2010

NUMERICAL MODELING OF THE DYNAMIC RESPONSE OF A MULTI-BILINEAR-SPRING SUPPORT SYSTEM

Trey D. Gilliam
University of Kentucky, treydgilliam@gmail.com

ABSTRACT OF THESIS

NUMERICAL MODELING OF THE DYNAMIC RESPONSE OF A MULTI-BILINEAR-SPRING SUPPORT SYSTEM

The Alpha Magnetic Spectrometer is an International Space Station Experiment that features a unique nonlinear support system with no previous flight heritage. The experiment consists of multiple straps with piecewise-linear stiffness curves that support a cryogenic magnet in three-dimensional space inside of a vacuum chamber. The stiffness curves for each strap are essentially bilinear and switch between two distinct slopes at a specified displacement. This highly nonlinear support system poses many questions in regards to feasible computational methods of analysis and possible response behavior. This thesis develops a numerical model for a multi-bilinear-spring support system motivated by the Alpha Magnetic Spectrometer design. Methods of analysis applied to the single bilinear oscillator served as the foundation of the model developed in this thesis. The model is developed using MATLAB and proves to be more computationally efficient than ANSYS finite element software. Numerical simulations contained herein demonstrate the variety of response behaviors possible in a multi-bilinear-spring support system, thus aiding future endeavors which may use a support system similar to the Alpha Magnetic Spectrometer. Classic nonlinear responses, such as subharmonic and chaotic, were found to exist.

KEYWORDS: Dynamic Response, Bilinear Stiffness Springs, Geometric Nonlinearities, Numerical Modeling, Space Applications

Trey Gilliam

July 30, 2010

NUMERICAL MODELING OF THE DYNAMIC RESPONSE OF A MULTI-BILINEAR-SPRING SUPPORT SYSTEM

By

Trey D. Gilliam

Suzanne Weaver Smith, Ph.D.
Director of Thesis

James M. McDonough, Ph.D.
Director of Graduate Studies

July 30, 2010

RULES FOR THE USE OF THESES

Unpublished theses submitted for the Master's degree and deposited in the University of Kentucky Library are as a rule open for inspection, but are to be used only with due regard to the rights of the authors. Bibliographical references may be noted, but quotations or summaries of parts may be published only with the permission of the author, and with the usual scholarly acknowledgments.

Extensive copying or publication of the thesis in whole or in part also requires the consent of the Dean of the Graduate School of the University of Kentucky.

A library that borrows this thesis for use by its patrons is expected to secure the signature of each user.

Name	Date

THESIS

Trey D. Gilliam

The Graduate School

University of Kentucky

2010

NUMERICAL MODELING OF THE DYNAMIC RESPONSE OF A MULTI-BILINEAR-SPRING SUPPORT SYSTEM

THESIS

A thesis submitted in partial fulfillment of the
requirements for the degree of Master of Science in
Mechanical Engineering in the College of Engineering
at the University of Kentucky

By

Trey D. Gilliam

Lexington, Kentucky

Director: Dr. Suzanne Weaver Smith, Professor of Mechanical Engineering

Lexington, Kentucky

2010

ACKNOWLEDGEMENTS

This thesis would not have been possible without the academic guidance of several individuals. I would like to thank my thesis advisor, Dr. Suzanne Weaver Smith, for providing me with the opportunity to attend graduate school and for her knowledge of linear and nonlinear dynamic analysis which greatly aided me during my studies. I wish to thank Dr. John Baker, who played a key role in assisting me with development of numerical models in this thesis and who, along with Dr. Keith Rouch, provided training in the use of ANSYS finite element software used for a portion of this thesis. Thanks are extended to all members of the Dynamic Structures and Controls Lab, who in various ways contributed to this work. I would also like to thank my Thesis Committee, Dr. Smith, Dr. Baker, and Dr. Rouch, for their time and effort given to improve this thesis.

I am extremely grateful for funding that I received from the University of Kentucky Center for Computational Sciences, the University of Kentucky Graduate School (Otis A. Singletary Fellowship), and the Kentucky Space Grant Consortium, all of which made it possible for me to attend graduate school.

I wish to thank members of the AMS-02 design team, Chris Tutt and Carl Lauritzen of Jacobs Engineering, for taking time out of their busy schedules to visit with us and provide valuable information about the system that motivated my thesis.

Most importantly, I am thankful for the many blessings God has bestowed upon my life. I wish to thank my family for the love and support they continue to provide, as well as my fiancée who, in addition to love and support outside of the classroom, has experienced countless hours of studying and late night work marathons in RGAN by my side.

TABLE OF CONTENTS

LIST OF TABLES

LIST OF FIGURES

Chapter 1: Introduction

The Alpha Magnetic Spectrometer (AMS) is an International Space Station experiment to be launched via shuttle in the second half of 2010. The project, under the sponsorship of the United States Department of Energy, is truly international in scope. The work effort spans over 15 different countries and various institutions and organizations including MIT, NASA and CERN [1].

Fundamentally, the AMS is a particle physics detector that uses a magnet to bend the path of charged cosmic particles as they pass through one of five on-board detectors. There are two different hardware versions of the Alpha Magnetic Spectrometer. AMS-01, which first flew aboard Discovery in 1998, utilized an ordinary magnet, while AMS-02 utilizes a large cryogenic superconducting magnet housed within a vacuum chamber. Evaporative cooling caused by the bleeding off of extremely cold liquid helium is used to keep the AMS-02 superconducting magnet cool and thus fully operational. A vacuum case serves as insulation of the complete magnet assembly, ensuring the helium itself remains cold and thus low temperatures are maintained during the experiment's planned three year lifespan.

Maintaining critically low temperatures required that a support system with minimal heat transfer be designed to mount the magnet within the vacuum chamber. The chosen system consists of 16 nonlinear straps that are fabricated with a low thermal conductivity material, further ensuring the cryogenic environment is not compromised by heat transfer to the magnet through the straps from outside the vacuum chamber. The support strap configuration and how they attach to the vacuum casing and magnet is presented in Figure 1.1 [2], [3].

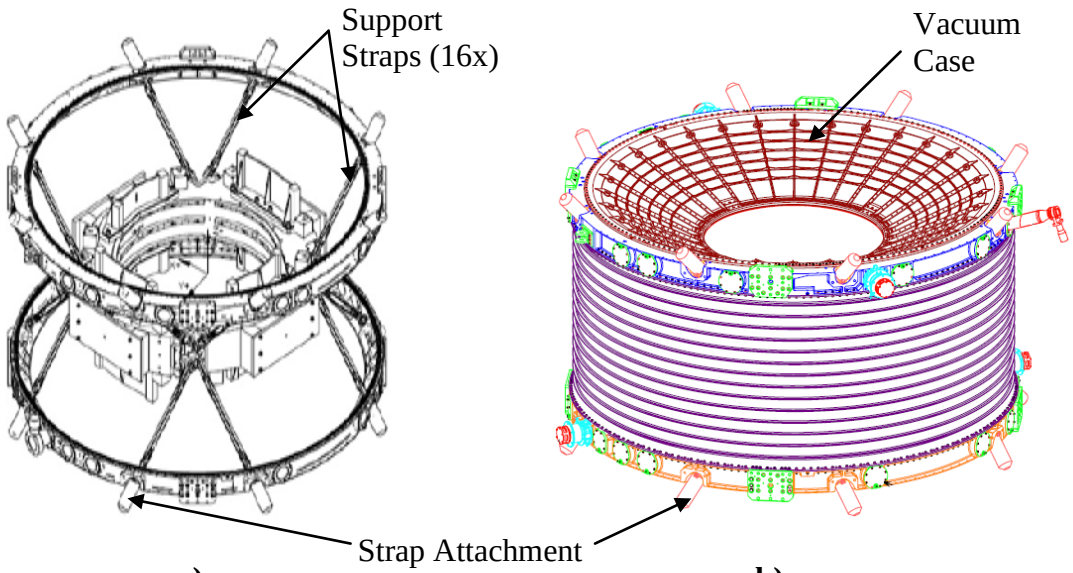

Figure 1.1: a) AMS-02 Magnet Support Straps [2], b) AMS-02 Magnet Vacuum Case [3]

The straps are considered nonlinear due an abrupt change in stiffness that occurs when any individual strap is stretched past a critical limit. The stiffness curves for each strap are actually piecewise-linear (PWL). PWL stiffness curves consist of various linear regions connected at points where stiffness changes, denoted as knees of the stiffness curve. The abrupt changes in stiffness of the PWL straps limit the range of magnet motion allowed and prevent an undesired source of heat transfer through contact with the walls of the vacuum case.

The actual straps used on the AMS-02 are bilinear or trilinear depending on the operation temperature. Representative stiffness models for AMS-02 straps are given in Figure 1.2. Each support strap is preloaded to a point within the yellow region on the curve at static equilibrium. The PWL stiffness curves globally appear bilinear, with distinct upper and lower stiffness values.

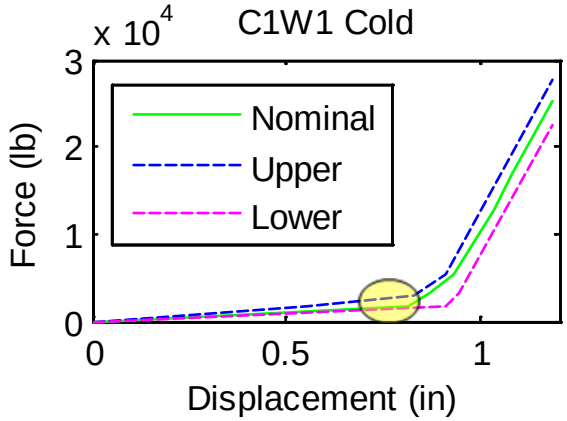

Figure 1.2: Representative AMS-02 Nonlinear Support Strap Stiffness Curve

The AMS-02 nonlinear support system is a new design with no prior flight heritage. The design poses many interesting challenges as a result of the nonlinear nature, such as determining a suitable method of analysis and exploring the wide range of possible response types. After the work for this thesis was completed, there was speculation as to which magnet, the AMS-01 or the AMS-02, would be used on the final International Space Station experiment [4]. All stated reasons of uncertainty associated with the AMS-02 cryogenic magnet were independent of the nonlinear support system and instead were inspired by the desired life span of the experiment. Regardless of which magnet is chosen for the final system, the PWL support strap system is a promising development for future space applications that may use the AMS-02 design as legacy.

The primary objective of this thesis is to develop a feasible method of computational analysis for a multi-bilinear-spring (MBS) support system motivated by the AMS-02 design that enables the range of possible nonlinear behavior to be studied. The system of interest consists of a point mass supported by four bilinear springs in a two-dimensional plane. The springs were assumed bilinear as a result of the essentially bilinear nature previously noted in the AMS-02 support strap stiffness curve. A general

bilinear spring consists of two distinct stiffness values, K_1 and K_2, joined together at a point that is called the knee of the stiffness curve, denoted by the letter s. Several examples of bilinear springs are given in Figure 1.3. Each of these is identical in extension, but differs in their compressive behavior. Additional information on each type of bilinear spring is provided in the introduction of Chapter 3. The four-spring MBS support system studied in this thesis, and presented in Chapter 3, is part of the larger class of PWL systems. Both single and multi-spring systems require nonlinear dynamic analysis.

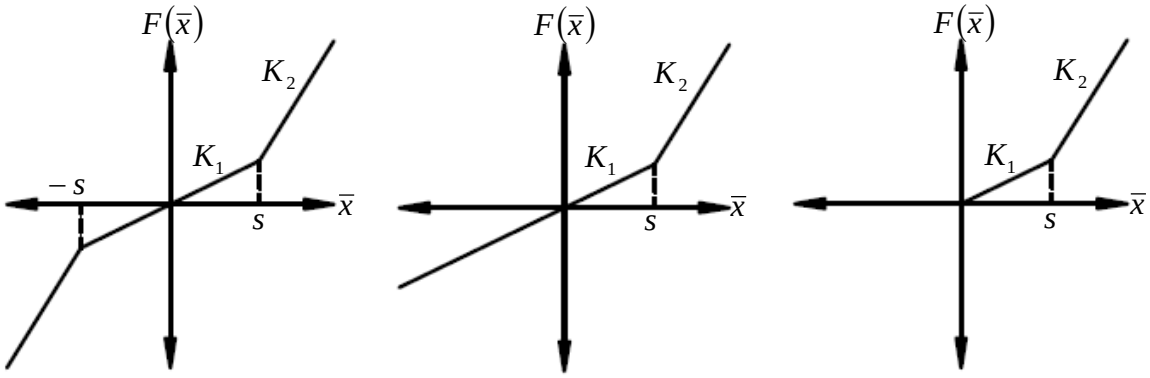

a) **b)** **c)**

Figure 1.3: Sample Bilinear Spring Stiffness Curves, a) Symmetric, b) Asymmetric with Compressive Resistance, c) Asymmetric with no Compressive Resistance

Chapter 2 of this thesis contains a brief summary of terminology necessary when studying nonlinear dynamics followed by a review of literature pertaining to nonlinear and PWL dynamic systems. Chapter 3 presents a derivation of equations of motion for two PWL systems. The single degree-of-freedom (DOF) bilinear oscillator is considered first, and serves as the starting point for a thorough derivation of the piecewise-continuous equations of motion for the two-dimensional four-spring MBS support system. Chapter 4 explores the potential energy associated with the MBS system in

different positions as well as variation of static equilibrium positions due to changes in system parameters. Chapter 5 contains dynamic simulation results primarily obtained via numerical integration of differential equations of motion in MATLAB. The familiar single bilinear oscillator is once again used as a starting point to motivate actions taken when exploring the more complicated four-spring MBS support system. Nonlinear behavior in the four-spring MBS support system is documented. Additional topics include comparison of numerical integration results with ANSYS nonlinear transient results and exploration of approximating bilinear stiffness curves with polynomials. Chapter 6, the final chapter of this thesis, contains a summary and conclusions as well as recommendations for future expansions of this work.

Chapter 2: Literature Review

2.1 Definitions

Nonlinear dynamics has a vast language not readily encountered in other fields of study. It is first necessary to summarize essential definitions prior to a review of the literature. Much of this language will also be used in subsequent chapters. The aim of this section is to improve the overall flow of the thesis and aid in understanding the material.

State variables refer to quantities used to describe the state of the system [5]. In dynamic analysis, position and velocity are frequently chosen as state variables. The space in which state variables evolve is known as the phase space.

Phase plane portraits are projections of state variable solutions onto the phase space [5]. For dynamic system analysis, phase plane portraits are frequently velocity plotted versus position. Solutions projected onto the phase space create trajectories in phase plane portraits. Periodic solutions are represented by closed-curve trajectories.

Poincaré maps are generated by marking the location of the system at particular state variables on the phase plane portrait at discrete time intervals. The forcing period is typically used as the discretized time interval.

Subharmonic responses occur at frequencies lower than the frequency of external forcing. Subharmonic responses are frequently denoted as period-k responses, where the response period is k times larger than the forcing period. Similarly, a superharmonic response occurs at a frequency greater than the frequency of external forcing.

Chaos is an apparently random response of a nonlinear system to a fixed excitation that occurs when “periodic excitation leads to a nonperiodic response” [6].

Nayfeh defines chaos as “a bounded steady state behavior that is not an equilibrium solution or a periodic solution or a quasiperiodic solution” as well as a “constrained random-like behavior” [5].

A bifurcation refers to a change in the number or type of solutions that occurs as a system parameter, such as forcing frequency or damping ratio, is varied in small intervals.

2.2 Introduction to Nonlinear Dynamic Analysis

Piecewise-linear dynamic systems, such as the Alpha Magnetic Spectrometer cryogenic magnet support structure, are part of a larger class known as nonlinear dynamic systems. The study of nonlinear dynamic systems has seen rapid growth in the last century as increases in scientific awareness and computational capacity have allowed researchers to explore these systems in great detail. Nonlinear system dynamic analysis frequently requires repetition of computationally expensive calculations that have been expedited with the advent of the modern computer. However, many of the methods and tools utilized today were developed during or adapted from early foundational studies of nonlinear systems.

French mathematician Henri Poincaré encountered nonlinear systems during his study of the n-body problem in celestial mechanics during the late 1800’s [5]. Poincaré is considered by many to be the father of chaos theory. Poincaré maps, named in honor of Henri Poincaré, have become a standard means of detecting chaos within a dynamic system. A more general discussion on nonlinear systems was documented in Den Hartog’s Mechanical Vibrations, originally published in 1934 [7]. A chapter of the text is devoted to systems with variable or nonlinear characteristics, whereby the mass,

damping, or stiffness are functions of time or displacement. Integration of governing equations of motion for free and forced vibrations are discussed for both mechanical and electrical systems. Subharmonic resonance, a phenomenon not possible in linear systems, was discussed. One of the earliest comprehensive textbooks on nonlinear dynamics, Minorsky's Introduction to Nonlinear Mechanics, was published in 1947 [8]. The text utilized topological methods of nonlinear analysis, such as phase plane plots, trajectories and bifurcation theory, as well as analytical methods popular at the time.

Numerous textbooks and journal articles have since been published within the field of nonlinear dynamics. Most modern texts on vibrations contain at least one chapter dedicated to nonlinear analysis [9]. Nonlinear systems exhibit many response characteristics that are not possible in their linear counterparts, such as the existence of multiple subharmonic responses. In cases where multiple responses are possible, the initial conditions of the system determine which motion is physically realized. This strong dependence on initial conditions has become a key trait of nonlinear systems. However, perhaps the most important aspect of research in the field of nonlinear dynamics is the discovery and establishment of the branch of physics known as chaos. Modern chaos theory has become a standard and acceptable aspect of nonlinear dynamic analysis.

Chaos, by nature, cannot be defined by a simple mathematical model. It is important to note that chaos is not completely random. Poincaré maps provide visual justification of the bounded nature of the seemingly random phenomenon. Harmonic and subharmonic responses are represented by a single or a finite number of points on the Poincaré map, respectively. Chaos is represented by strange attractors on the maps.

Strange attractors, such as the famous Lorenz attractor, are composed of an infinite number of points arranged in bounded, fractal shapes. A truly random phenomenon would not have recognizable attractors on the Poincaré map, but rather a completely random distribution of points with no bounds or shapes.

Bifurcation diagrams are another tool frequently used to identify chaotic motion. Bifurcation diagrams often reveal repeated period doubling as the path to chaos in nonlinear systems. A period-1 response may bifurcate into a period-2 response. The period-2 response has a period that is twice that of the period-1 response. Thus, in forced systems, two forcing periods will occur before the period-2 response begins to repeat. In general, a period-k response has a period that is k times larger than the forcing period for the system. These period doublings, or triplings in some instances, continue to occur as the system parameter is varied until chaotic motion appears. It is possible for regions of chaotic motion to once again become harmonic or subharmonic as the system parameter is varied.

Ueda successfully simulated chaos exhibited by Duffing's equation using analog and digital computers in 1980 [10]. Duffing's equation is a second order differential equation with cubic stiffness nonlinearity. Ueda found that forced Duffing oscillatory systems exhibited harmonic, subharmonic, ultrasubharmonic and chaotic response for certain system parameters (damping and forcing amplitude). These regions were identified on a damping-forcing amplitude parameter plane. This parameter plane was reproduced by Thompson and Stewart and has been included for reference in Figure 2.1 [11]. Twenty-one major regions were identified, ranging from strictly chaotic, periodic, or subharmonic responses to coexisting chaotic, periodic or subharmonic responses. In

agreement with typical chaotic systems, the obtained response varied with initial conditions.

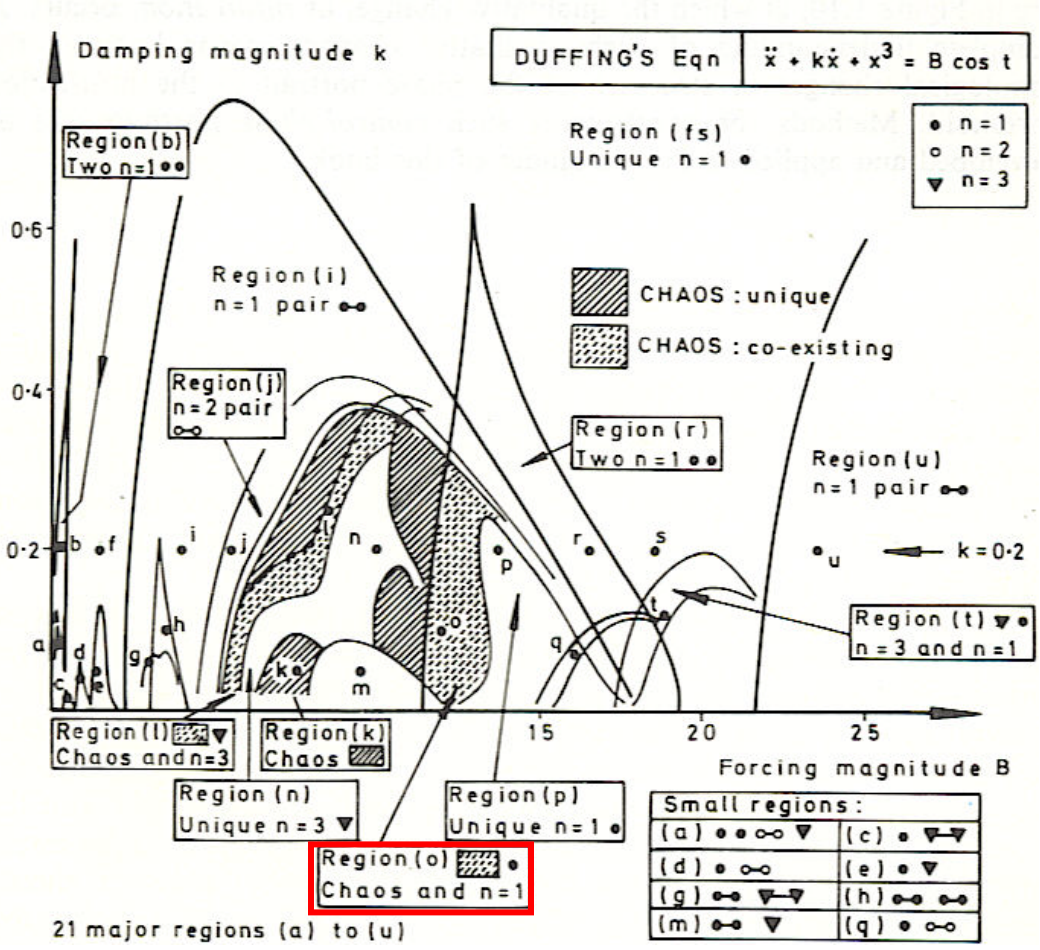

Figure 2.1: Damping-Forcing Amplitude Parameter Plane for Duffing's Equation, created by Ueda [10]. Thompson and Stewart Reproduction is Presented with Permission (Copyright © 1986 John Wiley & Sons) [11].

Phase plane plots highlighted various regions of coexisting responses as well as detected chaotic regions. Figure 2.2, the result of numerical simulations reproducing Ueda [10], demonstrates the nonlinear system's dependence on initial conditions. For given values of damping and forcing amplitude, the response is chaotic or period-1 depending on the initial position and velocity. These parameter values correspond to

Region (o) as noted in Figure 2.1. The nonlinear behavior of Duffing's equation has also been explored experimentally and results compare well with Ueda's paper [12].

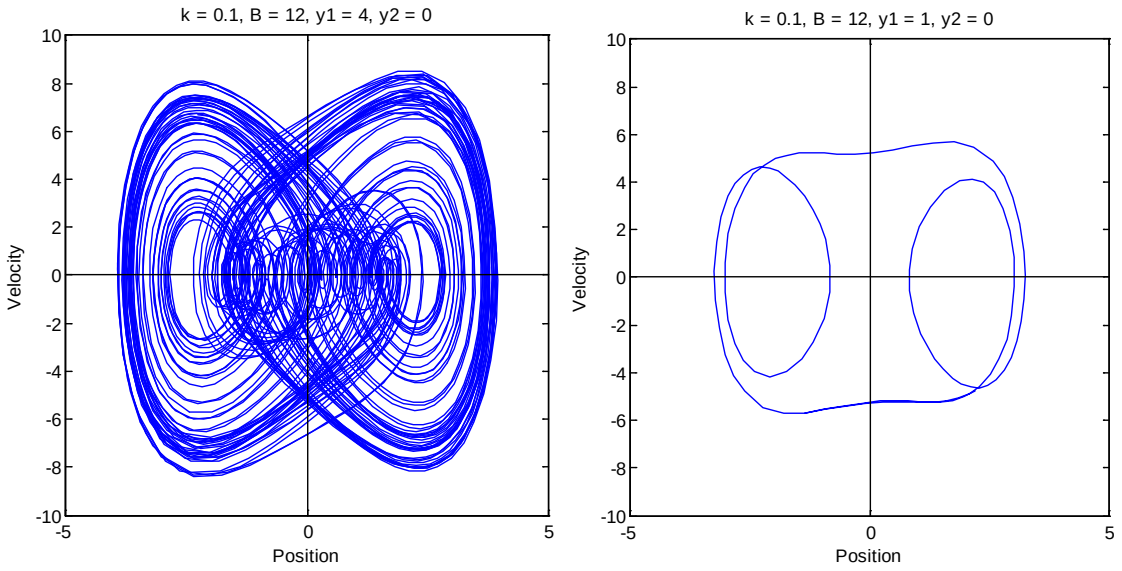

Figure 2.2: Coexisting chaotic and period-1 trajectories, recreated from Ueda [10]

2.3 Introduction to Piecewise Linear Dynamic Systems

Bilinear springs, the specific focus of the effort in this thesis, belong to the subset of general nonlinear systems known as piecewise-linear (PWL). Their name is derived from the fact that the governing differential equations of motion can be written by piecing together two or more linear equations at distinct locations. When the governing equation switches from one linear solution to another, the system response changes abruptly. This abrupt change in behavior is often caused by physical contact with another object or a change in material properties designed to alter the system response. Impact oscillators, such as a bouncing ball contacting a rigid surface [13], mooring lines [14], [15], [16], spring mass systems with clearance [17], [18], [19], [20], preloaded compliance systems [21], elastic beams with nonlinear boundary conditions [22], and cracked concrete

structures [23] are all examples of piecewise linear dynamic systems. All of these examples use modeling equations composed of a series of linear differential equations.

Den Hartog was perhaps the first individual to research PWL dynamic systems. During the 1930's, Den Hartog published two papers that investigated one-dimensional, single DOF spring mass systems with PWL stiffness behavior [24], [25]. In 1932, Den Hartog and Mikina obtained the steady state solution for an oscillatory system with initial spring set [24]. The solution was obtained by piecing together the linear solutions which pertained to the two portions of the oscillatory motion. The second order differential equation of motion was nondimensionalized, boundary conditions were imposed, and an equation which governed the shape of the response was obtained. Numerical methods were required to solve transcendental equations in time to determine the actual maximum response amplitude for a given forcing function.

Four years later, Den Hartog and Heiles investigated the steady state response of a symmetric bilinear oscillator [25]. Denoting the lower portion of the stiffness curve K_1, and the upper portion of the stiffness curve K_2, the response amplitude was plotted for various forcing frequencies and K_1/K_2 ratios of 0, 0.5, 2, and ∞. It was determined that bilinear system response with large forcing approached that of a purely linear system with stiffness K_2. For cases where external forcing did not engage the second portion of the stiffness curve, the system behaved as the expected linear spring mass structure with stiffness K_1.

Chaotic solutions of single DOF PWL oscillators were discovered in the early 1980's [26]. After the work of Ueda and others in years prior, chaos was an accepted aspect of general nonlinear dynamic systems. Previously studied systems were typically

nonlinear because of the presence of terms that were not first order in time dependent variables. Unlike these systems, PWL oscillators possess differential equations that are first order in the dependent variables but still exhibit chaotic response. Schulman studied the case of a single DOF forced oscillator with stiffness K_1 for x > 0 and stiffness K_2 for x < 0 in 1983. This system is a simplistic model of the human eardrum, where the elastic coefficient is larger for inward displacement than it is for outward displacement [26]. Damping time, defined as the inverse of the nondimensionlized damping coefficient, was chosen as the varied system parameter. The damping times at which period doublings occurred were presented in tabular form and ranges of damping time that resulted in chaotic motion were discovered. A maximum value of damping time above which no chaotic solutions were found was discussed within the paper.

In the same year of Schulman's study, Shaw and Holmes published an article on periodically forced piecewise linear oscillators where harmonic, subharmonic, and chaotic responses were found to exist [17]. Their general model was a single DOF asymmetric bilinear oscillator with two stiffness values, K_1 and K_2, and critical knee location at displacement value x0. Two distinct scenarios, one with x0 = 0 and the other an impact oscillator with $K_2 = \infty$, were discussed. The governing differential equations of motion were written in piecewise form. This resulted in two second order differential equations because of the two potential stiffness values. Exact solutions governing the motion in each region were obtained with traditional ODE theory. Each occurrence of the knee location x0, which serves as the switching point between the two solutions, was located using simple Newton-Rhapson iterations on digital computers. The times at which x0 was reached are referred to as crossing times, and these times were determined

through use of the Newton-Rhapson scheme. The use of digital computers allowed Shaw and Holmes to locate the crossing points with high precision. Locating the crossing point was the only approximation in their model since exact ODE solutions were used rather than numerical ODE methods to predict the motion for time spans between back-to-back crossing point times.

For the special case x0 = 0, Shaw and Holmes located a series of period doubling bifurcations and presented a case with coexisting stable period-1 and period-3 motions. Analysis of the impact oscillator ($K_2 = \infty$) was simplified by taking the time of flight during impact to be zero. A coefficient of restitution model was implemented to account for energy loss during the impact. Digital computation was only needed to locate one crossing time (the time at which the impact occurred). A bifurcation diagram was constructed by carrying out a large number of simulations on the computer. A variety of single impact and period-k orbits were found. Orbits up to period-32 were observed for the impact oscillator. Strange attractors were discovered for various impact oscillator cases, but no rigorous mathematical theory was utilized to confirm that chaos was present. At the time of publication, fairly general mathematical theory had been completed for one-dimensional mappings, but not for two dimensions, limiting the authors to digital evidence of chaotic responses.

2.4 Methods of Analysis for Nonlinear Dynamic Systems

Solutions for nonlinear dynamic problems where the exact time histories are not easily obtained or are potentially nonexistent are obtained with a variety of methods. If an analytical solution is obtainable without extremely large increases in computation time, this will be the most desirable due to the low amount of error introduced.

Complications in deriving closed form solutions and complexity of calculation normally lead researchers to utilize approximate methods of solution. Perturbation theory, harmonic balance, and numerical integration are a few of the approximate techniques frequently used to solve nonlinear dynamic problems. Other methods, such as mapping dynamics [27] and graph theory [28] can also be applied to nonlinear system analysis, but are not addressed in this review due to their infrequent use compared to other methods of analysis. Each method has inherent benefits and drawbacks, as well as others that depend on the particular nonlinearity being modeled. For example, numerical integration allows for the full time history to be obtained, while harmonic balance methods provide the steady state motion only. Depending on the desired outcome, the lack of transient solution information may be acceptable.

Very few papers have made use of closed form solution techniques for piecewise-linear systems. Shaw and Holmes used exact solutions for each linear region of the piecewise linear system, but used digital computers to approximate the switching point between their two governing differential equation solutions [17]. This solution type is not truly closed form. Additionally, piecing together closed form solutions for a simple one-dimensional, single DOF PWL oscillator is easily done, but higher order systems would require complex theory to obtain the solutions in each PWL region. Chicurel-Uziel presented an exact, closed-form solution for a piecewise-linear spring and mass system that could be written in a single equation [29]. Their methodology was to use the Heaviside unit step function to write a single equation of motion. The unit step function can be used to activate different portions of the PWL stiffness curve. The author suggests that a closed algebraic expression for the Heaviside unit step function is possible, but

most likely software such as Mathematica or Maple would be used to handle the function and make calculations. This approach is not typically seen in other PWL studies.

Perturbation theory is based on the idea of splitting a problem into the combination of a solvable problem and a small perturbation parameter, ε [30]. Allowing ε to tend to 0 results in a problem where the solution is easily obtained. Modifications are then made to account for the effect of the small perturbation, ε, from the easily obtained solution. By accounting for small deviations from linear problems, perturbation theory can be used to solve problems with relatively weak nonlinearities, such as certain instances of cubic stiffness nonlinearities. The abrupt changes encountered in PWL oscillators imply they are strongly nonlinear systems, thus classical perturbation methods, such as Krylov-Bogoliubov-Mitropolsky and multiple scales, are not appropriate solution techniques [31], [32].

The harmonic balance method (HBM) is a frequency domain approach used to obtain steady state solutions of nonlinear dynamic systems. This method is capable of handling systems with strong nonlinearities. In cases where more accurate periodic solutions are desired, the HBM must be reformulated to add additional harmonic terms [31]. Cheung and Lau proposed using the incremental harmonic balance method (IHBM) for nonlinear periodic vibrations in 1981 [33]. A series of solutions are obtained in a step-by-step manner until the desired solution accuracy is obtained. Choosing a suitably small increment almost guarantees that the IHBM will converge regardless of the complicated response nature. The authors demonstrated proper application of their proposed IHBM on thin-walled plates and shallow shell problems. Their results compared well with previously published results [33].

Lau and Zhang extended IHBM analysis to systems with PWL stiffness [34]. Plots of response amplitude versus forcing frequency were generated for two classic PWL stiffness examples. The first, a single DOF system with clearance, gave rise to superharmonic and subharmonic resonances. The second example was a single DOF system with symmetric PWL stiffness, also known as a symmetric bilinear spring. The authors presented a convergence study for the second case. Time histories for two different forcing frequencies were tabulated for three, five, and eight harmonic term models. Three-harmonic-term models provided very good results when compared to the higher-order models, but it is still recommended to use more harmonic terms when analyzing superharmonic and subharmonic resonances. Both stable and unstable vibration states are obtained with the IHMB, contrary to numerical integration. This facilitates stability analysis of PWL systems [34].

In 2003, Xu et al applied the IHBM to a single DOF oscillator with both PWL stiffness and damping terms [31]. Period-3 responses were discovered with the IHBM. Chaotic responses arising from successive period doubling bifurcations were also found, in agreement with Li and Yorke's famous assertion that existence of period-3 motion implies chaotic motion will also occur [35]. Xu et al compared many of their results with fourth order Runge-Kutta simulations and the two methods matched extremely well. Successful applications suggest the IHBM is a promising solution technique to analyze forced periodic vibrations of PWL systems.

Numerical integration schemes are perhaps the most prevalent nonlinear response analysis technique seen in the literature. High-order Runge-Kutta (RK) methods allow for full time histories of motion with both the transient and steady state solutions to be

accurately obtained. RK methods are criticized for being time consuming when conducting parametric studies or if unstable solutions are desired [31]. However, once equations of motion are obtained, RK schemes are easily implemented and compute reasonably quickly on modern computers. RK schemes have been used in general nonlinear dynamic problems as well as PWL problems.

Ravindra and Mallik used RK to numerically integrate the governing equation of motion for a harmonically excited mass and isolator with cubic stiffness and pth-power damping nonlinearities [36]. A parametric study revealed that while critical forcing values at which bifurcations occured changed as the the power of damping and damping ratio varied, the bifurcation structure of this Duffing type oscillator was not affected by the specific power of the nonlinearity. Changes in the nonlinear damping model showed potential for passive control of chaos. Nayfeh et al used a fifth and six-order RK scheme when studying the nonlinear free and forced responses of a buckled beam [37]. RK56 results obtained with a digital computer agreed with analytical solutions obtained with an analog computer. Kahraman also used RK56 when numerically simulating the response of a one-dimensional single DOF PWL oscillator with a clearance deadzone [20]. Previous studies on PWL oscillators that used RK schemes to obtain accurate results were listed in Kahraman's paper. Due to its frequent use as the approximate solution technique of choice and as a benchmark for validating new methods of nonlinear system analysis, RK is an extremely promising method when considering numerical modeling of multi-bilinear-spring support systems.

The time step of integration is a key parameter when numerically integrating equations of motion. All numerical integration schemes, such as RK or Newmark's

method, require that a finite time step be selected. Larger time steps generally imply less accurate results. In theory, an infinite number of time steps in a given simulation time would result in the highest accuracy obtainable, but this is not possible due to limitations in computational capacity. If a chosen time step is too small, numerical error can be introduced via subtractive cancellation. Subtractive cancellation occurs when the computer attempts to take the difference between two extremely small numbers [38]. If the precision required to accurately represent the difference is higher than the computers binary representation capacity, errors are introduced. This provides a realistic lower bound for time steps of integration. However, it is still important to select a time step that accurately resolves the dynamic behavior of the system.

Koh and Liaw studied the effects of time step size on a bilinear system response [39]. A one-dimensional single DOF spring mass model with symmetric bilinear stiffness behavior was simulated numerically with Newmark's method. As a general rule of thumb, the authors state that the number of time steps per natural period of the structural system in its linear range should be at least ten. In cases where the bilinear stiffness hardens at the knee, this criterion for time step is more stringent. The validity of this statement was analyzed parametrically by running simulations with an increasing number of time steps per forcing period.

The authors found that an insufficient number of time steps per forcing cycle resulted in incomplete chaotic attractors and false existence of subharmonic responses [39]. A critical number of time steps per forcing cycle was found to exist. If the number of time steps was below this critical value, there was a potential for false or incomplete results, and if the number of time steps was above this number, the results appeared

unchanged. In some cases, an insufficient number of time steps resulted in the correct chaotic attractor shape, but points on the Poincaré map tended to stay in the top or bottom of the attractor for long periods of time, rather than being evenly distributed as seen in cases with more time steps.

Furthermore, it was determined that an even number of time steps per forcing cycle resulted in more accurate simulations than an odd number. The critical number of time steps per forcing period, above which spurious results were not seen, was found to be higher for the odd case than the even case. This effect is believed to be a result of the difficulty in representing a symmetric sine wave (the forcing function) with an odd number of segments. The odd representation does not preserve symmetry of each half sine wave. As the number of odd time steps increases, this effect becomes less noticeable. Practically speaking, using an odd number of time steps per forcing cycle, rather than an even number, required that more time steps be used to obtain accurate results for the bilinear system. The authors also made note that chaotic time histories are greatly affected by the number of time steps, even if the number is above the critical amount. In light of the variation of response with time step, it is advised that numerical simulations of chaotic time histories be viewed in a more qualitative than quantitative light.

2.5 PWL System Studies of Interest and Adaptations

Hossain et al studied the effect of the bilinear spring stiffness ratio on obtaining chaotic motion from quasi-periodic motion [18]. A single DOF asymmetric bilinear spring mass system with clearance was experimentally and numerically simulated. The asymmetric nature is intended to account for preloaded conditions that may be present in

the spring. A small spring could be inserted into the clearance region, allowing the clearance stiffness to range from 0 to an arbitrary small amount, denoted K_1. The second portion of the stiffness curve was denoted by stiffness K_2. Numerical and experimental results revealed that multiple periodic motions occurred more frequently when the ratio K_1/K_2 was decreased from 0.25 to 0 [18]. Similarly, bifurcation analysis revealed that larger chaotic regions of motion occurred in the case of $K_1/K_2 = 0$, suggesting that more chaotic and subharmonic motions result for a free clearance system than one with a low stiffness spring inserted in the clearance. Decreasing the value of the clearance ratio, a measure of the length of the clearance region, also resulted in more chaotic motion.

In addition to spring stiffness and clearance ratios in a bilinear system, Hossain et al investigated the effect of preloading in an asymmetric single DOF bilinear model of a clutch-power transmission [19]. This paper made use of the low stiffness clearance spring addressed in their work on stiffness ratio effects. Physically, elastic materials such as rubber are often used to lessen the harsh nonlinearity of a true bilinear spring with zero stiffness clearance region. Numerical and experimental studies were conducted for a range of preloaded initial conditions. By setting the initial preload, a new equilibrium position for the spring mass system was set, governing how close the system was to the knee in the bilinear stiffness model. The equilibrium position proved to greatly affect the nonlinear dynamic response. Specifically, chaotic responses occurred more frequently for cases where the initial preload was close to the knee in the stiffness curve. Discrepancies between numerical and experimental results were present due to friction and inability to match damping coefficients, yet both methods demonstrated qualitative

similarities and both revealed the increase in chaotic motion for preloading conditions near the knee.

Previously addressed papers on PWL systems presented foundational studies and exploration of key behavior parameters, such as stiffness ratios and location of the knee in the stiffness model. A portion of the literature on PWL systems has simply aimed to further explore the nonlinear behavior that may arise from the case of harmonically forcing a system with PWL stiffness. Often times a new method of analysis is presented to effectively conduct bifurcation and stability analysis, such as Cao et al's use of the Chen-Langford method to obtain averaged system equations for an asymmetric PWL oscillator [40]. Other researchers have further expanded the analysis by exploring more involved forcing functions than simple harmonic. Choi and Noah examined the response of a PWL oscillator subjected to multiple harmonic forces at different frequencies [41]. The fixed point algorithm (FPA), previously referred to as the "shooting method," was used to identify stable and unstable solutions for multiple forcing frequency systems applied to an offshore articulated loading platform. Such a system consists of an asymmetric bilinear stiffness curve which softens at the knee ($K_2 < K_1$). Articulated loading platforms subjected to two different forcing frequencies were found to exhibit chaotic motion more frequently than forcing the system at a single frequency.

Narayanan and Sekar added flow-induced excitations in addition to harmonic forcing when modeling the vibration of a square prism in fluid flow [32]. The prism is modeled as a single DOF asymmetric PWL oscillator with softening nonlinearity. Vortex shedding and galloping are sources of flow-induced excitation a square prism in fluid flow may encounter. The Fast-Galerkin and Runge-Kutta methods of analysis were

compared and displayed high levels of agreement for this particular model. Typical nonlinear responses, such as subharmonic and chaotic, were found. Initial condition maps visually characterized system response by clarifying which initial conditions lead to specific responses. Overall, the dynamic behavior with flow induced excitations was qualitatively similar to the simple case of harmonic forcing.

Xueqi et al presented a two-step method to identify parameters of symmetric PWL oscillators from experimental data [42]. While nonlinear system identification has frequently been addressed, very few have considered the case of PWL systems. System parameters that are identified include mass, damping, lower stiffness (K_1), upper stiffness (K_2), and the location of the knee in the stiffness curve. The Legendre polynomial approximation is a key aspect of the two step method. PWL stiffness curves are represented by their Legendre polynomials curve fittings. Assuming that position, velocity, acceleration, and forcing are known at each point in the experimental data, the first step is to use the direct parameter estimation method to estimate the mass and Legendre polynomial coefficients from the assumed general form of spring mass system equations. Identification of the stiffness properties is achieved by relating Legendre polynomial coefficients to the desired parameters. The author presents the Legendre polynomial curve fitting process when applied to PWL systems by means of the least squares method. This allows for the relationship between stiffness and Legendre coefficients to be determined in advance. This relationship is then used in the reverse order when translating estimated Legendre coefficients from the experimental data into stiffness curve properties. The method was verified by treating numerical integration results obtained from fourth-order Runge-Kutta as experimental data. The two-step

method was applied, and estimated parameters were compared to those used in the numerical simulation. For high-order Legendre polynomial approximations, results were almost identical to the original simulation values. The authors note that their method accurately obtains parameters without need of search procedures or iterations.

Most of the literature on PWL oscillators is dedicated to one-dimensional, single DOF systems, such as a single mass and bilinear spring oscillator. Studies presented up to this point in this review have dealt with this particular case. Other studies have extended the scope to one-dimensional multiple DOF systems that consist of several masses connected in series by linear springs and one location where stiffness changes. Often this is achieved by applying a physical stop in one blocks' path of motion, thus creating an impact oscillator, or by inserting a clearance region, creating a bilinear spring acting on one mass. Wagg and Bishop explored modeling techniques for an N-DOF impact oscillator system using a coefficient of restitution model [43]. In their study, only the Nth mass is assumed to impact a rigid wall, at which point the restitution model is introduced. The authors explore the relationship between modal energy and the coefficient of restitution; connections are made to physical systems such as an impacting beam [43]. Additional studies of one-dimensional multiple DOF oscillators with PWL stiffness in different regions include [44], [45], [46], and [47].

Piecewise systems are not limited to PWL applications. Piecewise nonlinear-linear systems, whereby a nonlinear stiffness/damping is connected to a region of linear stiffness/damping, have also been addressed in the literature. Ji and Hansen developed an approximate solution and carried out numerical integration with Runge-Kutta schemes for a one-dimensional single DOF piecewise nonlinear-linear system [48]. Many of the

previously discussed phenomena, such as chaotic motions and coexisting subharmonic responses depending on initial conditions, were discovered. The authors employed the same notion of joining various solution regions at a specific location in space and time as seen in PWL system analysis.

A recent dissertation submitted at Ohio State University explored the dynamic response of piecewise nonlinear oscillators with time varying stiffness coefficients [49]. The author presented a classification system for general piecewise systems that included PWL time invariant, PWL time varying, piecewise nonlinear time invariant, and piecewise nonlinear time varying. Papers previously addressed in this literature review focus on what the author terms PWL time invariant, whereas the main objective of the dissertation was to develop a general method to obtain the steady state response of piecewise nonlinear time varying systems. The proposed methodology made use of the multi-term HBM and discrete Fourier transforms. Single DOF and multiple DOF systems were considered. For further information in regards to piecewise systems with time varying coefficients, consult [49]. The focus of this work remains the PWL time-invariant bilinear spring featured in MBS support systems.

2.6 Accounting for Geometric Nonlinearities

A key difference between the Alpha Magnetic Spectrometer cryogenic magnet support system and the literature previously addressed is the existence of multiple PWL spring supports. Literature provides a thorough treatment of one-dimensional single DOF PWL spring oscillators, but not systems that consist of multiple PWL springs or multiple DOF in the same context as the aforementioned support system. Previously discussed multiple DOF PWL oscillators discussed one-dimensional motion of several masses

connected by springs in series. The AMS consists of a single mass supported by an array of multiple straps, each of which is PWL in nature. The magnet is able to move in all three dimensions. Additional complications in modeling arise due to the existence of several locations where the governing equations of motion change. Each individual strap has its own PWL stiffness curve, resulting in multiple knees in the behavior, whereas one-dimensional single DOF PWL oscillators had a single location where the equations must switch.

Geometric nonlinearities must also be accounted for in systems such as the AMS support structure. As the magnet moves in three-dimensional space, the strap orientation will change with respect to the original configuration. Depending on the amplitude of motion, the corresponding changes in angles of the straps with respect to the global x, y and z axes will lead to variations in the stiffness component in each of those directions. Euromech (European Mechanics Society) colloquium 483, entitled *Geometrically non-linear vibrations of structures*, consisted of presentations over recent geometric nonlinearity research. A special issue in the *Journal of Sound and Vibration* contained extended versions of some papers presented at the colloquium and is available for consultation [50]. Kovacic et al studied a vibration isolator that consisted of three springs, a vertical spring which was linear and two oblique springs which had cubic stiffness nonlinearities [51]. The physical arrangement, shown in Figure 2.3, of the oblique springs required that geometric nonlinearities also be addressed.

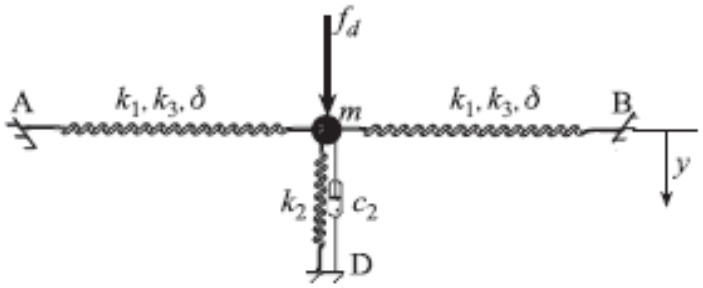

Figure 2.3: Isolator with Linear Vertical Spring and Nonlinear Oblique Springs, Copied from [51] with Permission (Copyright © 2008 Elsevier Ltd)

Introducing nonlinear oblique springs, as opposed to solely linear, proved desirable for static characteristics, but the nonlinearity, in combination with the geometric nonlinearity, allowed for undesired dynamic response. Period doubling bifurcations were found to occur for certain combinations of system parameters. Period-doubling bifurcations are a common route to chaos, and such a response is not desired for vibration isolation. The authors note that for certain ranges of forcing frequency, no bifurcations were discovered.

The analysis of moored bodies is one area of research that simultaneously encompasses PWL nonlinearities and geometric nonlinearities simultaneously. Mooring lines are frequently modeled in a manner similar to impact oscillators (ie taut and slack behavior only), and are used to restrain vessels, buoys, and similar structures in bodies of water. Plaut and Farmer studied motion of a breakwater anchored to the sea floor by mooring lines that were modeled as inextensible cables [14]. Their general two-dimensional model is seen in Figure 2.4.

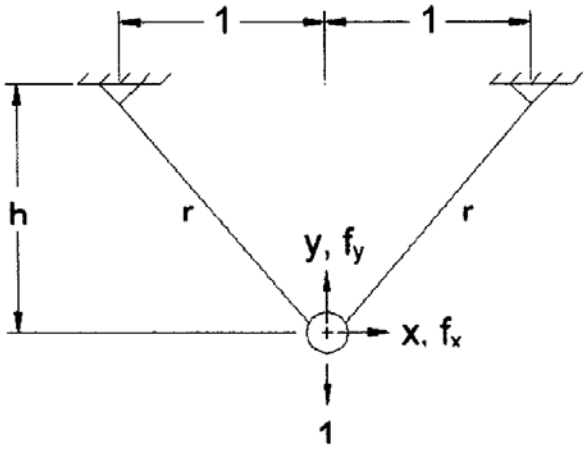

Figure 2.4: Point Mass and Inextensible Mooring Cable Breakwater Model, Copied from [14] with Permission (Copyright © 2000 Kluwer Academic Publishers)

A survey of possible motions for the point mass in two-dimensions, as well as results for a rigid body model, was presented in the paper via two-dimensional trajectory plots and phase plane portraits. Plaut et al also extended the study to three-dimensions and found chaotic motions were possible [15]. One-dimensional surge motion of a moored vessel has been studied by Gottlieb and Yim using four mooring lines [52] and by Umar et al using six mooring lines [53]. Subharmonic and chaotic motions were discovered at various system parameter combinations in both one-dimensional surge motion studies. Similar nonlinear responses are anticipated in PWL support structures, such as the AMS-02 strap system, due to physical similarities to the moored body problem.

2.7 Alpha Magnetic Spectrometer

The AMS-02 support strap system is a complex PWL oscillator with multiple PWL straps and three-dimensional motion. Due to its complexity, many of the analysis tools discussed in this review are not readily applicable. Structural verification of the AMS-02 support strap system began with modeling a two strap in-line configuration with closed-form techniques, but dynamic response analysis for the complete AMS-02 magnet

support system with 16 straps was carried out in NASTRAN software [2]. The AMS-02 support straps are initially preloaded to a force value just prior to the first change in stiffness behavior. Limitations in NASTRAN implied there was no direct method for preloading the elements used to model support straps [2]. This difficulty was overcome by shifting the origin of each strap's stress-strain curve to correspond to the preloaded condition. The validity of this approach will be explored further in Chapter 4.

2.8 Concluding Remarks

Future on-orbit systems may make use of PWL support structures similar to the AMS-02 design. A review of the literature on PWL dynamic systems revealed most of the focus to date has been on one-dimensional, single DOF systems, with less work available on two and three-dimensional systems with multiple PWL supports. This work effort is motivated by the AMS-02 support strap system, but aims to provide a more general understanding of the possible motions for this unique design, as well as identify and develop additional simulation methodology for similar systems. The existence of classic nonlinear responses is also of interest. In the chapters to follow, equations of motion are derived and nondimensionalized for a multi-bilinear-spring (MBS) support system with four bilinear springs supporting a single point mass in a two-dimensional plane. Many of the techniques discussed in this literature review are applied to numerical simulations of this MBS support system.

Chapter 3: Developing Numerical Models

3.1 Introduction to Bilinear Springs

A four-spring MBS support system will be the main focus of this work. Justification for choosing this two-dimensional, two DOF system is given later in this chapter. However, thorough understanding of the equations of motion for a one-dimensional, single DOF bilinear spring mass oscillator, as addressed in much of the literature review, is required prior to developing equations of motion for the MBS system with additional springs and higher dimensions of motion.

A general bilinear spring consists of two distinct stiffness values, K_1 and K_2, implying the restoring force is piecewise-linear (PWL) in nature. In this work, the location at which the stiffness changes is referred to as the knee of the bilinear spring stiffness model, denoted by the letter *s*. This variable will always be a positive value, and will be preceded by a negative sign if required in equations. Bilinear springs can be classified by their behavior under tension or compression. A brief overview of different types of bilinear springs is given in this section, but the discussion does not include all possible configurations.

For a symmetric bilinear spring, the compressive region of the stiffness curve is a reflection of the tensile region. A symmetric bilinear spring has two knee locations, one under tension and one under compression. The PWL restoring force for a symmetric bilinear spring is

$$F(\bar{x}) = \begin{cases} K_2'\bar{x} + (K_2' - K_1)s, & \bar{x} < -s \\ K_1\bar{x}, & |\bar{x}| \le s \\ K_2\bar{x} + (K_1 - K_2)s, & \bar{x} > s \end{cases} \tag{3.1}$$

K_2 and K_2', seen in Equation 3.1, are assumed to be equal for the symmetric bilinear spring. Often times a symmetric bilinear spring stiffness curve may be shifted with respect to the origin to account for preloading. In this case, the plane of symmetry simply shifts from the origin to another location of the force-versus-displacement curve. The symmetric bilinear spring stiffness curve with and without preloading is seen in Figure 3.1.

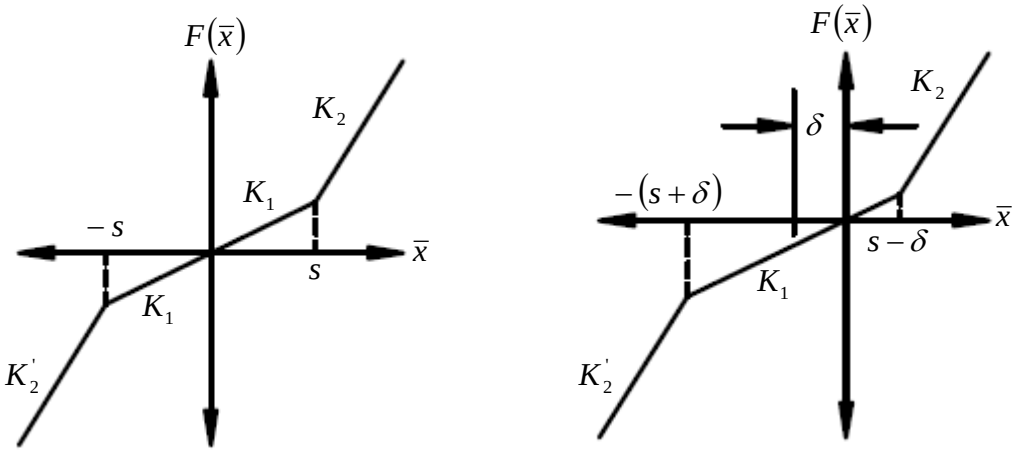

a) **b)**

Figure 3.1: Symmetric Bilinear Spring Stiffness Model, a) without preload, b) with preload

Any deviation that does not allow for a plane of symmetry, such as K_2' having a different value from K_2, results in what will be referred to as an asymmetric bilinear spring. An asymmetric bilinear spring with no knee under compression maintains the stiffness value K_1 for all $\bar{x} \leq s$. The PWL restoring force for the asymmetric bilinear spring with a tension knee but no knee under compression is

$$F(\bar{x}) = \begin{cases} K_1\bar{x}, & \bar{x} \leq s \\ K_2\bar{x} + (K_1 - K_2)s, & \bar{x} > s \end{cases} \tag{3.2}$$

Figure 3.2 illustrates the stiffness curve for an asymmetric bilinear spring with no compressive knee.

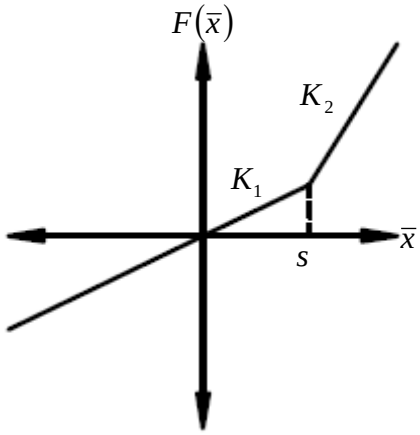

Figure 3.2: Asymmetric Bilinear Spring with Compressive Resistance Stiffness Model

The last situation presented is an asymmetric bilinear spring with no compressive resistance. The PWL restoring force for the asymmetric bilinear spring with no compressive resistance is

$$F(\bar{x}) = \begin{cases} 0, & \bar{x} \le 0 \\ K_1 \bar{x}, & 0 < \bar{x} \le s \\ K_2 \bar{x} + (K_1 - K_2)s, & \bar{x} > s \end{cases} \tag{3.3}$$

A classic example of the zero compressive resistance bilinear spring is a tension only mooring line. In that particular case, the knee of the stiffness curve is located at the origin, implying a stiffness of K_2 for any positive displacement, and zero stiffness otherwise. The general stiffness model for an asymmetric bilinear spring with zero compressive resistance is given in Figure 3.3a). One should note that shifting the origin of Figure 3.3a), as is done in Figure 3.3b), results in an asymmetric bilinear spring with an artificial region of compressive resistance and changes the location of the knee with respect to the newly placed origin.

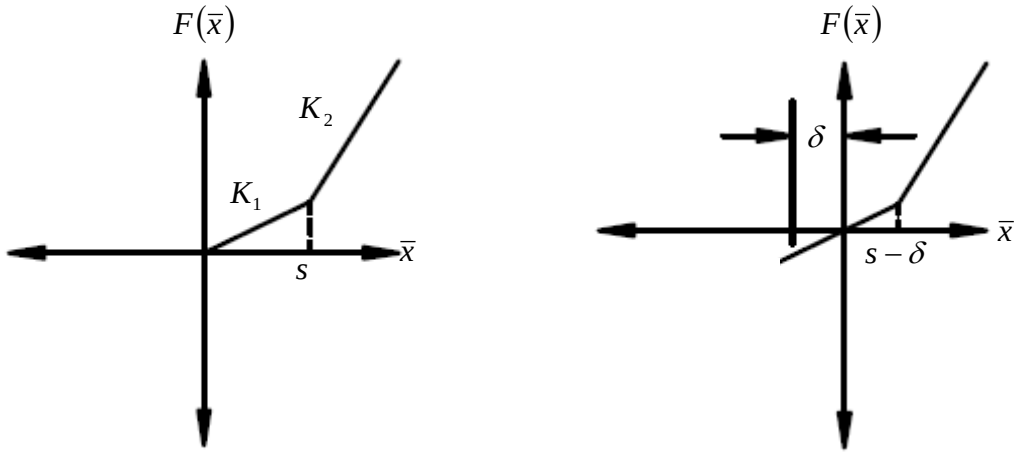

a) **b)**

Figure 3.3: Asymmetric Bilinear Spring with no Compressive Resistance, a) general curve, b) with origin shift

This artificial compression region is of finite length, governed by the distance that the origin was shifted. The significance of this shifting is addressed later when potential energy of the MBS support system is discussed in Chapter 4. As previously mentioned, there are other adaptations, such as combining two opposing bilinear springs, which could be presented but are excluded from the present work because they are not as central to the thesis as these models.

3.2 One-Dimensional Single DOF Bilinear Oscillator Equations of Motion

Development of the equations of motion for the MBS support system started with modeling the simplified asymmetric bilinear spring oscillator with no compressive knee. First consider the simple linear oscillator in Figure 3.4 where $\bar{x}$ is measured with respect to the equilibrium position. The equation of motion can be derived using Newton's Second Law.

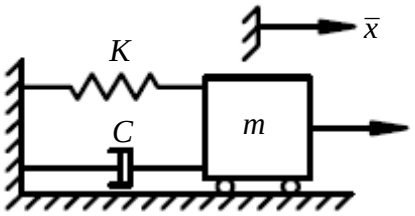

Figure 3.4: Simple Linear Oscillator

$$\xrightarrow{+} \sum F = m\frac{d^2}{d\bar{t}^2}(\bar{x}) \tag{3.4}$$

$$-K\bar{x} - C\frac{d}{d\bar{t}}(\bar{x}) + \bar{A}\sin(\bar{\omega}\bar{t}) = m\frac{d^2}{d\bar{t}^2}(\bar{x}) \tag{3.5}$$

$$m\frac{d^2}{d\bar{t}^2}(\bar{x}) + C\frac{d}{d\bar{t}}(\bar{x}) + K\bar{x} = \bar{A}\sin(\bar{\omega}\bar{t}) \tag{3.6}$$

The solution to this second order differential equation is readily obtained via traditional ODE theory, via numerical ODE solution schemes such as Runge-Kutta, or may be found in standard vibration texts [9].

Similarly, for the asymmetric bilinear spring with a tension knee at a displacement value of s and $\bar{x}$ measured with respect to the equilibrium position, Newton's Second Law yields

$$\xrightarrow{+} \sum F = m\frac{d^2}{d\bar{t}^2}(\bar{x}) \tag{3.7}$$

$$m\frac{d^2}{d\bar{t}^2}(\bar{x}) = \begin{cases} -K_1\bar{x} - C\dfrac{d}{d\bar{t}}(\bar{x}) + \bar{A}\sin(\bar{\omega}\bar{t}), & \bar{x} \le s \\ -\left(K_2\bar{x} + (K_1 - K_2)s\right) - C\dfrac{d}{d\bar{t}}(\bar{x}) + \bar{A}\sin(\bar{\omega}\bar{t}), & \bar{x} > s \end{cases} \tag{3.8}$$

$$\begin{cases} m\dfrac{d^2}{d\bar{t}^2}(\bar{x}) + C\dfrac{d}{d\bar{t}}(\bar{x}) + K_1\bar{x} = \bar{A}\sin(\bar{\omega}\bar{t}), & \bar{x} \le s \\ m\dfrac{d^2}{d\bar{t}^2}(\bar{x}) + C\dfrac{d}{d\bar{t}}(\bar{x}) + \left(K_2\bar{x} + (K_1 - K_2)s\right) = \bar{A}\sin(\bar{\omega}\bar{t}), & \bar{x} > s \end{cases} \tag{3.9}$$

Mass normalization yields

$$\begin{cases} \dfrac{d^2}{d\bar{t}^2}(\bar{x}) + \dfrac{C}{m}\dfrac{d}{d\bar{t}}(\bar{x}) + \Omega_1^2\bar{x} = \dfrac{\bar{A}}{m}\sin(\bar{\omega}\bar{t}), & \bar{x} \le s \\ \dfrac{d^2}{d\bar{t}^2}(\bar{x}) + \dfrac{C}{m}\dfrac{d}{d\bar{t}}(\bar{x}) + \left(\alpha\Omega_1^2\bar{x} + \left(\Omega_1^2 - \alpha\Omega_1^2\right)s\right) = \dfrac{\bar{A}}{m}\sin(\bar{\omega}\bar{t}), & \bar{x} > s \end{cases} \tag{3.10}$$

where, $\Omega_1^2 = K_1/m$. The bilinear spring stiffness ratio, defined as $\alpha = K_2/K_1$, has also been introduced. Finally, the equation of motion is written in dimensionless form,

$$\begin{cases} \ddot{x} + (2\zeta)\dot{x} + x = A\sin(\omega t), & x \le 1 \\ \ddot{x} + (2\zeta)\dot{x} + (\alpha x + (1-\alpha)) = A\sin(\omega t), & x > 1 \end{cases} \tag{3.11}$$

where $x = \bar{x}/s$, $t = \bar{t}\Omega_1$, $\zeta = C/2m\Omega_1$, $A = \overline{A}/sK_1$, and $\omega = \overline{\omega}/\Omega_1$. An overdot now represents differentiation with respect to dimensionless time, t.

The dimensionless equation of motion for the asymmetric bilinear spring oscillator with tension knee is piecewise-linear in nature due to the two distinct governing differential equations of motion. The appropriate differential equation to use depends on the value of the dimensionless position. When obtaining the solution for a particular span of dimensionless time, there are several options. The simplistic nature of the differential equations implies that exact solutions could be written for each region of motion. Each occurrence of the switching point could then be located with a Newton-Rhapson scheme, as previously mentioned in the literature review [17].

A general solution may also be obtained by implementing a numerical ODE solution scheme that is capable of changing which equation is integrated depending on the value of x. Many computer software packages, such as MAPLE or MATLAB have predefined numerical ODE solvers, including Runge-Kutta schemes with varying orders of accuracy, capable of solving user defined systems of equations. The MATLAB *ode45* command is an explicit one-step Runge-Kutta solver based on the Dormand-Prince method [56]. For a general differential equation, *ode45* will numerically solve and provide a solution over the desired time duration. While the overall desired simulation

time for an asymmetric bilinear spring is user defined, specifying this time span is not sufficient to solve the problem.

The time of flight in each region of motion is not known ahead of time, and must therefore be determined during integration. The event location property of the *ode45* command can be used to successfully locate the switching points in time. Specifically, zeros of user defined event functions are intelligently detected during integration. Once a particular event occurs, the user can specify whether or not to stop integration. An alternation scheme can then be developed to simulate the asymmetric bilinear spring oscillator. Initial conditions determine which portion of the piecewise-linear equation of motion should be used to start the simulation, and that equation will be numerically integrated until the event function detects that a knee has been reached. When the knee is reached, integration will be stopped and the state variables will be stored. For a single asymmetric bilinear spring, the occurrence of the knee implies switching to the second differential equation. The Runge-Kutta scheme is called again with initial conditions governed by the ending state variables of the last numerical integration pass. This alternating process is continued until the full simulation time is realized. Appendix A contains the MATLAB code with this logic implemented for a single asymmetric bilinear oscillator.

Alternately, the MATLAB *switch* command could be used without starting and stopping integration. The *switch* command allows several cases to be defined yet have a single case execute based on a changing status variable. This approach, however, does not intelligently locate the switching points. Rather, at each time step, MATLAB checks if it has moved beyond the switching point, and if so, it changes equations, implying the

switching point location is not fully resolved. Overstepping the switching point, even by small amounts, may potentially alter the dynamic response, and thus is not desired behavior. The *ode45* event detection capabilities, which do allow for intelligent location of switching points, will be used instead. A review of typical one-dimensional, single DOF bilinear oscillator dynamic simulations using this approach is given in the preliminary section of Chapter 5.

3.3 MBS Support System Equations of Motion

This section details the derivation of equations of motion via Newton's Second Law for a two-dimensional, two DOF support system consisting of four bilinear springs. The system was obtained by collapsing the magnet to a point mass in a top-view of the AMS-02 strap support system, seen in Figure 3.5. The general schematic is given in Figure 3.6. This new system reduces the level of complexity as compared to the full AMS-02 geometry, yet still serves as an appropriate phenomenological representation, as discussed later in this section. The point mass assumption implies that rotational degrees-of-freedom, which would be present when considering a rigid mass, are neglected in this study.

The anchor points where one end of each spring attaches are considered fixed in space and in-line with the x and y axes of the two-dimensional plane. The undeformed length of each spring can be less than or equal to the distance from the origin of the plane to its corresponding anchor point. If the undeformed length is equal to that distance, the springs are assumed to be "cut-to-length" and possess an asymmetric bilinear stiffness model (the springs experience tension and compression as the mass oscillates). The "cut-

to-length" assumption implies there is no initial preload in any of the springs and that the equilibrium position corresponds to the origin of the two-dimensional plane.

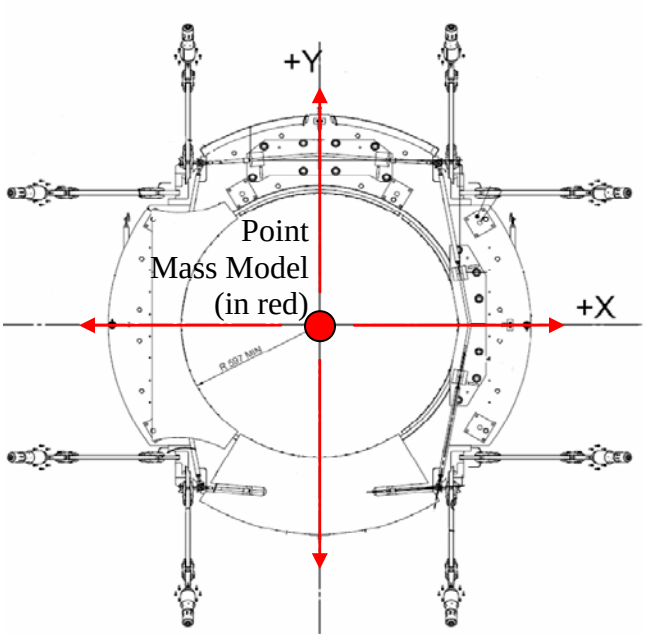

Figure 3.5: Top-View of AMS-02 Magnet and Support Straps [2]

If the undeformed length of each spring is less than the distance from the origin to each corresponding anchor point, the springs are initially preloaded. This scenario is similar to the physical AMS-02 support straps, which are tension-only elements that are stretched and attached to the magnet. In the four-spring MBS system, each individual spring is assumed to have an asymmetric bilinear stiffness curve with no compressive resistance (individual springs always remain in tension as the mass oscillates). Each spring applies a different force on the mass and provides a component of the total resultant force. Due to the preloaded initial state, the equilibrium position is not guaranteed to coincide with the origin of the plane, and its location is governed by the location of anchor points and each spring's parameter definitions.

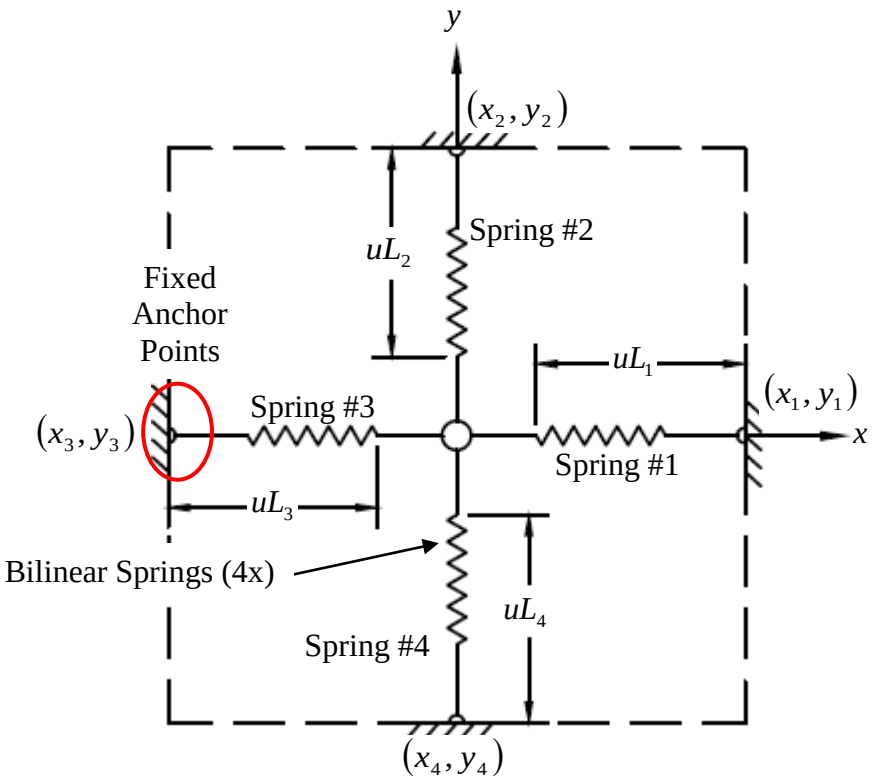

a)

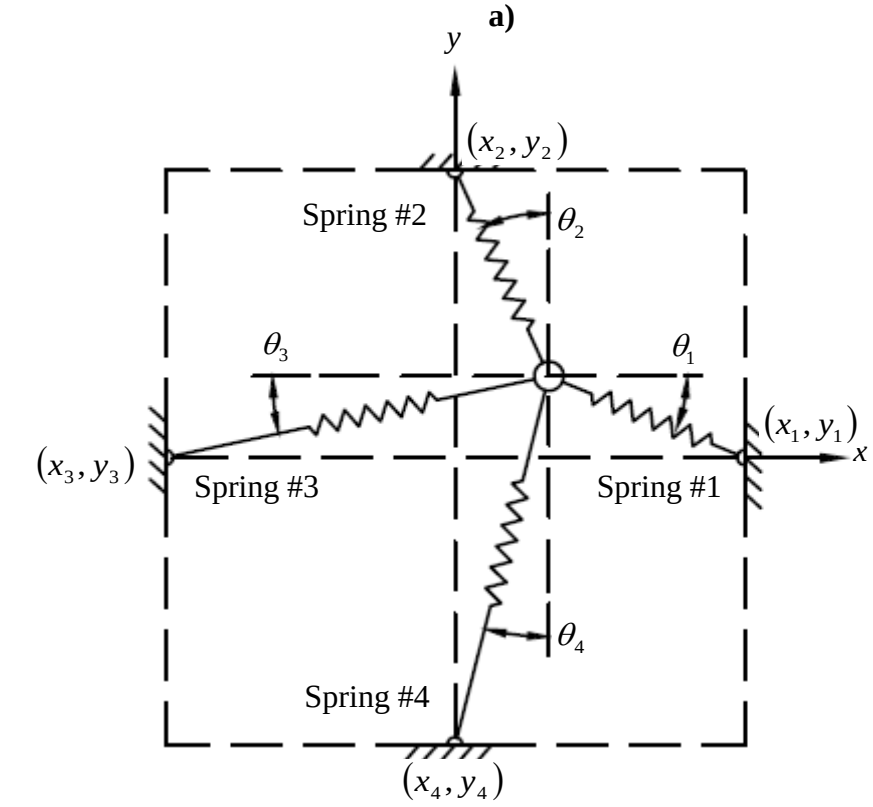

b)

Figure 3.6: Schematic of MBS Support System with Four Bilinear Springs: a) Undeformed Lengths and Anchor Coordinate Definitions, b) Angle Definitions

Geometric nonlinearities must now be accounted for in addition to the bilinear stiffness curve of each individual support spring. As the mass moves in the two-dimensional plane, the orientation of the straps will change with respect to the original configuration as seen in Figure 3.6b. These geometric nonlinearities will be addressed by calculating the angle of the springs at each iteration and updating the equations of motion accordingly. Geometric nonlinearities were a non-issue in the case of one-dimensional bilinear spring mass oscillators of one, or even multiple, DOF. Even in higher dimensions, such as the system of interest in Figure 3.6, geometric nonlinearities may be a non-issue if large displacement of the mass is not possible. However, in the general sense, whereby the mass is allowed to move throughout the two-dimensional plane with large or small amplitude displacement, the geometric nonlinearity cannot be ignored. The effect of the geometric nonlinearity when large amplitude displacement occurs is discussed in more detail in Chapter 5. The presence of both geometric and bilinear nonlinearities makes the four-spring MBS an appropriate phenomenological representation of the AMS-02 support structure.

The single asymmetric bilinear spring had a piecewise equation of motion that consisted of two options. The governing equations of motion for the four-spring MBS support system will be piecewise with 16 different differential equation sets, where each set consists of two equations, one for each independent DOF. The total number of piecewise differential equation sets for a MBS support system is governed by the simple equation

$$Number \quad of \quad Sets = (2)^{Number \quad of \quad Bilinear \quad Springs} \tag{3.12}$$

The number of equations in each set depends on the dimension of the model in consideration. This equation is applicable for any system where no more than two regions of the bilinear spring stiffness curve are encountered during the motion of interest. For example, a system consisting of asymmetric bilinear springs with no compressive resistance would not follow this equation if all three regions of the stiffness curve were encountered during the motion. Spring deformations are assumed to be within reasonable bounds given the physical constraints of the system, implying factors such as material failure and additional nonlinear end effects are not considered. A MBS support system, similar to the AMS support strap system, consisting of 16 bilinear springs would have $2^{16} = 65{,}536$ differential equation sets. If a full three-dimensional model were considered, each of these sets would contain three differential equations, one for each independent DOF, for a total of 196,608 equations.

As previously stated, the two-dimensional nature of the four-spring MBS support system implies the system has two independent DOF. The 2 DOF chosen to develop the equations of motion align with the horizontal and vertical directions of the original model configuration, labeled as $\bar{x}$ and $\bar{y}$, respectively. The bars are used to denote dimensioned quantities. Nondimensional quantities, in contrast, will use symbols without additional overbars.

The governing differential equations of motion in each direction are once again obtained via Newton's 2nd Law. The equations of motion are initially developed in detail for the case where all springs are assumed to be stretched to a value below the knee of their individual stiffness curves. Viscous damping and general harmonic forcing are assumed present in the $\bar{x}$ and $\bar{y}$ directions. The equations of motion are easily adapted

to accommodate different force disturbances, but harmonic forcing only is presented here for simplicity. Appendix B contains the MATLAB script capable of simulating the four-spring MBS support system.

For $\left(\sqrt{(\bar{x}_1-\bar{x})^2+\bar{y}^2}-u\bar{L}_1\right)\le s_1$, $\left(\sqrt{\bar{x}^2+(\bar{y}_2-\bar{y})^2}-u\bar{L}_2\right)\le s_2$,

$$\left(\sqrt{(\bar{x}-\bar{x}_3)^2+\bar{y}^2}-u\bar{L}_3\right)\le s_3,\ \left(\sqrt{\bar{x}^2+(\bar{y}-\bar{y}_4)^2}-u\bar{L}_4\right)\le s_4$$

In the horizontal direction

$$\overset{+}{\rightarrow}\sum F_{\bar{x}}=m\frac{d^2}{d\bar{t}^2}(\bar{x}) \tag{3.13}$$

$$\begin{aligned}
&K_{11}\left(\sqrt{(\bar{x}_1-\bar{x})^2+\bar{y}^2}-u\bar{L}_1\right)\cos\left(a\tan\left(\frac{\bar{y}}{(\bar{x}_1-\bar{x})}\right)\right)...\\
&-K_{21}\left(\sqrt{\bar{x}^2+(\bar{y}_2-\bar{y})^2}-u\bar{L}_2\right)\sin\left(a\tan\left(\frac{(\bar{y}_2-\bar{y})}{\bar{x}}\right)\right)...\\
&-K_{31}\left(\sqrt{(\bar{x}-\bar{x}_3)^2+\bar{y}^2}-u\bar{L}_3\right)\cos\left(a\tan\left(\frac{\bar{y}}{(\bar{x}-\bar{x}_3)}\right)\right)...\\
&-K_{41}\left(\sqrt{\bar{x}^2+(\bar{y}-\bar{y}_4)^2}-u\bar{L}_4\right)\sin\left(a\tan\left(\frac{(\bar{y}-\bar{y}_4)}{\bar{x}}\right)\right)-C\frac{d}{d\bar{t}}(\bar{x})+\bar{A}_x\sin(\bar{\omega}_x\bar{t})=m\frac{d^2}{d\bar{t}^2}(\bar{x})
\end{aligned} \tag{3.14}$$

Similarly, in the vertical direction

$$+\uparrow\sum F_{\bar{y}}=m\frac{d^2}{d\bar{t}^2}(\bar{y}) \tag{3.15}$$

$$\begin{aligned}
&-K_{11}\left(\sqrt{(\bar{x}_1-\bar{x})^2+\bar{y}^2}-u\bar{L}_1\right)\sin\left(a\tan\left(\frac{\bar{y}}{(\bar{x}_1-\bar{x})}\right)\right)...\\
&+K_{21}\left(\sqrt{\bar{x}^2+(\bar{y}_2-\bar{y})^2}-u\bar{L}_2\right)\cos\left(a\tan\left(\frac{(\bar{y}_2-\bar{y})}{\bar{x}}\right)\right)...\\
&-K_{31}\left(\sqrt{(\bar{x}-\bar{x}_3)^2+\bar{y}^2}-u\bar{L}_3\right)\sin\left(a\tan\left(\frac{\bar{y}}{(\bar{x}-\bar{x}_3)}\right)\right)...\\
&-K_{41}\left(\sqrt{\bar{x}^2+(\bar{y}-\bar{y}_4)^2}-u\bar{L}_4\right)\cos\left(a\tan\left(\frac{(\bar{y}-\bar{y}_4)}{\bar{x}}\right)\right)-C\frac{d}{d\bar{t}}(\bar{y})+\bar{A}_y\sin(\bar{\omega}_y\bar{t})=m\frac{d^2}{d\bar{t}^2}(\bar{y})
\end{aligned} \tag{3.16}$$

These equations are simplified through introduction of several parameters. The lower stiffness of Springs 2 through 4 are scaled in relation to the lower stiffness of Spring 1 with the primary stiffness ratio, denoted β and subscripted accordingly, such that $K_{21} = \beta_2 K_{11}$, $K_{31} = \beta_3 K_{11}$, $K_{41} = \beta_4 K_{11}$. Furthermore, each spring has a bilinear spring stiffness ratio, denoted α and subscripted accordingly, where $K_{12} = \alpha_1 K_{11}$, $K_{22} = \alpha_2 K_{21} = \alpha_2 \beta_2 K_{11}$, $K_{32} = \alpha_3 K_{31} = \alpha_3 \beta_3 K_{11}$, and $K_{42} = \alpha_4 K_{41} = \alpha_4 \beta_4 K_{11}$. Introducing these definitions and normalizing with respect to mass yields

$$\begin{aligned}
&\Omega_1^2\left(\sqrt{(\bar{x}_1-\bar{x})^2+\bar{y}^2}-u\bar{L}_1\right)\cos\left(a\tan\left(\frac{\bar{y}}{(\bar{x}_1-\bar{x})}\right)\right)\ldots\\
&-\beta_2\Omega_1^2\left(\sqrt{\bar{x}^2+(\bar{y}_2-\bar{y})^2}-uL_2\right)\sin\left(a\tan\left(\frac{(\bar{y}_2-\bar{y})}{\bar{x}}\right)\right)\ldots\\
&-\beta_3\Omega_1^2\left(\sqrt{(\bar{x}-\bar{x}_3)^2+\bar{y}^2}-u\bar{L}_3\right)\cos\left(a\tan\left(\frac{\bar{y}}{(\bar{x}-\bar{x}_3)}\right)\right)\ldots\\
&-\beta_4\Omega_1^2\left(\sqrt{\bar{x}^2+(\bar{y}-\bar{y}_4)^2}-u\bar{L}_4\right)\sin\left(a\tan\left(\frac{(\bar{y}-\bar{y}_4)}{\bar{x}}\right)\right)-\frac{C}{m}\frac{d}{d\bar{t}}(\bar{x})+\frac{\bar{A}_x}{m}\sin(\bar{\omega}_x\bar{t})=\frac{d^2}{d\bar{t}^2}(\bar{x})
\end{aligned} \tag{3.17}$$

and

$$\begin{aligned}
&-\Omega_1^2\left(\sqrt{(\bar{x}_1-\bar{x})^2+\bar{y}^2}-u\bar{L}_1\right)\sin\left(a\tan\left(\frac{\bar{y}}{(\bar{x}_1-\bar{x})}\right)\right)\ldots\\
&+\beta_2\Omega_1^2\left(\sqrt{\bar{x}^2+(\bar{y}_2-\bar{y})^2}-u\bar{L}_2\right)\cos\left(a\tan\left(\frac{(\bar{y}_2-\bar{y})}{\bar{x}}\right)\right)\ldots\\
&-\beta_3\Omega_1^2\left(\sqrt{(\bar{x}-\bar{x}_3)^2+\bar{y}^2}-u\bar{L}_3\right)\sin\left(a\tan\left(\frac{\bar{y}}{(\bar{x}-\bar{x}_3)}\right)\right)\ldots\\
&-\beta_4\Omega_1^2\left(\sqrt{\bar{x}^2+(\bar{y}-\bar{y}_4)^2}-u\bar{L}_4\right)\cos\left(a\tan\left(\frac{(\bar{y}-\bar{y}_4)}{\bar{x}}\right)\right)-\frac{C}{m}\frac{d}{d\bar{t}}(\bar{y})+\frac{\bar{A}_y}{m}\sin(\bar{\omega}_y\bar{t})=\frac{d^2}{d\bar{t}^2}(\bar{y})
\end{aligned} \tag{3.18}$$

where $\Omega_1^2 = K_{11}/m$. Finally, the equations of motion are written in dimensionless form

For $\left(\sqrt{(x_1-x)^2+y^2}-uL_1\right)\le 1$, $\left(\sqrt{x^2+(y_2-y)^2}-uL_2\right)\le \sigma_2$,

$$\left(\sqrt{(x-x_3)^2+y^2}-uL_3\right)\le\sigma_3,\ \left(\sqrt{x^2+(y-y_4)^2}-uL_4\right)\le\sigma_4$$

$$\begin{aligned}
&\left(\sqrt{(x_1-x)^2+y^2}-uL_1\right)\cos\left(a\tan\left(\frac{y}{(x_1-x)}\right)\right)...\\
&-\beta_2\left(\sqrt{x^2+(y_2-y)^2}-uL_2\right)\sin\left(a\tan\left(\frac{(y_2-y)}{x}\right)\right)...\\
&-\beta_3\left(\sqrt{(x-x_3)^2+y^2}-uL_3\right)\cos\left(a\tan\left(\frac{y}{(x-x_3)}\right)\right)...\\
&-\beta_4\left(\sqrt{x^2+(y-y_4)^2}-uL_4\right)\sin\left(a\tan\left(\frac{(y-y_4)}{x}\right)\right)-(2\zeta)\dot{x}+A_x\sin(\omega_x t)=\ddot{x}
\end{aligned}\tag{3.19}$$

and

$$\begin{aligned}
&-\left(\sqrt{(x_1-x)^2+y^2}-uL_1\right)\sin\left(a\tan\left(\frac{y}{(x_1-x)}\right)\right)...\\
&+\beta_2\left(\sqrt{x^2+(y_2-y)^2}-uL_2\right)\cos\left(a\tan\left(\frac{(y_2-y)}{x}\right)\right)...\\
&-\beta_3\left(\sqrt{(x-x_3)^2+y^2}-uL_3\right)\sin\left(a\tan\left(\frac{y}{(x-x_3)}\right)\right)...\\
&-\beta_4\left(\sqrt{x^2+(y-y_4)^2}-uL_4\right)\cos\left(a\tan\left(\frac{(y-y_4)}{x}\right)\right)-(2\zeta)\dot{y}+A_y\sin(\omega_y t)=\ddot{y}
\end{aligned}\tag{3.20}$$

where $x=\bar{x}/s_1$, $y=\bar{y}/s_1$, $t=\bar{t}\Omega_1$, $\zeta=C/2m\Omega_1$, $A_x=\bar{A}_x/s_1K_{11}$, $A_y=\bar{A}_y/s_1K_{11}$ $\omega_x=\bar{\omega}_x/\Omega_1$, $\omega_y=\bar{\omega}_y/\Omega_1$, $uL_1=u\bar{L}_1/s_1$, $uL_2=u\bar{L}_2/s_1$, $uL_3=u\bar{L}_3/s_1$, $uL_4=u\bar{L}_4/s_1$, $\sigma_2=s_2/s_1$, $\sigma_3=s_3/s_1$, and $\sigma_4=s_4/s_1$. An overdot now represents differentiation with respect to dimensionless time.

The same process is used to write the remaining 15 of 16 cases in dimensionless form. Each spring's corresponding contributions to the equations of motion have two options, depending on whether or not the spring is stretched past its knee. The two options each spring can contribute to the equations of motion are listed below

Spring 1, x direction contribution options

$$\begin{cases} \left(\sqrt{(x_1-x)^2+y^2}-uL_1\right)\cos(\theta_1), & \left(\sqrt{(x_1-x)^2+y^2}-uL_1\right)\le 1 \\ \left(\alpha_1\left(\sqrt{(x_1-x)^2+y^2}-uL_1\right)+(1-\alpha_1)\right)\cos(\theta_1), & \left(\sqrt{(x_1-x)^2+y^2}-uL_1\right)>1 \end{cases} \tag{3.21}$$

where $\theta_1 = a\tan\left(\frac{y}{(x_1-x)}\right)$

Spring 1, y direction contribution options

$$\begin{cases} -\left(\sqrt{(x_1-x)^2+y^2}-uL_1\right)\sin(\theta_1), & \left(\sqrt{(x_1-x)^2+y^2}-uL_1\right)\le 1 \\ -\left(\alpha_1\left(\sqrt{(x_1-x)^2+y^2}-uL_1\right)+(1-\alpha_1)\right)\sin(\theta_1), & \left(\sqrt{(x_1-x)^2+y^2}-uL_1\right)>1 \end{cases} \tag{3.22}$$

Spring 2, x direction contribution options

$$\begin{cases} -\beta_2\left(\sqrt{x^2+(y_2-y)^2}-uL_2\right)\sin(\theta_2), & \left(\sqrt{x^2+(y_2-y)^2}-uL_2\right)\le \sigma_2 \\ -\left(\alpha_2\beta_2\left(\sqrt{x^2+(y_2-y)^2}-uL_2\right)+(\beta_2-\alpha_2\beta_2)\sigma_2\right)\sin(\theta_2), & \left(\sqrt{x^2+(y_2-y)^2}-uL_2\right)>\sigma_2 \end{cases} \tag{3.23}$$

where $\theta_2 = a\tan\left(\frac{(y_2-y)}{x}\right)$

Spring 2, y direction contribution options

$$\begin{cases} \beta_2\left(\sqrt{x^2+(y_2-y)^2}-uL_2\right)\cos(\theta_2), & \left(\sqrt{x^2+(y_2-y)^2}-uL_2\right)\le \sigma_2 \\ \left(\alpha_2\beta_2\left(\sqrt{x^2+(y_2-y)^2}-uL_2\right)+(\beta_2-\alpha_2\beta_2)\sigma_2\right)\cos(\theta_2), & \left(\sqrt{x^2+(y_2-y)^2}-uL_2\right)>\sigma_2 \end{cases} \tag{3.24}$$

Spring 3, x direction contribution options

$$\begin{cases} -\beta_3\left(\sqrt{(x-x_3)^2+y^2}-uL_3\right)\cos(\theta_3), & \left(\sqrt{(x-x_3)^2+y^2}-uL_3\right)\le \sigma_3 \\ -\left(\alpha_3\beta_3\left(\sqrt{(x-x_3)^2+y^2}-uL_3\right)+(\beta_3-\alpha_3\beta_3)\sigma_3\right)\cos(\theta_3), & \left(\sqrt{(x-x_3)^2+y^2}-uL_3\right)>\sigma_3 \end{cases} \tag{3.25}$$

Where $\theta_3 = a\tan\left(\frac{y}{(x-x_3)}\right)$

Spring 3, y direction contribution options

$$\begin{cases} -\beta_3\left(\sqrt{(x-x_3)^2+y^2}-uL_3\right)\sin(\theta_3), & \left(\sqrt{(x-x_3)^2+y^2}-uL_3\right)\le\sigma_3 \\ -\left(\alpha_3\beta_3\left(\sqrt{(x-x_3)^2+y^2}-uL_3\right)+(\beta_3-\alpha_3\beta_3)\sigma_3\right)\sin(\theta_3), & \left(\sqrt{(x-x_3)^2+y^2}-uL_3\right)>\sigma_3 \end{cases} \tag{3.26}$$

Spring 4, x direction contribution options

$$\begin{cases} -\beta_4\left(\sqrt{x^2+(y-y_4)^2}-uL_4\right)\sin(\theta_4), & \left(\sqrt{x^2+(y-y_4)^2}-uL_4\right)\le\sigma_4 \\ -\left(\alpha_4\beta_4\left(\sqrt{x^2+(y-y_4)^2}-uL_4\right)+(\beta_4-\alpha_4\beta_4)\sigma_4\right)\sin(\theta_4), & \left(\sqrt{x^2+(y-y_4)^2}-uL_4\right)>\sigma_4 \end{cases} \tag{3.27}$$

Where $\theta_4 = a\tan\left(\frac{(y-y_4)}{x}\right)$

Spring 4, y direction contribution options

$$\begin{cases} -\beta_4\left(\sqrt{x^2+(y-y_4)^2}-uL_4\right)\cos(\theta_4), & \left(\sqrt{x^2+(y-y_4)^2}-uL_4\right)\le\sigma_4 \\ -\left(\alpha_4\beta_4\left(\sqrt{x^2+(y-y_4)^2}-uL_4\right)+(\beta_4-\alpha_4\beta_4)\sigma_4\right)\cos(\theta_4), & \left(\sqrt{x^2+(y-y_4)^2}-uL_4\right)>\sigma_4 \end{cases} \tag{3.28}$$

These individual contributions can be used to quickly generate equations of motion for each remaining scenario. The following demonstrates the end result for the case where Springs 1, 3, and 4 are below the knee of their stiffness curve but Spring 2 is above its knee.

For $\left(\sqrt{(x_1-x)^2+y^2}-uL_1\right)\le 1$, $\left(\sqrt{x^2+(y_2-y)^2}-uL_2\right)>\sigma_2$,

$$\left(\sqrt{(x-x_3)^2+y^2}-uL_3\right)\le\sigma_3,\ \left(\sqrt{x^2+(y-y_4)^2}-uL_4\right)\le\sigma_4$$

$$\begin{aligned}
&\left(\sqrt{(x_1-x)^2+y^2}-uL_1\right)\cos(\theta_1)\ldots\\
&-\left(\alpha_2\beta_2\left(\sqrt{x^2+(y_2-y)^2}-uL_2\right)+(\beta_2-\alpha_2\beta_2)\sigma_2\right)\sin(\theta_2)\ldots\\
&-\beta_3\left(\sqrt{(x-x_3)^2+y^2}-uL_3\right)\cos(\theta_3)\ldots\\
&-\beta_4\left(\sqrt{x^2+(y-y_4)^2}-uL_4\right)\sin(\theta_4)-(2\zeta)\dot{x}+A_x\sin(\omega_x t)=\ddot{x}
\end{aligned} \tag{3.29}$$

and

$$\begin{aligned}
&-\left(\sqrt{(x_1-x)^2+y^2}-uL_1\right)\sin(\theta_1)\ldots\\
&+\left(\alpha_2\beta_2\left(\sqrt{x^2+(y_2-y)^2}-uL_2\right)+(\beta_2-\alpha_2\beta_2)\sigma_2\right)\cos(\theta_2)\ldots\\
&-\beta_3\left(\sqrt{(x-x_3)^2+y^2}-uL_3\right)\sin(\theta_3)\ldots\\
&-\beta_4\left(\sqrt{x^2+(y-y_4)^2}-uL_4\right)\cos(\theta_4)-(2\zeta)\dot{y}+A_y\sin(\omega_y t)=\ddot{y}
\end{aligned} \tag{3.30}$$

3.4 MBS Support System Equations of Motion via Finite Element Method Formulation

Equations of motion for one-dimensional spring mass systems are frequently derived with the Finite Element Method (FEM) formulation. Global mass, damping, and stiffness matrices are quickly assembled using superposition of the individual element matrices and allow for quick derivation of the governing differential equations of motion. In theory, this same process happens behind the scenes in FEM software packages such as ANSYS. However, deriving the equations of motion by hand allows for a more thorough understanding of the FEM and gives the user the freedom to obtain transient simulation data with other numerical integration tools, such as MATLAB Runge-Kutta. Efforts were made to derive the equations of motion for the four spring MBS support system via the FEM and the appropriate transformation matrices. However, it was found that underlying assumptions of the model and applied methodology resulted in inaccurate

numerical time histories. The derivation and validation processes are presented in detail for others that may consider this approach. In this section, the equations of motion have not been nondimensionalized, and all springs are assumed to be linear and cut-to-length, implying only the geometric nonlinearity is being addressed.

The four spring MBS support system discussed in this work consists of elements that are rotated with respect to the global $\bar{x}$ and $\bar{y}$ directions. Prior to assembling a global stiffness matrix with superposition, a rotation matrix must be used to transform each element's local stiffness matrix to the proper global orientation. Each element is rotated in the $\bar{x}\bar{y}$ plane with respect to the $\bar{z}$ axis. For a general two node axial element, such as a spring, rotated through an angle φ, where + φ is always measured counterclockwise from global to local, $-\pi \le \varphi \le \pi$, the rotation matrix is given by

$$T = \begin{bmatrix} C\phi & S\phi & 0 & 0 \\ -S\phi & C\phi & 0 & 0 \\ 0 & 0 & C\phi & S\phi \\ 0 & 0 & -S\phi & C\phi \end{bmatrix} \tag{3.31}$$

For a spring element between nodes *i* and *j* with stiffness *k*, the global stiffness matrix is then given by

$$\underline{k} = T^T \hat{k} T = k \begin{bmatrix} C^2\phi & C\phi S\phi & -C^2\phi & -C\phi S\phi \\ & S^2\phi & -C\phi S\phi & -S^2\phi \\ & & C^2\phi & C\phi S\phi \\ & \textit{Symmetry} & & S^2\phi \end{bmatrix} \begin{Bmatrix} \bar{x}_i \\ \bar{y}_i \\ \bar{x}_j \\ \bar{y}_j \end{Bmatrix} \tag{3.32}$$

This technique can be used to generate the global stiffness matrix for the MBS support system presented in Section 3.3. The model is initially developed with the assumption of linear springs; implying geometric nonlinearities are the only nonlinearities present.

Consider the system model, composed of five nodes and four elements, presented in Figure 3.7. Recall the cut-to-length assumption is utilized for this section.

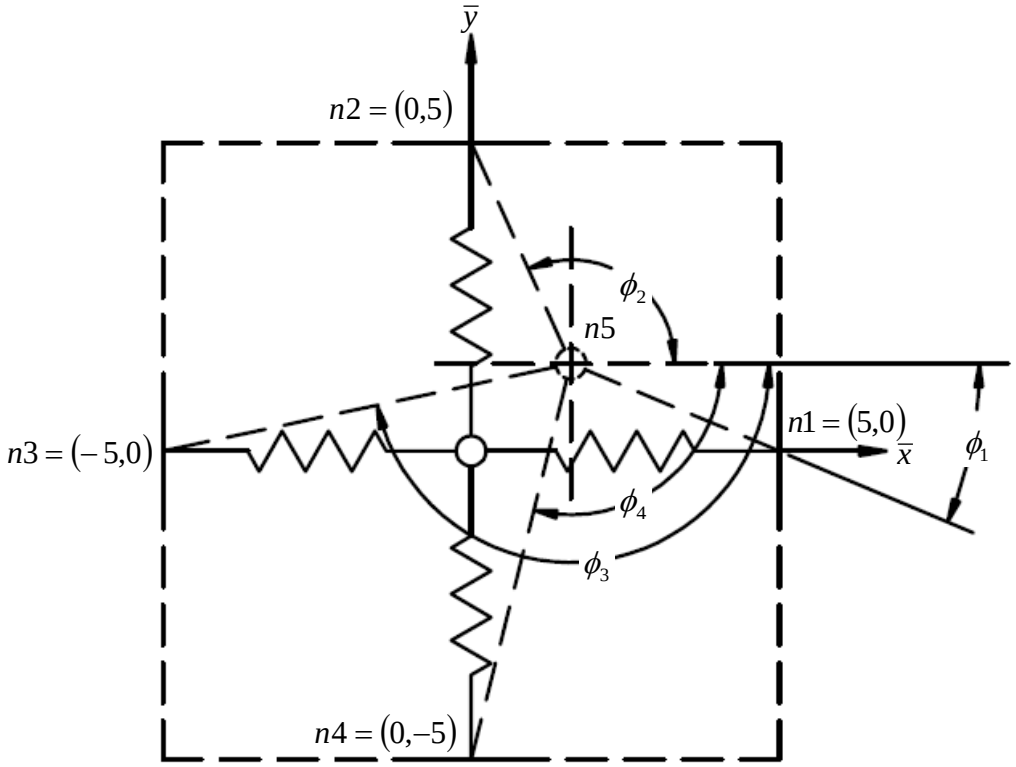

Figure 3.7: FEM Node Definitions for Multi-Linear Spring Support Model

Applying Equation 3.32 to each of the four springs produces the following global stiffness matrices for each spring element. The red lines cross out parts of the matrices where boundary conditions are applied, accounting for the fixed anchor nature of nodes 1-4.

Spring 1 Global Stiffness Matrix

$$\underline{k} = k_{11}\begin{bmatrix} C^2\phi_1 & C\phi_1 S\phi_1 & -C^2\phi_1 & -C\phi_1 S\phi_1 \\ C\phi_1 S\phi_1 & S^2\phi_1 & -C\phi_1 S\phi_1 & -S^2\phi_1 \\ & & C^2\phi_1 & C\phi_1 S\phi_1 \\ & \textit{Symmetry} & & S^2\phi_1 \end{bmatrix}\begin{Bmatrix} \bar{x}_5 \\ \bar{y}_5 \\ \bar{x}_1 \\ \bar{y}_1 \end{Bmatrix} \tag{3.33}$$

Spring 2 Global Stiffness Matrix

$$\underline{k} = k_{21}\begin{bmatrix} C^2\phi_2 & C\phi_2 S\phi_2 & -C^2\phi_2 & -C\phi_2 S\phi_2 \\ C\phi_2 S\phi_2 & S^2\phi_2 & -C\phi_2 S\phi_2 & -S^2\phi_2 \\ & & C^2\phi_2 & C\phi_2 S\phi_2 \\ & \textit{Symmetry} & & S^2\phi_2 \end{bmatrix}\begin{Bmatrix} \bar{x}_5 \\ \bar{y}_5 \\ \bar{x}_2 \\ \bar{y}_2 \end{Bmatrix} \tag{3.34}$$

Spring 3 Global Stiffness Matrix

$$\underline{k} = k_{31}\begin{bmatrix} C^2\phi_3 & C\phi_3 S\phi_3 & -C^2\phi_3 & -C\phi_3 S\phi_3 \\ C\phi_3 S\phi_3 & S^2\phi_3 & -C\phi_3 S\phi_3 & -S^2\phi_3 \\ & & C^2\phi_3 & C\phi_3 S\phi_3 \\ & \textit{Symmetry} & & S^2\phi_3 \end{bmatrix}\begin{Bmatrix} \bar{x}_5 \\ \bar{y}_5 \\ \bar{x}_3 \\ \bar{y}_3 \end{Bmatrix} \tag{3.35}$$

Spring 4 Global Stiffness Matrix

$$\underline{k} = k_{41}\begin{bmatrix} C^2\phi_4 & C\phi_4 S\phi_4 & -C^2\phi_4 & -C\phi_4 S\phi_4 \\ C\phi_4 S\phi_4 & S^2\phi_4 & -C\phi_4 S\phi_4 & -S^2\phi_4 \\ & & C^2\phi_4 & C\phi_4 S\phi_4 \\ & \textit{Symmetry} & & S^2\phi_4 \end{bmatrix}\begin{Bmatrix} \bar{x}_5 \\ \bar{y}_5 \\ \bar{x}_4 \\ \bar{y}_4 \end{Bmatrix} \tag{3.36}$$

These four matrices are added together for the total global stiffness matrix after boundary conditions have been applied. The resulting matrix is given by

(3.37)

$$[k] = \begin{bmatrix} k_{11}C^2\phi_1 + k_{21}C^2\phi_2 + k_{31}C^2\phi_3 + k_{41}C^2\phi_4 & k_{11}C\phi_1 S\phi_1 + k_{21}C\phi_2 S\phi_2 + k_{31}C\phi_3 S\phi_3 + k_{41}C\phi_4 S\phi_4 \\ k_{11}C\phi_1 S\phi_1 + k_{21}C\phi_2 S\phi_2 + k_{31}C\phi_3 S\phi_3 + k_{41}C\phi_4 S\phi_4 & k_{11}S^2\phi_1 + k_{21}S^2\phi_2 + k_{31}S^2\phi_3 + k_{41}S^2\phi_4 \end{bmatrix}$$

For a point mass positioned at node 5, the mass matrix is of the form

$$[m] = \begin{bmatrix} m & 0 \\ 0 & m \end{bmatrix} \tag{3.38}$$

The damping matrix is of the form

$$[c] = \begin{bmatrix} c_{11} & c_{12} \\ c_{21} & c_{22} \end{bmatrix} \tag{3.39}$$

The differential equations of motion are then obtained via the following formula

$$[m]\begin{Bmatrix}\ddot{x}\\ \ddot{y}\end{Bmatrix}+[c]\begin{Bmatrix}\dot{x}\\ \dot{y}\end{Bmatrix}+[k]\begin{Bmatrix}x\\ y\end{Bmatrix}=\begin{Bmatrix}f_x\\ f_y\end{Bmatrix} \tag{3.40}$$

In order to numerically integrate with MATLAB, the equations must be converted to state space form. This is accomplished by making the following definitions:

$$\{q\}=\begin{Bmatrix}x\\ y\\ \dot{x}\\ \dot{y}\end{Bmatrix} \qquad \{\dot{q}\}=\begin{Bmatrix}\dot{x}\\ \dot{y}\\ \ddot{x}\\ \ddot{y}\end{Bmatrix} \qquad \{u\}=\begin{Bmatrix}0\\ 0\\ f_x\\ f_y\end{Bmatrix} \quad [I]=\begin{bmatrix}1 & 0\\ 0 & 1\end{bmatrix} \quad [0]=\begin{bmatrix}0 & 0\\ 0 & 0\end{bmatrix} \tag{3.41}$$

From these definitions we can write

$$\begin{bmatrix}-[I] & [0]\\ [c] & [m]\end{bmatrix}\{\dot{q}\}+\begin{bmatrix}[0] & [I]\\ [k] & [0]\end{bmatrix}\{q\}=\{u\} \tag{3.42}$$

Solving for $\{\dot{q}\}$yields

$$\{\dot{q}\}=-\begin{bmatrix}-[I] & [0]\\ [c] & [m]\end{bmatrix}^{-1}\begin{bmatrix}[0] & [I]\\ [k] & [0]\end{bmatrix}\{q\}+\begin{bmatrix}-[I] & [0]\\ [c] & [m]\end{bmatrix}^{-1}\{u\} \tag{3.43}$$

This form of the equations is ready to be numerically integrated with the MATLAB *ode45* command. Recall the present state of the equations assumes the four springs are linear, and only geometric nonlinearities are taken into account. At this point in time, verification of the code was accomplished by comparing free vibration results to those obtained from the Newton's 2nd Law formulation. Significant discrepancies at early stages of simulations were found between the two methods. In Chapter 5, the Newton's 2nd Law formulation is verified and proven to match results from ANSYS, allowing one to assume that the FEM formulation developed here is indeed incorrect. Test cases with different initial conditions were conducted with the following system parameters: $K_1 = K_2$

= K_3 = K_4 = 125, m = 5, and $u\bar{L}_1 = u\bar{L}_2 = u\bar{L}_3 = u\bar{L}_4 = 5$. Results of two particular cases are shown in Figures 3.8 and 3.9 to demonstrate the error associated with the FEM formulation detailed in this section.

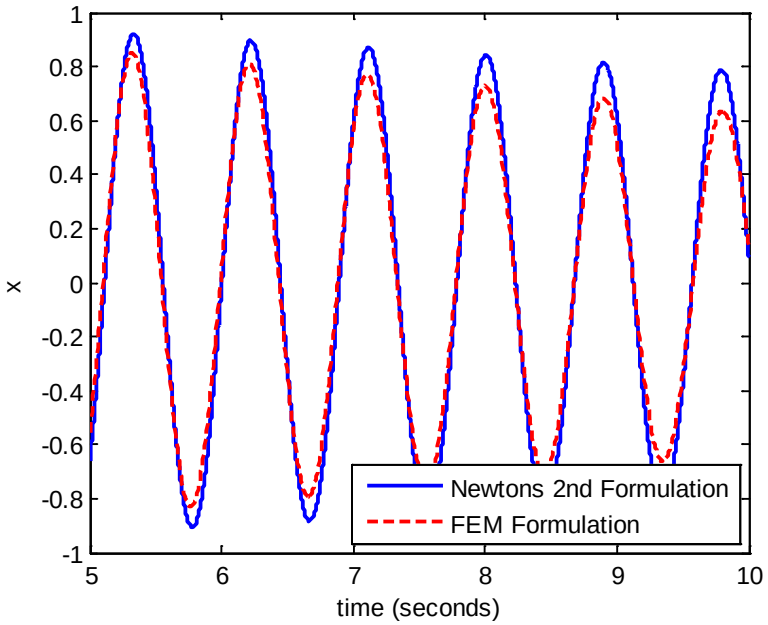

a)

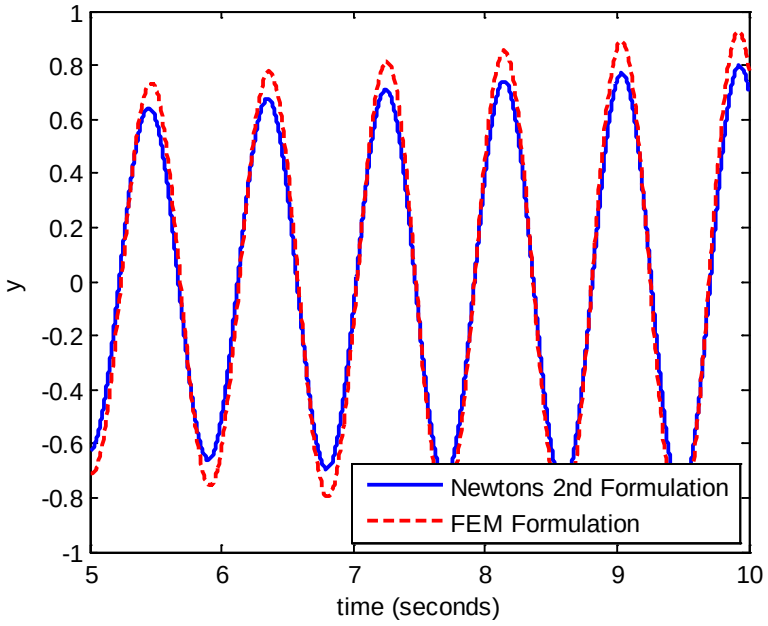

b)

Figure 3.8: FEM Formulation Validation Test Case 1, IC (1.0, 0.5), a) x time history, b) y time history

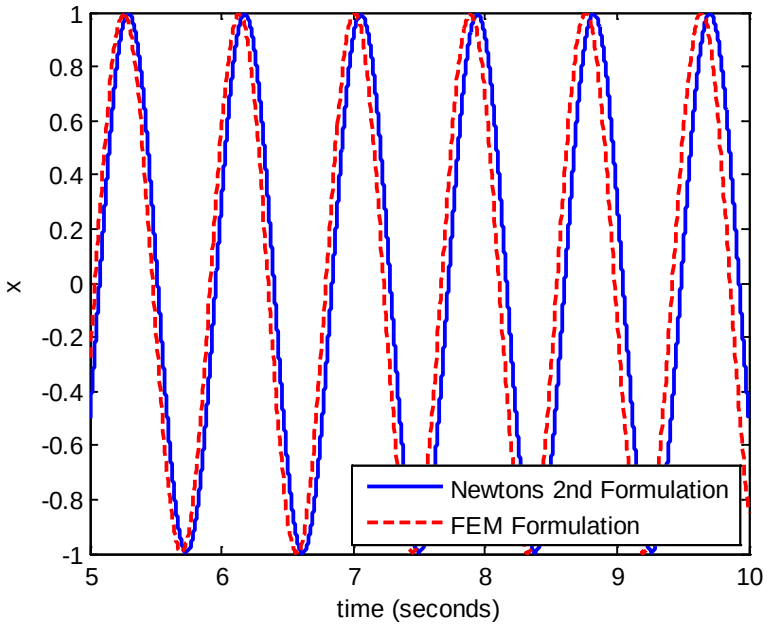

a)

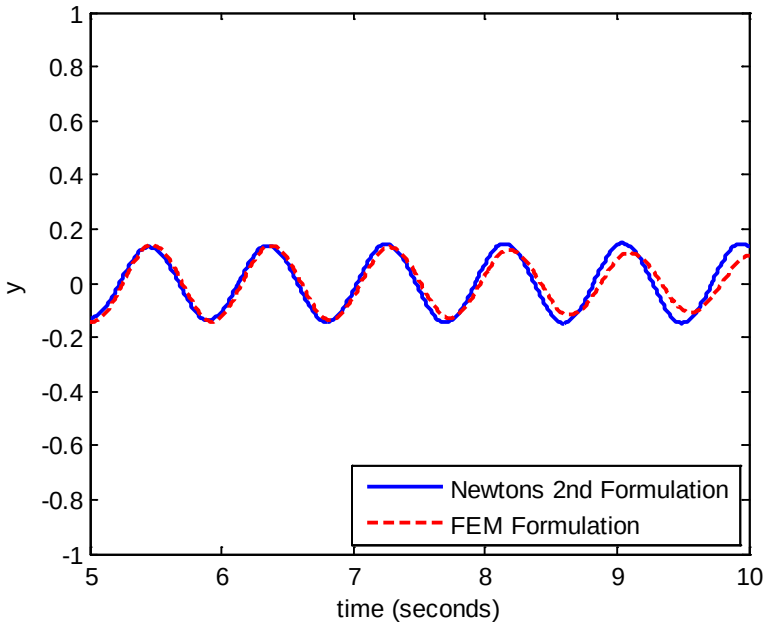

b)

Figure 3.9: FEM Formulation Validation Test Case 2, IC (1.0, 0.1), a) x time history, b) y time history

While qualitatively similar, the time histories reveal significant quantitative deviation at early stages of the simulation. These differences continue in magnitude for longer

simulations. These results motivated further analysis of the FEM formulation to determine the source of error. The answer is discovered by considering the simplified case given in Figure 3.10, where only Spring 3 remains in the model. System parameters are maintained from the previous test cases, that is, $K_3 = 125$, $m = 5$, and $u\bar{L}_3 = 5$.

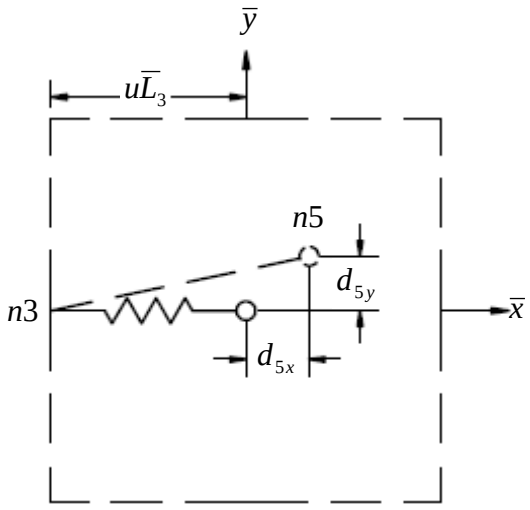

Figure 3.10: FEM Node Definitions for Simplified Linear Spring Support Model

Assume that a known displacement is imposed at node 5, such that $d_{5x} = 1$ and $d_{5y} = 0.5$. The static force in the spring is computed via

$$Spring\_Force = K_3 \times \left(\sqrt{\left(u\bar{L}_3 + d_{5x}\right)^2 + \left(d_{5y}\right)^2} - u\bar{L}_3 \right) \tag{3.44}$$

$$Spring\_Force = 125 \times \left(\sqrt{(5+1)^2 + (0.5)^2} - 5 \right) = 127.6 \tag{3.45}$$

Using the FEM formulation presented above, the force would be computed in the following manner.

$$\phi_3 = -\pi + a\tan\left(\frac{0-0.5}{-5-1}\right) = -3.058 rad \tag{3.46}$$

$$[k] = k_3 \begin{bmatrix} C^2\phi_3 & C\phi_3 S\phi_3 \\ C\phi_3 S\phi_3 & S^2\phi_3 \end{bmatrix} = \begin{bmatrix} 124.14 & 10.34 \\ 10.34 & 0.862 \end{bmatrix} \tag{3.47}$$

$$Spring\_Force = [k]\{d\} = \begin{bmatrix} 124.14 & 10.34 \\ 10.34 & 0.862 \end{bmatrix} \begin{Bmatrix} 1 \\ 0.5 \end{Bmatrix} = \begin{Bmatrix} 129.31 \\ 10.78 \end{Bmatrix} \tag{3.48}$$

$$Spring\_Force = \sqrt{129.31^2 + 10.78^2} = 129.8 \tag{3.49}$$

The two methods do not yield a consistent spring force value. It is worth noting that the force yielded by the FEM formulation would be correct if the total stretch in the spring was equal to the total displacement of node 5. However, this assumption is incorrect for any instance where the imposed displacement is not in line with the spring's initial orientation. Even if the imposed displacement at node 5 was such that it resulted in the correct force for Spring 3, adding the remaining spring supports would result in additional inaccuracies, as it is not possible to displace node 5 along the original orientation of all four springs at the same time. This revelation led to the decision to end pursuit of FEM formulated equations and to move forward with use of the Newton's 2nd Law formulation.

The Newton's 2nd law formulation will be used to study nonlinear dynamic behavior of the four-spring MBS support system in Chapter 5. Prior to that, a study of potential energy associated with various four-spring MBS systems is presented in Chapter 4.

Chapter 4: Potential Energy

4.1 Introduction

One unanswered question regarding MPWL support systems such as the AMS-02 strap system was whether or not it was possible to have multiple equilibrium states. The question is answered by looking for the possibility of multiple local potential energy minimums. Recall that the AMS-02 system consists of 16 PWL straps that are each ideally preloaded to a position just prior to the knee of their stiffness curves. Assuming all springs are perfectly identical in length and stiffness characteristics, one would accurately expect a single equilibrium state to be located in the center of the bounding space. However, statistical variations and manufacturing anomalies in the straps prevent the real world system from consisting of 16 truly identical PWL straps. Variations must be expected in upper and lower stiffness values, knee locations, and undeformed lengths of the springs. In some cases, it is possible for a preloaded spring to initially be past its stiffness knee.

The aim of this section is to explore potential energy curves that result when various system parameters are allowed to vary, as well as to explore the differences between the cut-to-length and preloaded model assumptions. In this chapter, the two-dimensional, two DOF MBS support system with four bilinear springs is the primary simulation model studied after an initial discussion of the PE for a single bilinear spring.

4.2 Deriving the Potential Energy Expression for a Single Bilinear Spring

The potential energy stored in a deformed linear spring can be found by integrating the restoring force with respect to the stretch in the spring

$$U = \int_0^{\bar{x}} kx' dx' = \frac{1}{2} k\bar{x}^2 \tag{4.1}$$

By definition, this value is the area under the force versus displacement curve when the spring is stretched by a value of $\bar{x}$.

The potential energy for an asymmetric bilinear spring with tension knee, s, and total stretch, $\bar{x}$, is found in the same manner

$$U = \begin{cases} \int_0^{\bar{x}} k_1 x' dx' = \frac{1}{2} k_1 \bar{x}^2, & \bar{x} \le s \\ \int_0^{s} (k_1 x') dx' + \int_s^{\bar{x}} \left(k_2 x' + (k_1 - k_2)s\right) dx' = \frac{1}{2} k_2 \bar{x}^2 + \frac{1}{2}(k_2 - k_1)s^2 + (k_1 - k_2)s\bar{x}, & \bar{x} > s \end{cases} \quad (4.2)$$

Making use of the bilinear spring stiffness ratio α, the scaled potential energy is given by

$$U_{scaled} = \begin{cases} \frac{1}{2}\bar{x}^2, & \bar{x} \le s \\ \frac{1}{2}\alpha\bar{x}^2 + \frac{1}{2}(\alpha - 1)s^2 + (1 - \alpha)s\bar{x}, & \bar{x} > s \end{cases} \quad (4.3)$$

where $U_{scaled} = U \big/ k_1$.

The scaled potential energy expression is piecewise continuous, just like the restoring force for a bilinear spring. The scaled PE curves consist of two distinct second order polynomials that meet at the knee of the bilinear spring. Figure 4.1 compares several scaled PE curves for different values of α.

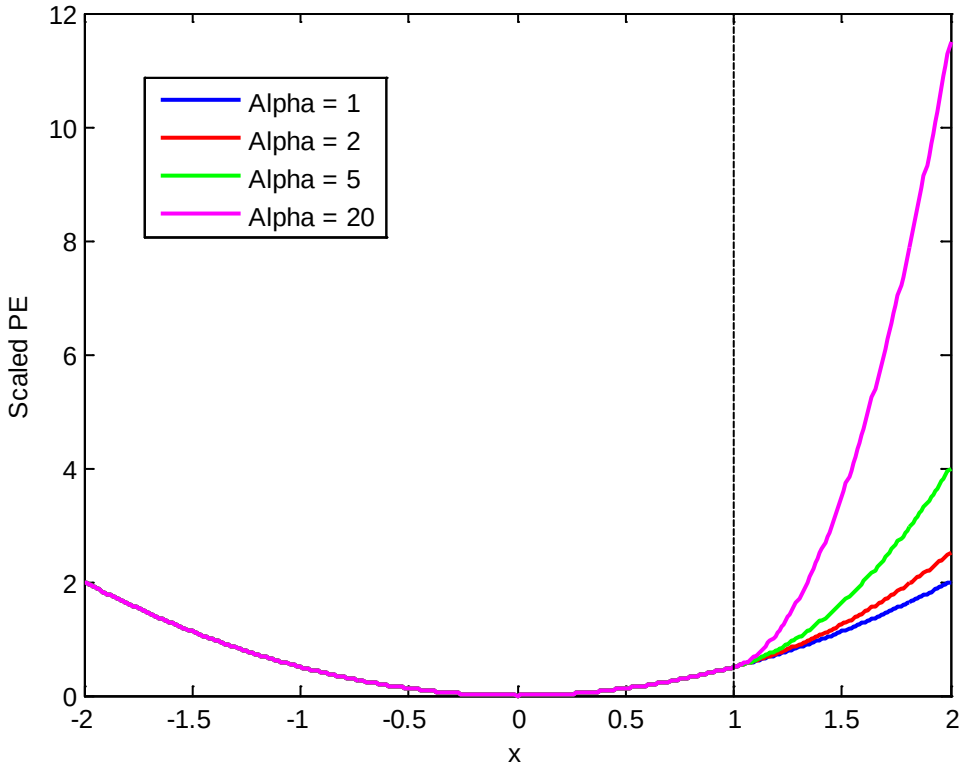

Figure 4.1: Single Bilinear Spring Scaled PE curves for various values of *α*

When α = 1, the scaled PE curve is a simple parabola. As α increases, the second derivative of the portion of Equation 4.3 for displacements past the knee, which is equal to α, also increases, which leads to the higher values of scaled PE past x = 1 seen in Figure 4.1. In all cases, the equilibrium position of the system corresponds to the minimum value of potential energy that occurs at the origin of the curves. This same concept of potential energy minimum and equilibrium extends to higher order systems and will be addressed in the discussion of energy plots for the MBS support system.

4.3 Scaled PE Study of MBS Support System

Equation 4.3 can be used to generate scaled PE plots for the four-spring MBS support system. The MBS system consists of fixed anchor points for each of the four bilinear springs. These anchor points define an overall bounding box for the system. The

potential energy plots are three-dimensional curves that show the total energy stored in all four springs if the mass were to be located at a particular x and y coordinate within the bounding space. Contour plots of the associated data reveal more information as to the shape of the energy curve and are included with each scaled PE surface plot. The total stretch in a particular spring, denoted by $\bar{x}$, is calculated from the coordinate location, the anchor point of the spring, and the undeformed length by

$$\bar{x}_{\#} = \sqrt{(x - x_{\#})^2 + (y - y_{\#})^2} - u\bar{L}_{\#} \tag{4.4}$$

For each (x,y) point in the region of interest, the stretch of Springs 1-4 is calculated, compared to the knee of each spring, and used to calculate the total potential energy of the system at that point. A typical scaled PE surface plot and associated contour for a four-spring MBS support system is featured in Figure 4.2. The MATLAB script used to calculate the scaled PE for the four-spring MBS is given in Appendix C.

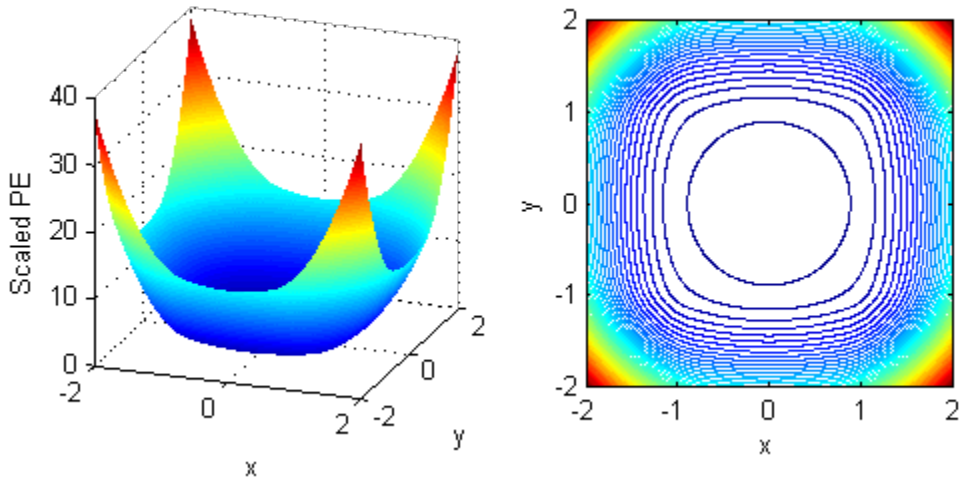

Figure 4.2: Scaled PE Surface and Contour Plots, $uL_1 = uL_2 = uL_3 = uL_4 = 5$, $s1 = 1$, $\sigma_2 = \sigma_3 = \sigma_4 = 1$, $\alpha_1 = \alpha_2 = \alpha_3 = \alpha_4 = 20$, $\beta_1 = \beta_2 = \beta_3 = \beta_4 = 1$

In this case, all of the springs are identical asymmetric bilinear springs that are assumed to be cut-to-length. The single equilibrium position, which corresponds to the minimum

scaled PE value of 0, is located at the origin of the two-dimensional plane. Identical spring definitions result in perfectly symmetric surface and contour plots.

Practically, the mass is not designed to move much beyond the knee of any given spring, as their intended purpose is to limit the motion of the supported mass. Thus in some cases, the energy study is focused on a smaller region of the overall bounding box dictated by the anchor points. The smaller region of focus is loosely chosen based on location of the knee-engagement curve. The knee-engagement curve is defined as the curve that bounds the region where all springs are below their corresponding knee. The curve is fully determinable and is a function of the undeformed lengths, knee locations, and anchor coordinates of each spring. The curve is determined by drawing a circle centered at each anchor point with a radius (undeformed length plus knee location) for the associated spring. This process is demonstrated in Figure 4.3 for symmetric springs.

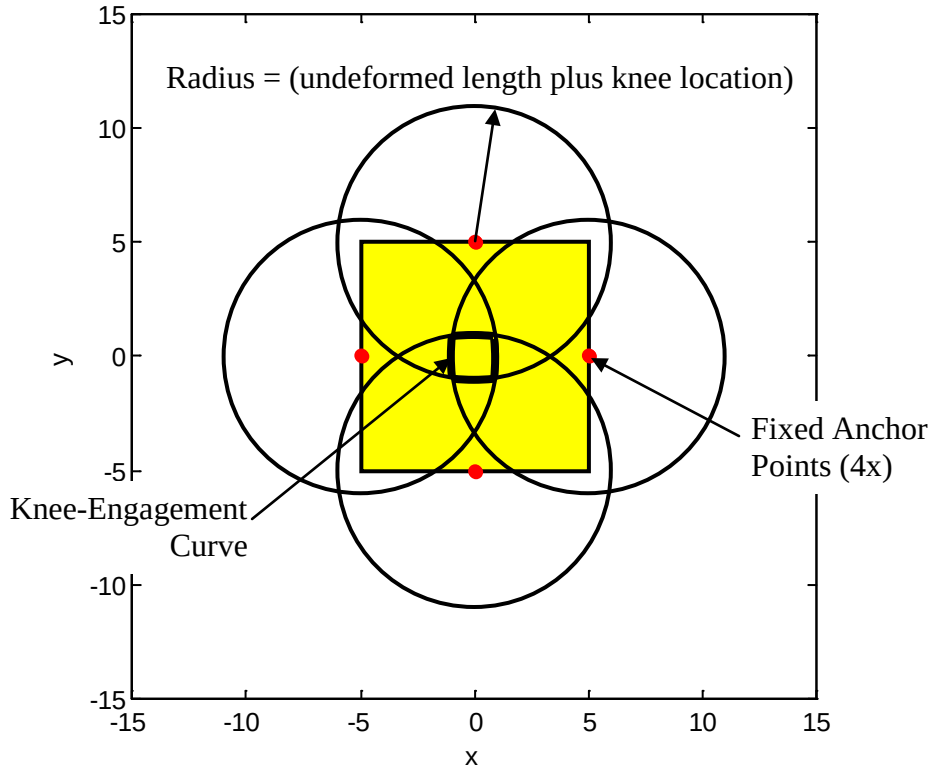

Figure 4.3: Determining the Knee-Engagement Curve

The red circles in Figure 4.3 represent the fixed anchor points of the four springs. The yellow shaded rectangle represents the global rectangular bounding box based on the fixed anchor points of the system. It is assumed that the mass will not move outside of the rectangular bounding box. The four black circles can be used to classify which springs are past their knee in various regions within the bounding box. The region contained in all four circles defines the knee-engagement curve. Figure 4.4 is a replot of Figure 4.3 with the axes adjusted to the rectangular bounding box.

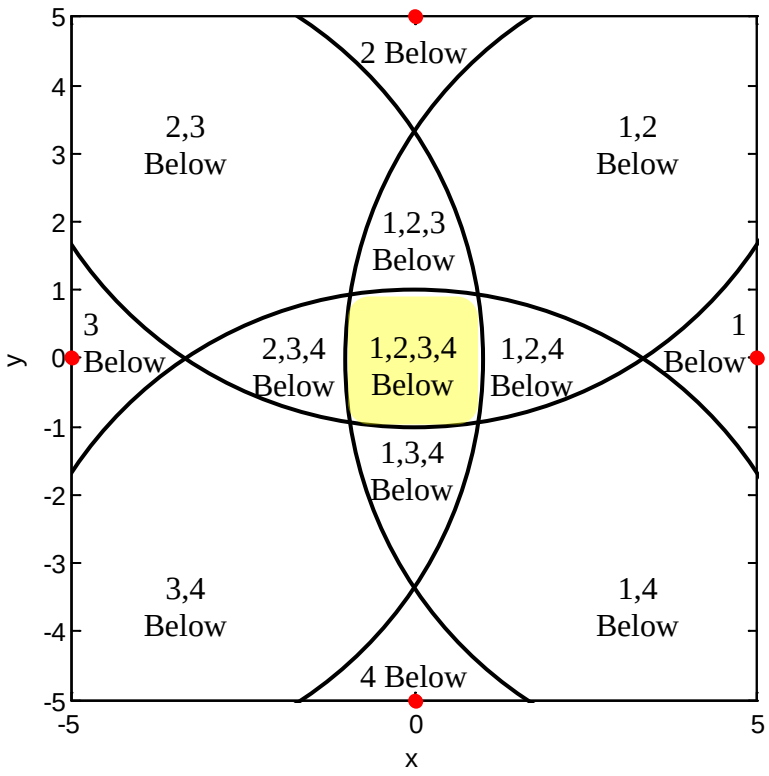

Figure 4.4: Classifying Knee Status of and Defining Knee-Engagement Curve

The plot contains labels that classify the knee status in each possible region. Spring numbers given in the region correspond to the springs which are not stretched past their knee in that zone. As previously mentioned, the knee-engagement curve bounds the region where all four springs are below their corresponding knee. By design, the mass is not intended to move very far outside of this curve, which motivates the decision to study

energy plots in a smaller space than that of the full bounding rectangle. Figure 4.5 demonstrates shifting the region of focus based on location of the knee-engagement curve on a scaled PE contour plot.

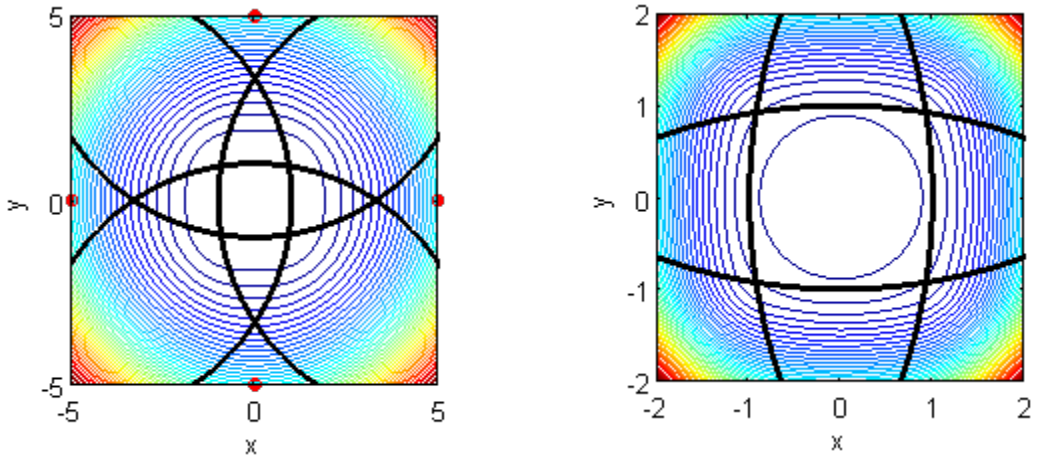

a) **b)**

Figure 4.5: Knee-Engagement Curve Overlapping Scaled PE Contour, a) Full Bounding Rectangle, b) Shifted Region of Focus

4.4 Cut-to-Length versus Preloaded Springs Assumptions

Most physical springs are not able to provide both tension and compression behavior relative to their undeformed state. The straps supporting the AMS-02 magnet, for example, offer no compressive resistance, and are preloaded to a position just prior to the knee of their force versus displacement curve. The straps always remain in tension during operation. Consultation with Jacobs Engineering team members responsible for designing and modeling AMS-02 straps led to the discovery that modeling this preloaded state was not directly possible in NASTRAN software used for their analysis. The elements used for defining straps did not allow for easy definition of a preloaded initial state. The work-around solution was to shift the origin of the element definition to the desired preloaded position and define the straps with no initial preload. This behavior is identical to creation of the asymmetric bilinear spring, as discussed in Chapter 3, by

shifting the origin of the asymmetric bilinear spring with no compressive resistance. In essence, the researchers shifted their preloaded model to a cut-to-length model. The validity of this approach is explored in this section through the study of scaled PE curves for both cases.

4.4.1 One-Dimensional Two Spring Support System

Initial studies of the preloaded versus cut-to-length configuration problem were conducted with a one-dimensional model including a mass and two bilinear springs supporting the mass. The general model for both cases is given in Figure 4.6.

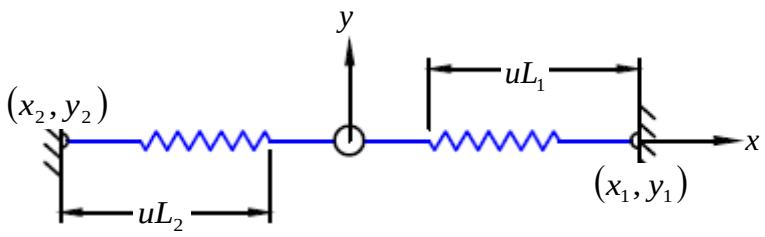

Figure 4.6: Two-Bilinear Spring In-Line Configuration

Case 1 represents the preloaded assumption. Case 1 is defined by the parameters given in Table 4.1. Case 2 represents the cut-to-length model, which is created from the preloaded model, and is similarly defined in Table 4.1. The key parameters to take note of are the undeformed lengths, uL_1 and uL_2, and the knee location, s_1. Both cases share common anchor points, but the knees are engaged at the same x coordinates relative to the fixed global coordinate system. This is accomplished by shifting the origin of the cut-to-length spring stiffness models, which results in a longer undeformed length and a knee location closer to the origin of the stiffness curve.

Figure 4.7 presents physical representations of the preloaded and cut-to-length assumptions. As previously stated, the undeformed lengths and knee locations are the key parameters which define the two models. The figure reveals how these two

parameters can be varied to yield the same knee engagement location in space for two different cases.

Table 4.1: Two Spring Preloaded vs. Cut-to-Length Parameter Definitions

Parameters	Case 1	Case 2
(x_1, y_1)	(5, 0)	(5, 0)
(x_2, y_2)	(-5, 0)	(-5, 0)
uL_1, uL_2	4.25	5
s_1	1	0.25
α1, α2	20	20
β2	1	1
σ2	1	1

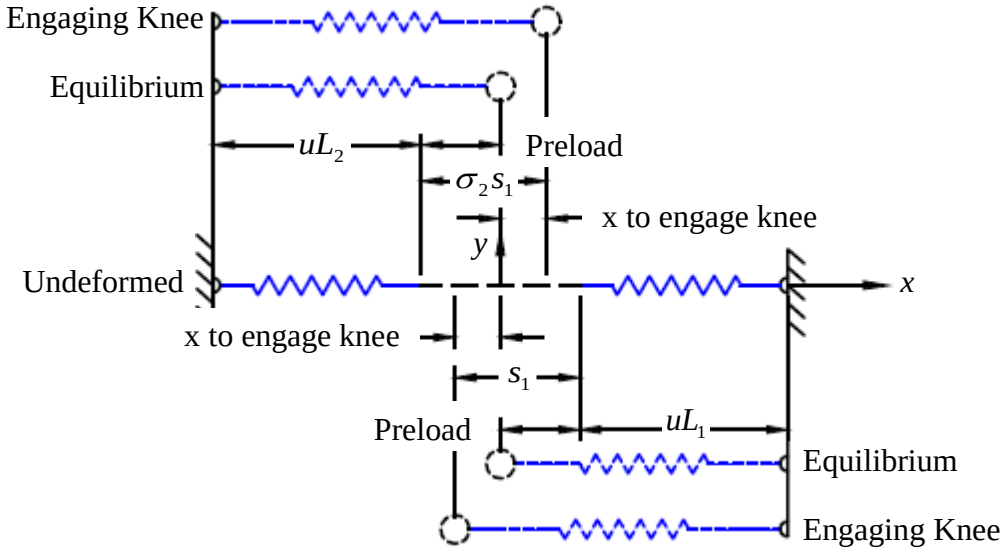

a)

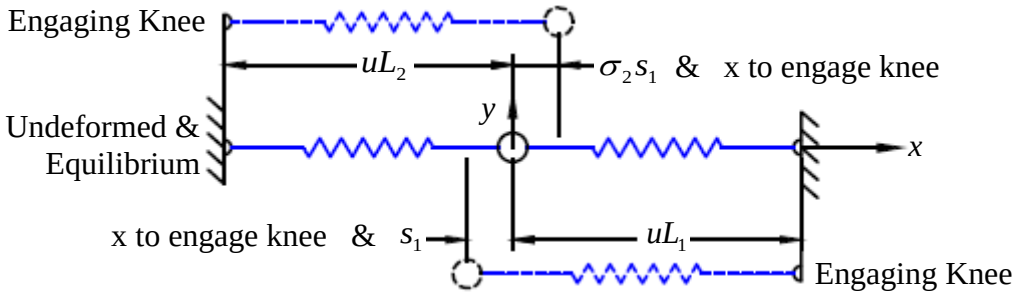

b)

Figure 4.7: Two-Bilinear Springs, a) Preloaded Configuration, b) Cut-to-Length Configuration

The scaled PE curves for Case 1 and Case 2 are both given in Figure 4.8 a). The plots reveal a high degree of qualitative similarity. A zero potential energy state is possible in the cut-to-length case, but not in the preloaded case, which is consistent with the underlying assumptions. However, the curves appear to be a simple translation of each other. Figure 4.8 b) plots Case 1 and Case 2 scaled PE curves on top of each other after shifting the minimum of the Case 1 curve to coincide with the Case 2 curve.

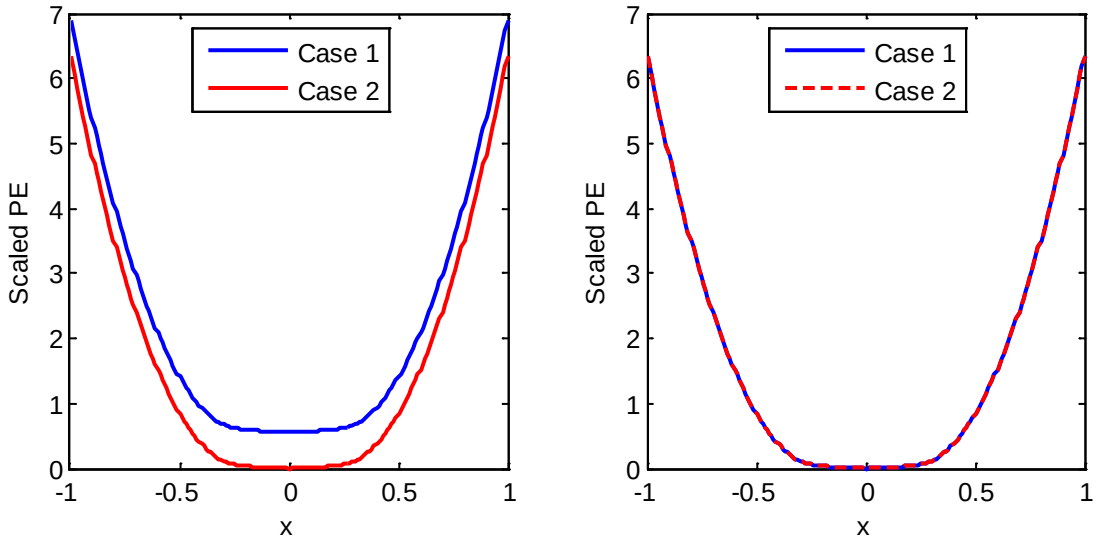

Figure 4.8: Scaled PE Curves for Two-Spring Model, a) Actual Curves, b) Shifted Curves with Coinciding Minimums

The curves overlap, suggesting they are perfect translations of each other. This fact is confirmed by calculating the potential energy at several points along the curve for each case and determining the shift between the curves at each point. Results of this study are given in Table 4.2.

Table 4.2: Calculating Translation between Two-Spring Preloaded and Cut-to-Length Configurations

Point of Interest	Scaled PE		
	Case 1	Case 2	Shift
-1	6.90625	6.34375	0.5625
-0.5	1.40625	0.84375	0.5625
0	0.5625	0	0.5625
0.5	1.40625	0.84375	0.5625
1	6.90625	6.34375	0.5625

Pure translation of the PE curves implies identical dynamic behavior. The concept is easily understood if one imagines a ball traversing the surface of the scaled PE curves, whereby a shift of the curve's height in space does not affect the resulting motion. For the case of one-dimensional two bilinear spring support systems, the cut-to-length model obtained by shifting the origin of the bilinear stiffness curves fully captures the dynamic response of the preloaded model.

4.4.2 Two-Dimensional Four-Spring Support System

Results of the one-dimensional two bilinear spring support system motivated further study of systems with additional DOF. The four-spring MBS support system introduced in Chapter 3 was used to compare the two-dimensional preloaded configuration (Case 1) versus cut-to-length configuration (Case 2). Each case is fully defined by the parameters given in Table 4.3.

Table 4.3: Four-Spring Preloaded vs. Cut-to-Length Parameter Definitions

Parameters	Case 1	Case 2
(x1, y1)	(5, 0)	(5, 0)
(x2, y2)	(0, 5)	(0, 5)
(x3, y3)	(-5, 0)	(-5, 0)
(x4, y4)	(0, -5)	(0, -5)
uL1, uL2, uL3, uL4	4.25	5
s1	1	0.25
α1, α2, α3, α4	20	20
β2, β3, β4	1	1
σ2, σ3, σ4	1	1

The scaled PE curves and associated contours for Case 1 and Case 2 are both shown in Figure 4.9.

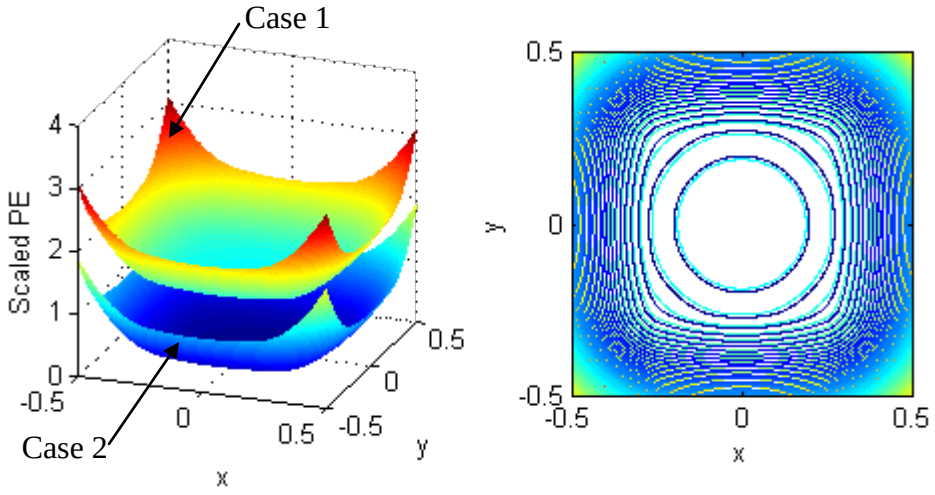

Figure 4.9: Scaled PE Curves and Associated Contours for Four-Spring MBS Model

The plots once again appear qualitatively very similar. The cut-to-length model (Case 2) has zero scaled PE at (0, 0), while the preloaded model (Case 1) has a finite value of scaled PE at (0, 0). Previously, this offset at the scaled PE minimum governed the translation value of the two curves. Figure 4.10 presents the surface plots for Case 1 and Case 2 on the same set of axes with Case 1 data shifted down so that the minimum value

coincides with the Case 2 minimum. Recall this implies that the curves are perfectly on top of each other at their global minimums.

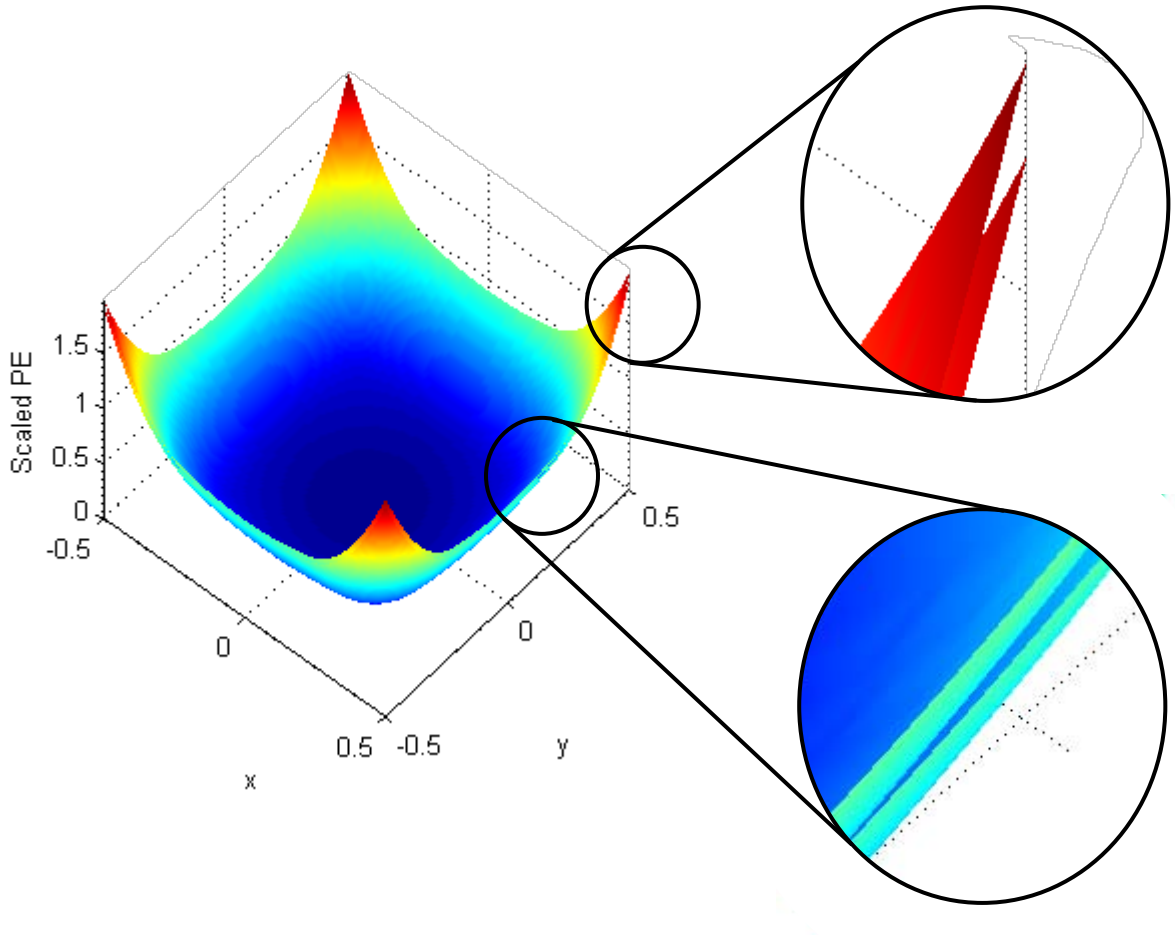

Figure 4.10: Shifted Scaled PE Curves and Associated Contours for Four-Spring MBS with Coinciding Minimums

Close inspection of the outer edges of the two curves plotted on top of each other reveals that scaled PE curves for Case 1 and Case 2 are not simply translations of each other as they were in the one-dimensional study. To quantify how large these differences are, the shift in scaled PE was calculated at a series of points for Case 1 and Case 2. The results of this study are given in Table 4.4.

Table 4.4: Calculating Translation between Four-Spring Preloaded and Cut-to-Length Configurations

	Scaled PE		
Point of Interest	**Case 1**	**Case 2**	**Shift**
(0, 0)	1.125	0.000	1.125
(0, 0.25)	1.197	0.063	1.134
(0, 0.5)	2.007	0.844	1.162
(0.25, 0.5)	2.110	0.938	1.172
(0.5, 0.5)	3.110	1.909	1.201

Rather than having a consistent translation at all points, the data implies that the deviation between scaled PE curves for the preloaded and cut-to-length models grows as you move further away from the scaled PE global minimum, contrary to the behavior seen in the two spring one-dimensional study. This behavior does not rely on the bilinear nature of the springs, and can be shown to occur because of the geometric nonlinearities present in the system by noting that the inconsistent translation discovered above occurs even if the four springs are assumed linear.

Fundamentally, different scaled PE curves imply different dynamic responses, suggesting that the work-around solution of shifting the origin of the bilinear stiffness curves to turn a preloaded configuration into a cut-to-length configuration does not perfectly capture the dynamics of the original problem for higher DOF systems, such as the AMS-02 support straps. This deviation was not originally anticipated, in light of the fact that the two scenarios have identical knee-engagement curves. Practically, the amount of deviation seen in the four-spring MBS cases, especially within the knee-engagement curve, is very slight. As a result, any deviation in the energy of the actual AMS-02 configuration and the cut-to-length model used for analysis may have proven

insignificant. However, in keeping with the real world motivation, the preloaded model will be used for all further study in this work.

4.5 Searching for Local Minimums in the Preloaded Four-Spring MBS Model

Returning to the question initially posed in this Chapter, this section explores whether or not local energy minimums that lead to multiple equilibrium positions can exist. Applying Newton's 2nd Law in each direction leads to two equations that can be solved for the two unknowns that mark the global PE minimum, but does not necessarily reveal if other local minimums have arisen due to variation in system parameters. A search for local scaled PE minimums was conducted with the four-spring MBS system by examining numerous cases with spring parameters randomly generated from specified statistical variations. The undeformed length of each spring, the bilinear spring stiffness ratio for each spring, the primary stiffness ratio for Springs 2-4, and the knee ratio for Springs 2-4 were all randomly chosen from pre-defined Gaussian distributions.

Table 4.5 contains the assumed nominal values and standard deviations associated with each parameter varied during the study. The standard deviations allow a 99.7% interval of confidence to be determined for each random parameter. Random numbers were always accepted except in cases where the undeformed length exceeded the distance between the origin and the corresponding anchor point. In other words, the cut-to-length assumption governed the upper limit for the undeformed length of each spring.

A total of 10,000 cases were run. In each case, the system parameters were randomly chosen from their Gaussian distribution and the total potential energy in the system was calculated via the methodology presented earlier in this chapter. Figure 4.11

displays the distribution of parameters used for Spring 2 definitions in the 10,000 cases. The Gaussian nature of the chosen parameters is easily discerned.

Table 4.5: Gaussian Distributions for Four-Spring MBS System Parameters

	Nominal	Standard Deviation		
(x_1, y_1)	(5, 0)	N/A		
(x_2, y_2)	(0, 5)	N/A		
(x_3, y_3)	(-5, 0)	N/A		
(x_4, y_4)	(0, -5)	N/A		
s_1	1	N/A	**99.7 % Range**	
uL_1, uL_2, uL_3, uL_4	4.25	0.2125	3.6125	4.8875
$\alpha_1, \alpha_2, \alpha_3, \alpha_4$	20	1.667	15	25
$\beta_2, \beta_3, \beta_4$	1	0.083	0.75	1.25
$\sigma_2, \sigma_3, \sigma_4$	1	0.083	0.75	1.25

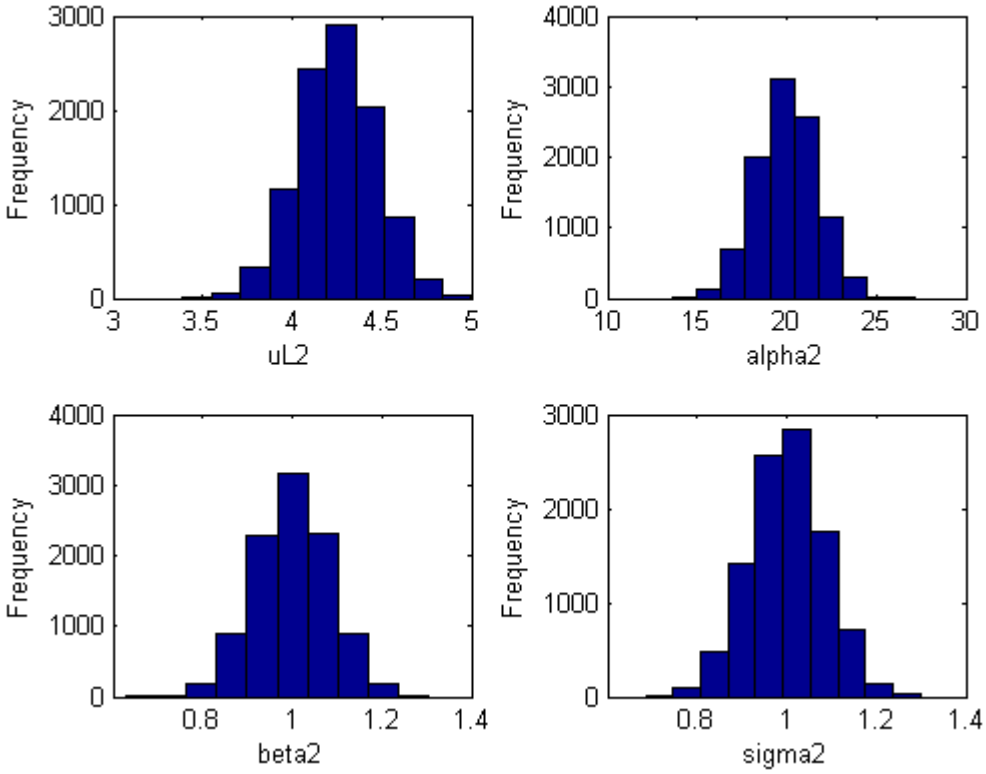

Figure 4.11: Histograms of Spring 2 Parameters Chosen from Gaussian Distributions

A MATLAB function developed by Carlos Adrián Vargas Aguilera at the University of Guadalajara [54] was used to locate any and all local minimums in the three-dimensional surface plot of scaled PE. In all 10,000 cases, only one local minimum was found and corresponded to the global minimum of the curve. This result suggests that multiple equilibrium positions are not possible in the four-spring MBS system. While it is believed the conclusion extends to higher dimensions, such as the full three-dimensional AMS-02 magnet strap support system, further investigation of that particular system would have to be completed to conclusively state multiple equilibrium positions are not a possibility.

The qualitative natures of the scaled potential energy surfaces were similar in all cases. The single potential energy minimum was located at the base of a general bowl-like shape for each case studied. Various examples of the scaled potential energy curves encountered in the study are presented in Figure 4.12 through 4.14. Tables 4.6, 4.7 and 4.8 contain the parameter definitions for the presented cases. The energy curves have different gradient values near their corresponding minimums, but globally they still fall under the bowl-like shape. The small blue "x's" in the contour plots mark the global minimum of the scaled PE curve.

Table 4.6: Parameter Definitions for Four-Spring MBS Energy Plot in Figure 4.12

Parameters	**Spring**			
	1	**2**	**3**	**4**
uL	4.262	3.963	4.390	3.992
α	22.454	17.971	19.565	18.054
β	N/A	0.997	1.080	0.962
σ	N/A	0.906	1.011	0.978

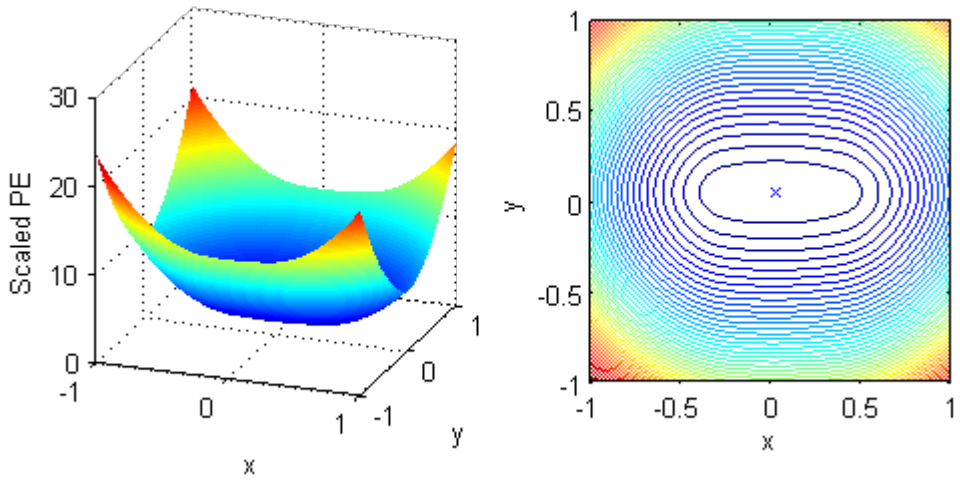

Figure 4.12: Four-Spring Scaled PE Example, Parameters Chosen from Gaussian Distributions (see Table 4.6)

Table 4.7: Parameter Definitions for Four-Spring MBS Energy Plots in Figure 4.13

Parameters	Spring			
	1	**2**	**3**	**4**
uL	4.448	4.299	4.564	4.235
α	17.801	20.019	18.350	21.897
β	N/A	0.946	0.943	0.962
σ	N/A	1.067	0.892	0.978

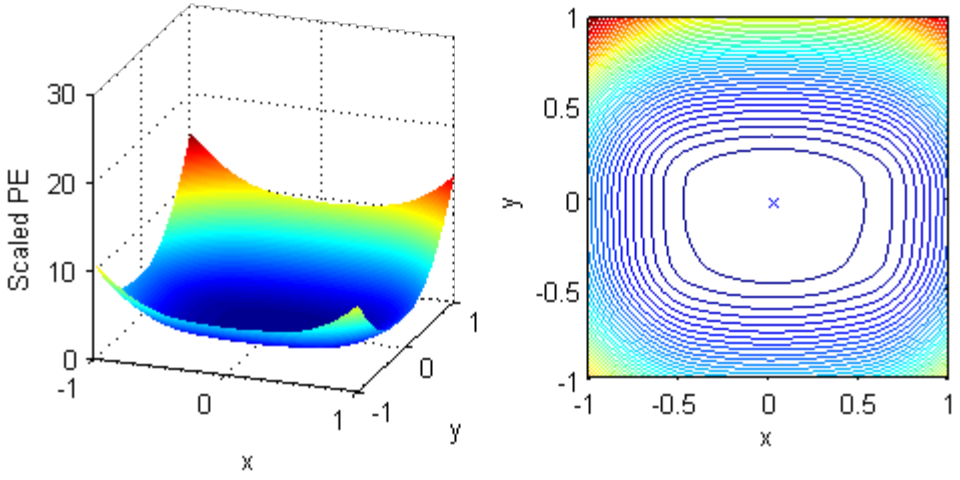

Figure 4.13: Four-Spring Scaled PE Example, Parameters Chosen from Gaussian Distributions (see Table 4.7)

Table 4.8: Parameter Definitions for Four-Spring MBS Energy Plots in Figure 4.14

Parameters	Spring			
	1	2	3	4
uL	4.071	4.299	4.070	4.124
α	19.449	20.830	19.589	19.800
β	N/A	1.124	1.055	0.995
σ	N/A	0.955	0.929	1.040

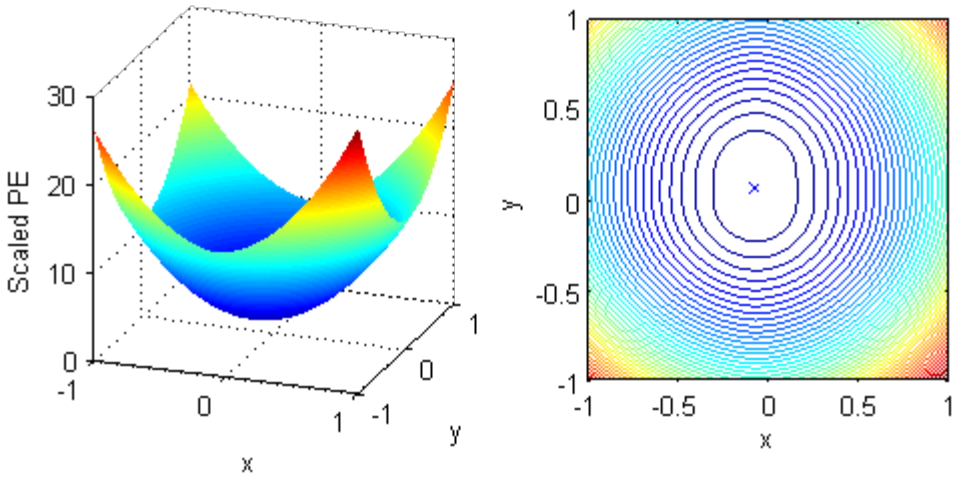

Figure 4.14: Four-Spring Scaled PE Example, Parameters Chosen from Gaussian Distributions (see Table 4.8)

The remaining cases had scaled PE curves that looked similar to those presented above with slight variations. Rather than provide exhaustive coverage of the types of bowl-like energy curves obtained, a study of the location of the global minimum is presented. The y-coordinates of the global minimum are plotted versus the x-coordinates of the global minimums in Figure 4.15.

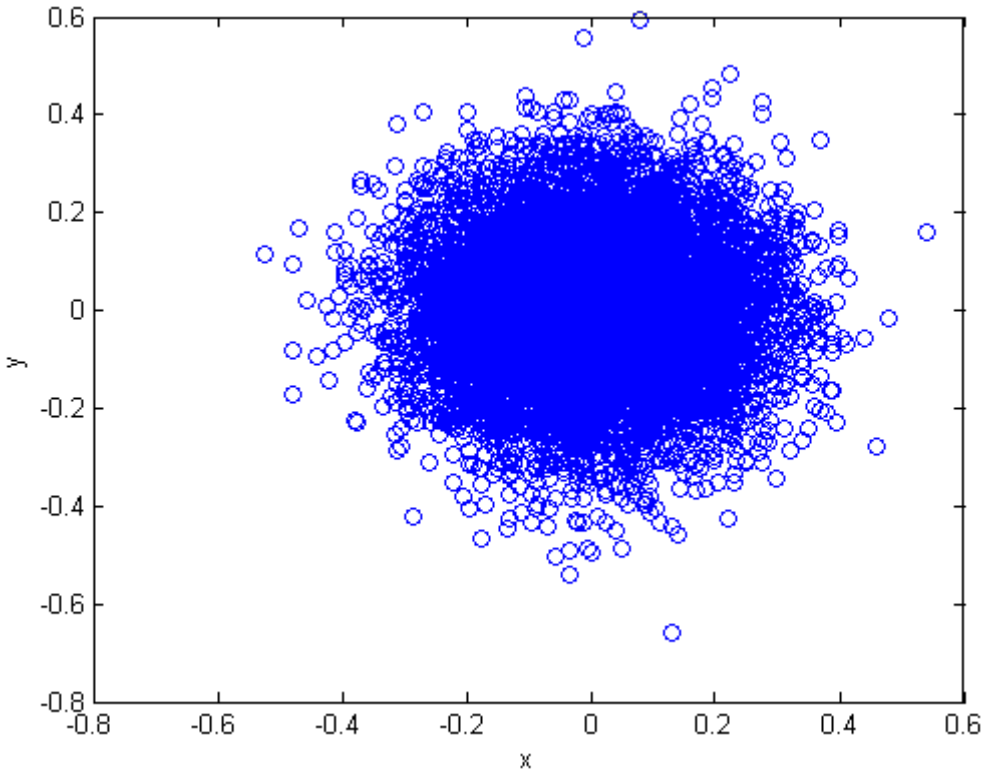

Figure 4.15: Coordinates of the Minimum in all 10,000 Scaled PE Study Cases

The figure reveals that the minimum of the scaled PE is still largely located near the origin of the system when parameters are chosen from their corresponding Gaussian distributions. A large portion of minimums have x and y-coordinates in the -0.4 to 0.4 range. The relative density of each minimum coordinate location is given by a three-dimensional histogram in Figure 4.16. This plot further reveals that the majority of cases had minimums at or extremely close to the origin. Thus, not only did all 10,000 cases feature a single equilibrium position, but the equilibrium locations in two-dimensional space for the were all very close together in light of the random variation in system parameters.

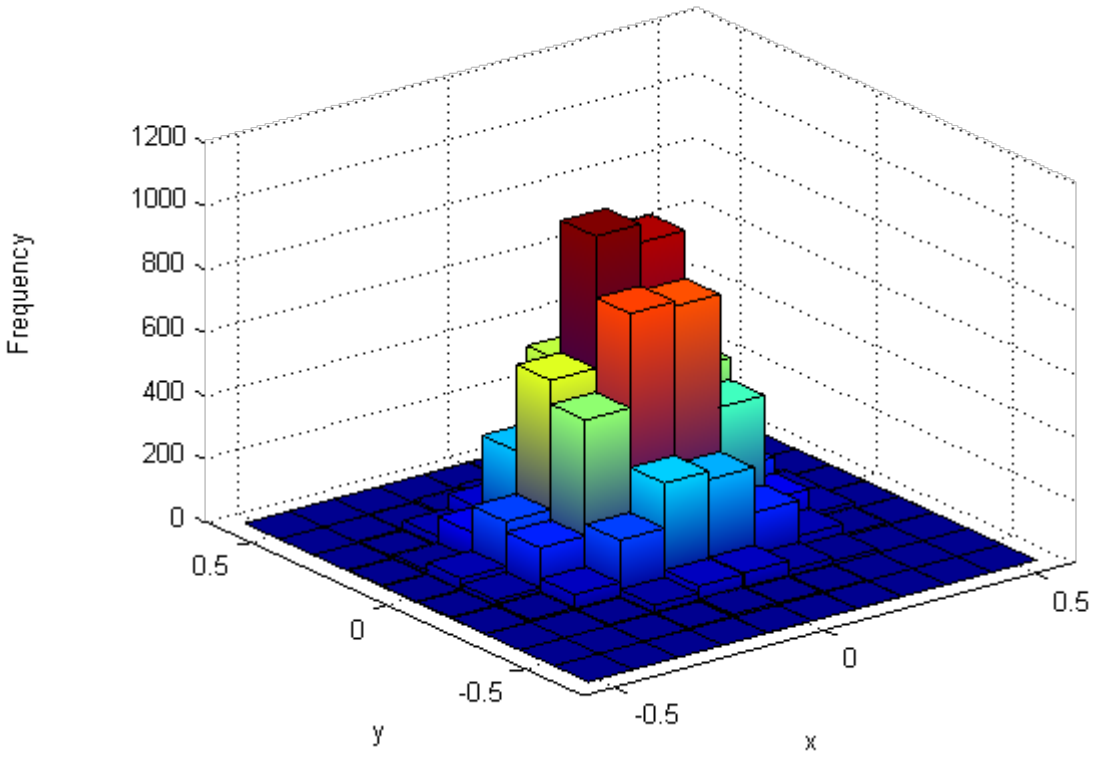

Figure 4.16: Three-Dimensional Histogram of Coordinates of the Global Minimum in all 10,000 Scaled PE Study Cases

4.6 Extreme Cases

Multiple equilibrium positions were determined not to exist in Section 4.5 when choosing parameters for the four-spring MBS system at random from Gaussian distributions. An additional question was whether scaled PE curves could take on shapes other than the general bowl-like configuration seen in Section 4.5. Practically, the answer is no when studying reasonable variation in springs which are designed to be similar in properties. This section presents the resulting scaled PE curves for two extreme cases that arise when the four springs are not nominally the same.

The first extreme case is that of one spring being extremely stiff in comparison to the others. In this case $\alpha_1 = \ldots = \alpha_4 = 20$, $\beta_2 = \beta_3 = 1$, $\sigma_2 = \ldots = \sigma_4 = 1$, and $\beta_4 = 50$, implying Spring 4 is fifty times stiffer than Springs 1 through 3. The scaled PE takes on

a horseshoe shape with a slight indention in the side of the curve seen in the plots of Figure 4.17.

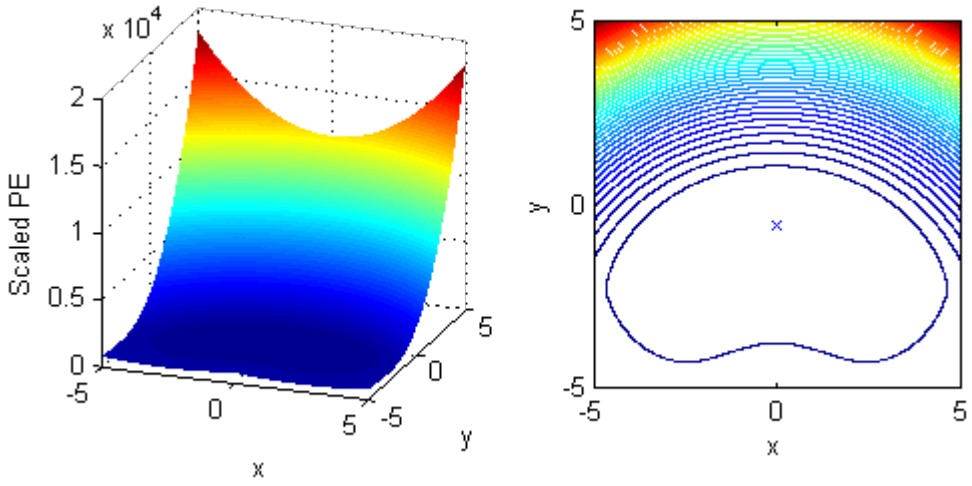

Figure 4.17: First Extreme Scaled PE Study Case

The scaled PE curve still only possesses a single local minimum in the presence of the horseshoe. Furthermore, the horseshoe is only seen when exploring regions of motion way outside of the knee-engagement curve, which contradicts the intended application whereby the knees prevent further motion in a particular direction. These facts, in addition to the impractical nature of having one spring fifty times stiffer than the rest, suggest that the horseshoe shaped curve is unlikely to be encountered in real applications.

Another extreme case is when one or multiple springs are missing and thus have zero stiffness. The second extreme case presented is missing Springs 2 and 3, implying Springs 1 and 4 are the only active support springs in the system. The associated energy plots are given in Figure 4.18. The two inactive springs result in one corner of the two-dimensional plane of motion having much lower scaled PE than the rest of the plane. However, just as previously encountered, there is only a single scaled PE minimum, denoted by the small "x" on the contour plot.

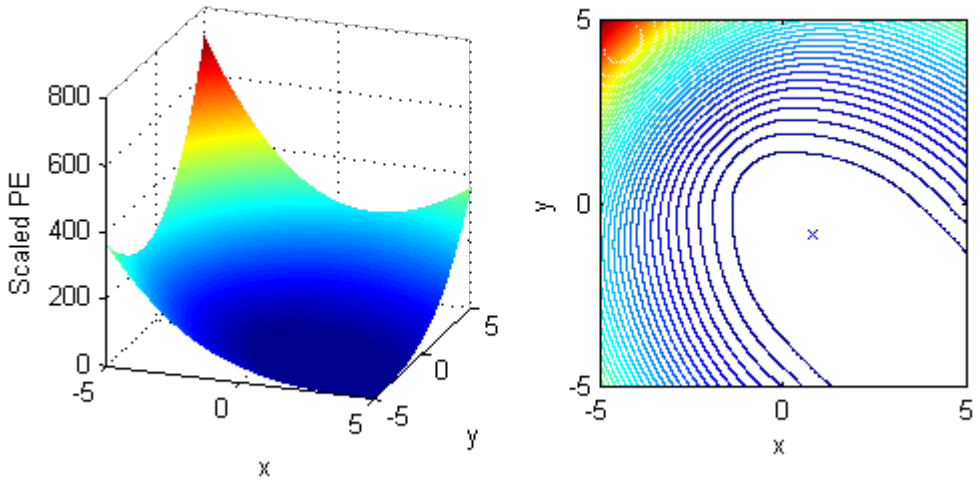

Figure 4.18: Second Extreme Scaled PE Study Case

This scenario is more plausible than the first extreme case. Springs may not intentionally be left out of the support system, but a malfunction or failure may lead to a similar situation.

The present chapter has resolved the differences between the preloaded and cut-to-length assumptions and found that the four-spring MBS system consists of a single equilibrium position in the form of a global PE minimum. The next chapter explores transient simulations of the four-spring MBS support system. Free and forced vibrations are considered, and the effects of the nonlinearities in the system are documented. Classic nonlinear behavior found in the single bilinear oscillator, and discussed in Chapter 2, is proven to exist in the four-spring MBS system.

Chapter 5: Dynamic Responses

5.1 Introduction

Numerical models developed in Chapter 3 can be used to simulate dynamic responses of the single bilinear oscillator and the four-spring MBS system. Free and forced responses reveal more information about how these nonlinear systems behave. The effect of a bilinear spring is first discussed in the single bilinear oscillator. Time histories and phase plane portraits provide a quick overview of nonlinear behavior, including subharmonic responses and bifurcations. Background knowledge obtained from studying the single bilinear oscillator lays the groundwork for studying the more complicated four-spring MBS system. This chapter also includes validation studies with ANSYS FEM software and a feasibility study of approximating bilinear stiffness curves with polynomials.

5.2 One-Dimensional Single DOF Bilinear Oscillator Transient Responses

In Chapter 3, the piecewise equation of motion for a single bilinear oscillator was developed. As previously discussed, the numerical integration scheme capable of switching between the two equations based on the active region of the stiffness curve is presented in Appendix A. This section provides a brief overview of the types of motion that arise in the single bilinear oscillator. Recall the equations were nondimensionalized such that the knee of the bilinear curve occurs at a dimensionless displacement of 1.

5.2.1 Single Bilinear Oscillator Free Response

The key parameter which defines the bilinear spring is the bilinear stiffness ratio, α. Figure 5.1 demonstrates the effect of increasing α in a given system's free response by

presenting the phase plane portrait and dimensionless time history for various values ranging from $\alpha = 1$ (linear oscillator) to $\alpha = 100$. In all cases, $A = \zeta = 0$.

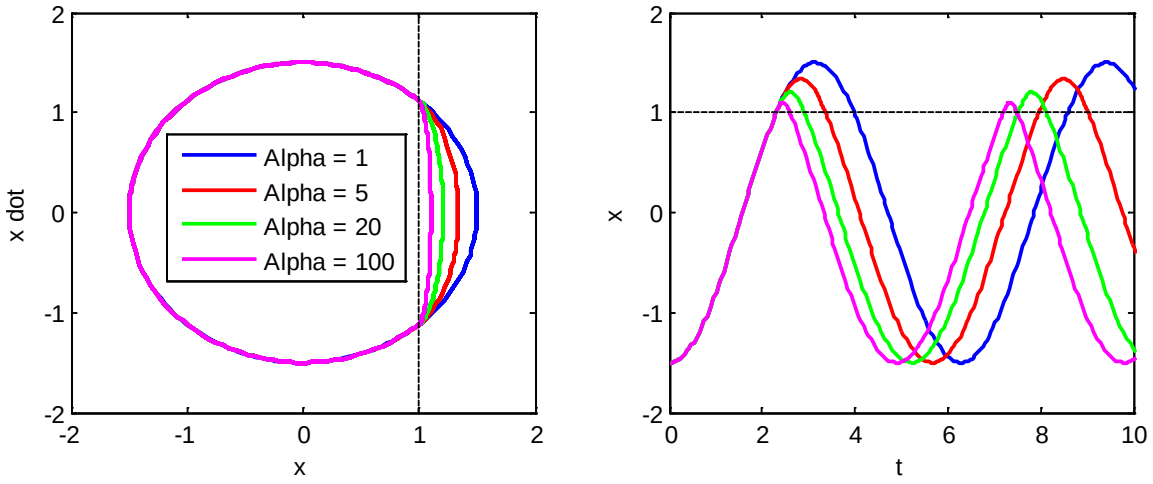

a) **b)**

Figure 5.1: Effect of Increasing α in Single Bilinear Oscillator Free Response, a) Phase Plane Portrait, b) Dimensionless Time History

When $\alpha = 1$, the system is equivalent to the simple mechanical oscillator, the phase plane portrait is a pure ellipse and the time history is a pure sine wave. As α increases, hitting the knee of the bilinear spring becomes more and more like hitting a wall. The limiting case of $\alpha = \infty$ is equivalent to a hard wall placed at the knee and is often referred to as an impact oscillator. It should be noted that as α increases, the natural frequency of the bilinear oscillator increases and the corresponding period decreases, as evident in the dimensionless time histories. This increase in response natural frequency implies that the system is sensitive to higher frequency forced disturbances for higher α.

5.2.2 Single Bilinear Oscillator Forced Response

The concept of subharmonic response can be demonstrated by adding harmonic forcing to the single bilinear oscillator. Figure 5.2 contains the dimensionless time history and phase plane portrait for a period-2 subharmonic response and is contrasted with a period-1 response in Figure 5.3. The forcing amplitude, frequency, and damping

ratio are given in the figure captions. Note that the only difference between the two systems is a slight increase in damping for the system in Figure 5.3 compared to that of Figure 5.2.

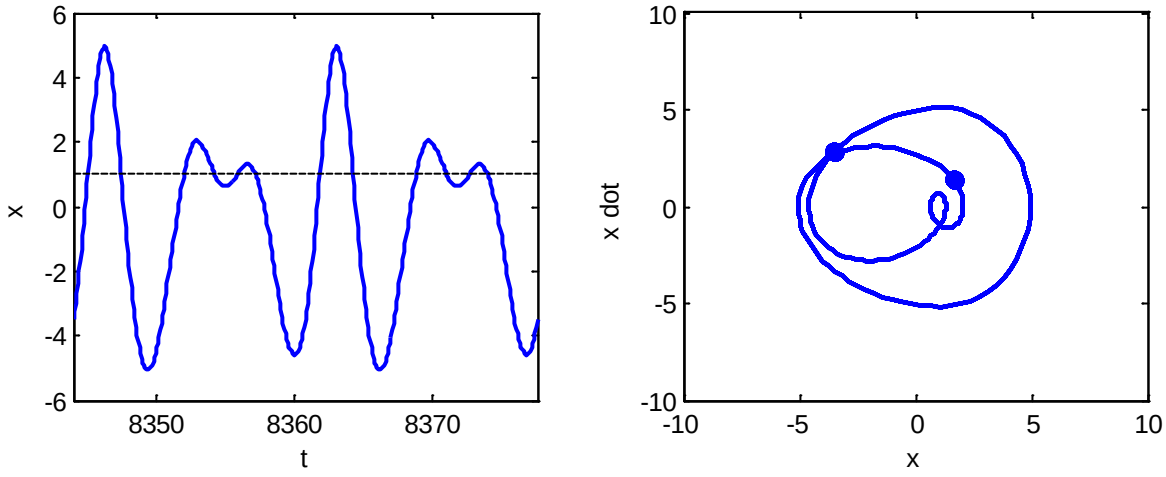

a) **b)**

Figure 5.2: Period-2 Response of Single Bilinear Oscillator (α = 2, ζ = 0.01, A = 2, ω = 0.75, IC = (0, 0))

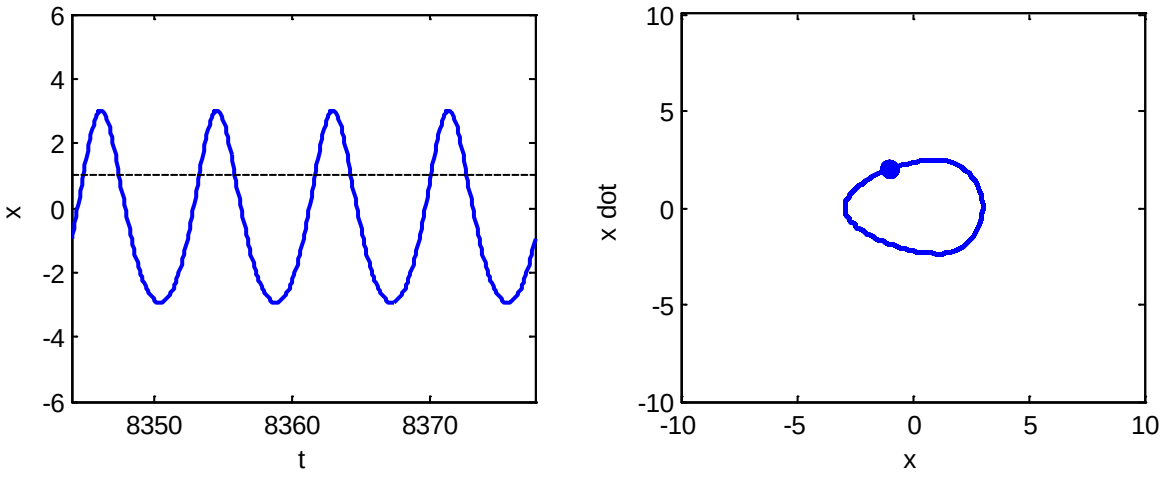

a) **b)**

Figure 5.3: Period-1 Response of Single Bilinear Oscillator (α = 2, ζ = 0.025, A = 2, ω = 0.75, IC = (0, 0))

The dots featured in the phase plane portraits correspond to sinusoidal forcing function cycles. When presented by themselves in the phase plane, these dots compose the

Poincaré map discussed in the definitions section of Chapter 2. The number of dots in the Poincaré map is directly correlated to the response type. One dot implies period-1, two dots imply period-2, and an infinite number of dots arranged in a strange attractor imply chaos. The dots of the Poincaré map can also be used to generate bifurcation diagrams.

Recall that a bifurcation fundamentally refers to a change in system response. These changes are frequently discovered by running numerous simulations with all parameters held constant but one. The bifurcation parameter is incrementally increased and the subsequent response is observed. A bifurcation found in the single bilinear oscillator from period-2 to period-1 motion is shown in Figure 5.4. The damping ratio ζ is used as the bifurcation parameter.

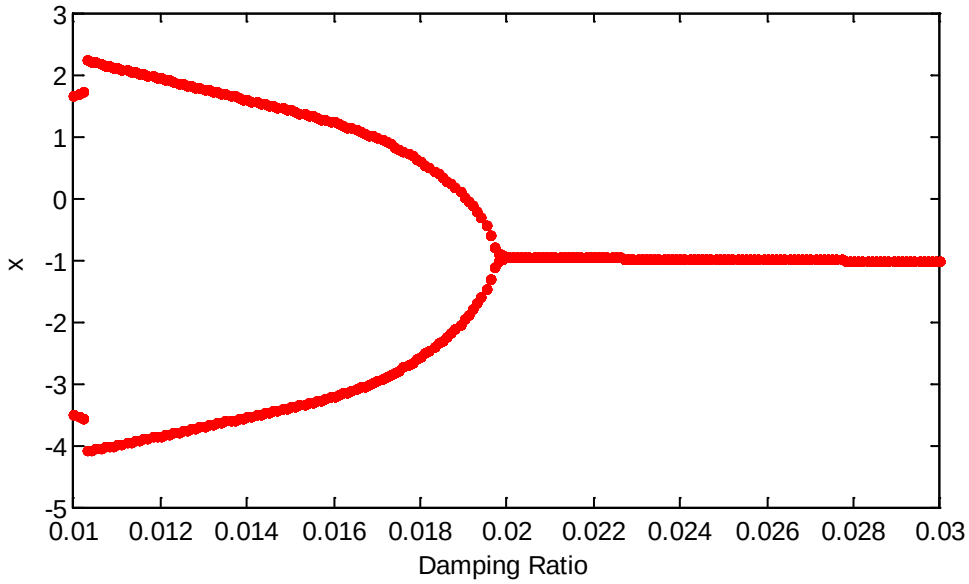

Figure 5.4: Single Bilinear Oscillator Bifurcation Diagram, ($\alpha = 2$, $A = 2$, $\omega = 0.75$, $\zeta = 0.01$ to 0.03)

The response type switches from period-2 to period-1 approximately at $\zeta = 0.02$. Slicing the bifurcation diagram at a particular value of the bifurcation parameter and counting the

dots yields the same information as counting dots on the Poincaré map. In fact, the x coordinate of the dots found in the phase plane portraits of Figures 5.1 and 5.2 correspond to the dots found in the bifurcation diagram at the respective damping ratios.

5.3 Four-Spring MBS Support System Transient Responses

The equations of motion for the two-dimensional four-spring MBS support system were derived in Chapter 3. The equations are piecewise, consisting of 16 possible differential equation sets depending on the active region of each spring's stiffness curve. Appendix B contains the MATLAB script used to numerically integrate and switch the active differential equation set employing the *ode45* event detection capabilities. The script can handle both free and forced response in the form of harmonic forcing. Additional forcing profiles could easily be implemented into the code, but are not studied in this work.

5.3.1 Four-Spring MBS Free Response

The geometric and bilinear nonlinearities present in the four-spring MBS system have two distinct effects on the free vibration response. Geometric nonlinearities arise due to large amplitude motion of the mass. The x and y components of each spring's force on the mass change as the angle of orientation changes with respect to the global x and y axes. Mathematically, the two differential equations of motion are coupled, whereby changes in the x coordinate affect the equation governing y motion, and vice versa. Physically, this leads to interaction of the underlying small motion x and y modes of vibration.

This phenomenon is demonstrated in the free response by setting the bilinear stiffness ratio, α, equal to one for each spring and providing reasonably large initial

conditions. Setting the bilinear stiffness ratio to one nullifies the effect of the bilinear spring, which results in linear springs, implying only geometric nonlinearities are present. The results are given in Figure 5.5.

Unless otherwise noted, the anchor points for all MBS simulations in this chapter are assumed equal to the values given in Table 5.1. Changing the location of anchor points was found to affect the dynamic response, particularly by altering the magnitude of the geometric nonlinearities. However, this notion is not explored further in this work but is noted as a potential area for future study.

Table 5.1: Fixed Anchor Points used for Four-Spring MBS Simulations

(x_1, y_1)	(5, 0)
(x_2, y_2)	(0, 5)
(x_3, y_3)	(-5, 0)
(x_4, y_4)	(0, -5)

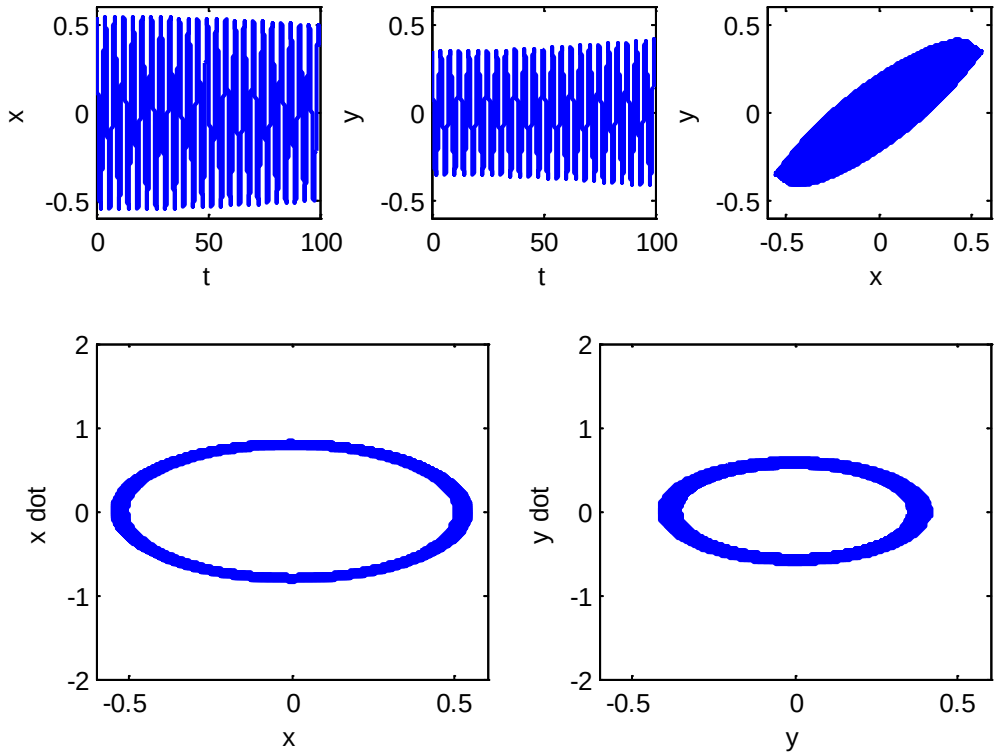

Figure 5.5: Free Vibration Demonstrating Effect of Geometric Nonlinearities, uL_1 = uL_2 = uL_3 = uL_4 = 4.25, α_1 = α_2 = α_3 = α_4 = 1, β_2 = β_3 = β_4 = 1, σ_2 = σ_3 = σ_4 = 1, IC = (0.55, 0.35, 0, 0)

The interaction between the two modes is seen in the dimensionless time histories, given in the upper left hand corner of Figure 5.5, through fluctuation in oscillation amplitude. The amplitude of oscillation in the x-direction gradually decreases as the amplitude of y-direction oscillation increase. Given different initial conditions in the x and y directions, the amplitude of oscillation in the x direction will eventually fluctuate from its starting value to the y direction starting value, and vice versa. The two-dimensional plane of motion, given in the upper right hand corner, and the phase plane portraits for each direction, given on the bottom row, also reflect the fluctuation in response amplitude. If the two initial conditions are identical, there is no interaction. This is seen in Figure 5.6. The motion trajectories in the x and y directions are identical, with no fluctuation in behavior between the two.

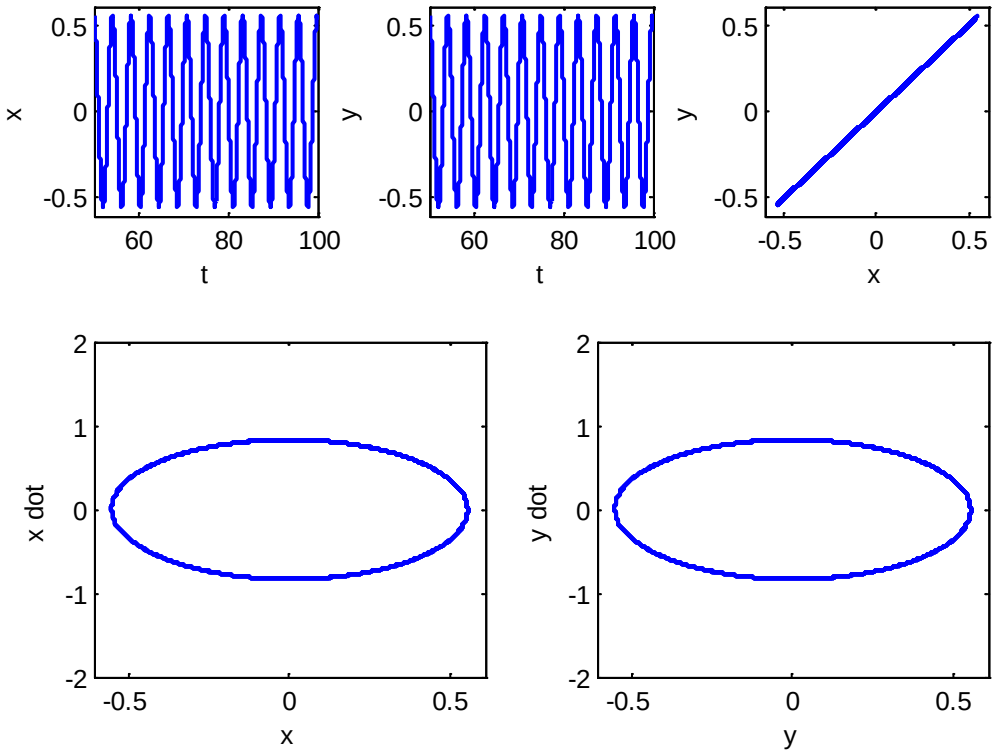

Figure 5.6: Free Vibration Demonstrating Effect of Geometric Nonlinearities, uL_1 = uL_2 = uL_3 = uL_4 = 4.25, α_1 = α_2 = α_3 = α_4 = 1, β_2 = β_3 = β_4 = 1, σ_2 = σ_3 = σ_4 = 1, IC = (0.55, 0.55, 0, 0)

The bilinear stiffness models of each spring in the MBS system effect the free vibration in a manner similar to the single bilinear oscillator. Previously with the single bilinear oscillator there was a single location in space where a knee was engaged. The four-spring MBS has four different knees that can be engaged independently at various locations in accordance with the knee-engagement curve discussed in Chapter 4. The simulation parameters used to generate Figures 5.7 and 5.8 are identical to those used in Figures 5.5 and 5.6, respectively, with the exception of the bilinear stiffness ratio, which now has a value greater than unity. Both figures demonstrate that the knees present in the system give the phase plane portraits rectangular shapes as opposed to the pure elliptical phase plane portraits seen when using linear springs. Changing the value of α for each spring changes how drastic the linear spring elliptical shape is altered, as previously noted with the single bilinear oscillator free response.

When the initial x and y-coordinates are different, as is the case in Figure 5.7, the interaction of the underlying modes of vibration is not as strong as that seen with linear springs. The amplitude of oscillation in the x and y-directions no longer fluctuates from one initial condition to the other. The fluctuation is much smaller and happens on a different time scale, suggesting the bilinearity negates some of the effect of the geometric nonlinearity. Furthermore, a much greater range is seen in the two-dimensional plane of motion. This behavior was seen in systems with various parameter definitions, but further study is required to fully understand the interaction between the bilinearity and the geometric nonlinearities in MBS support systems.

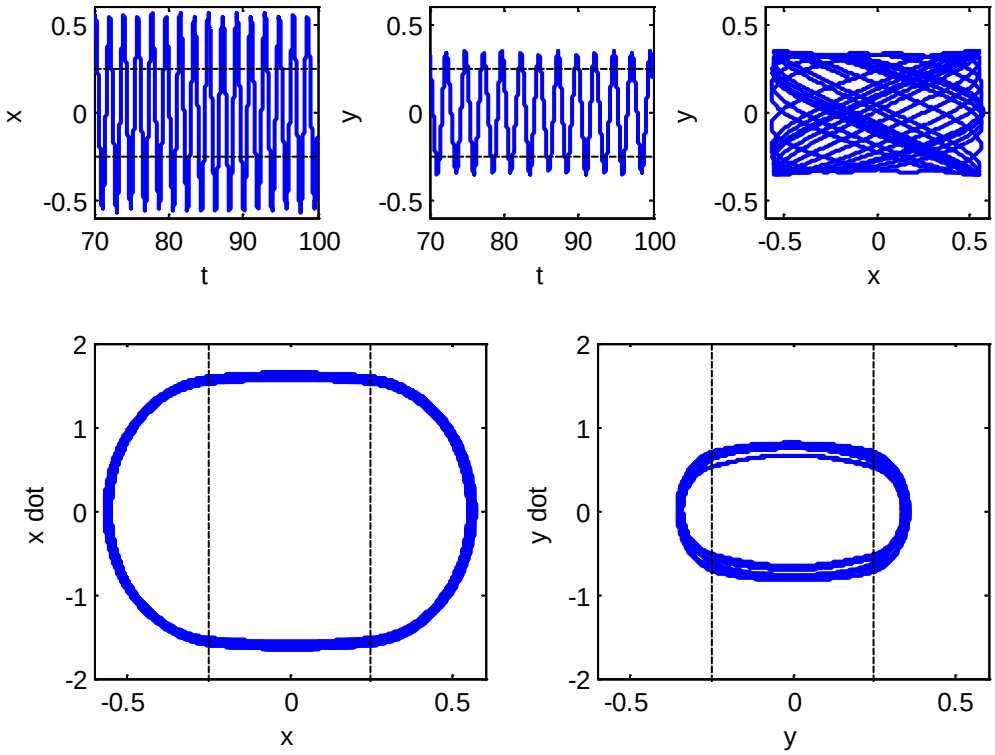

Figure 5.7: Free Vibration with Bilinear Springs, $uL_1 = uL_2 = uL_3 = uL_4 = 4.25$, $\alpha_1 = \alpha_2 = \alpha_3 = \alpha_4 = 20$, $\beta_2 = \beta_3 = \beta_4 = 1$, $\sigma_2 = \sigma_3 = \sigma_4 = 1$, IC = (0.55, 0.35, 0, 0)

When the initial conditions in the x and y-directions are identical, the MATLAB script does not yield the correct response with α greater than unity. It appears as though the bilinear nature of the support springs leads to fluctuations in the oscillation amplitude in both directions, as seen in Figure 5.8. This behavior is contrary to the linear spring equivalent, whereby identical initial conditions correctly resulted in no fluctuation of amplitude. The discrepancy is a direct result of issues associated with the MATLAB ode45 event detection function used to locate knees in space and time. The default event detection function is capable of handling simultaneous events, as is required by the case of identical initial conditions. However, when repeatedly detecting events and resuming integration, an apparent glitch in the default algorithm causes issues when a change in the number of events occurs from one stop to the next. In other words, if at some point in a

given simulation two events were detected simultaneously and at the next stopping point only one event was detected, there may be an issue. Due to numerical error, theoretically simultaneous events will not always be detected as such, implying this problem will inevitably be encountered in certain situations.

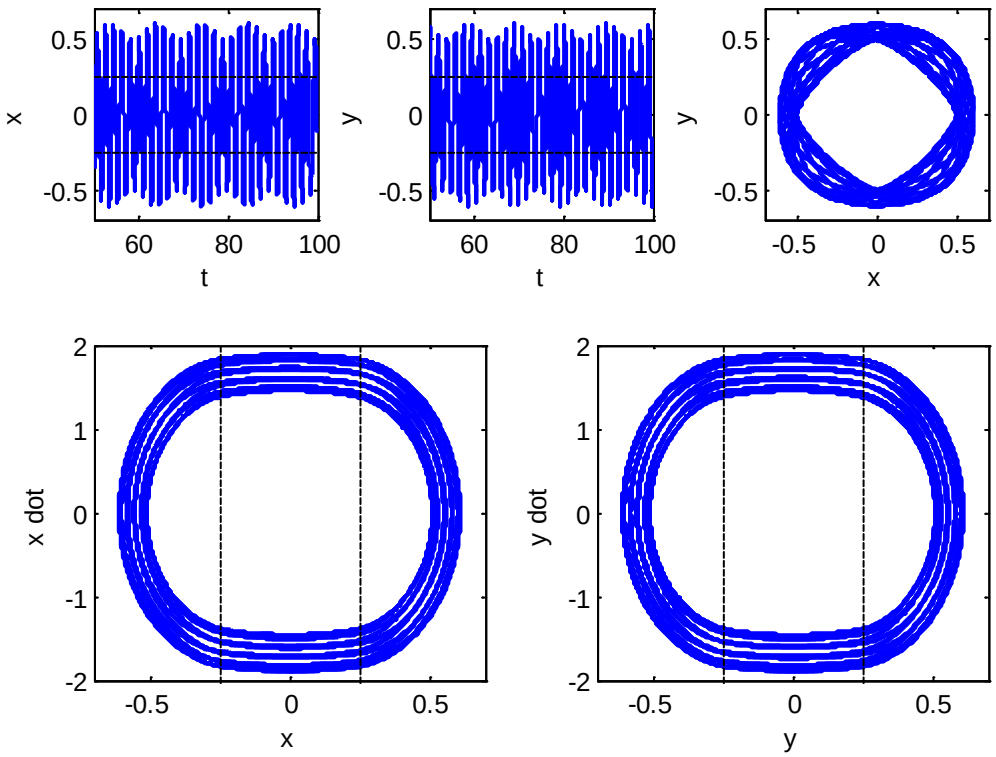

Figure 5.8: Free Vibration with Bilinear Springs, $uL_1 = uL_2 = uL_3 = uL_4 = 4.25$, $\alpha_1 = \alpha_2 = \alpha_3 = \alpha_4 = 20$, $\beta_2 = \beta_3 = \beta_4 = 1$, $\sigma_2 = \sigma_3 = \sigma_4 = 1$, IC = (0.55, 0.55, 0, 0)

Resolution of this issue was sought through modifying the associated default MATLAB scripts and through contact with MathWorks employees. A formal solution was not found at the time of this writing, which led to the following work-around solution. When identical initial conditions are desired, a very small discrepancy must be included between the numbers, forcing what normally would be simultaneous events to be separated by extremely small differences in space and time. This methodology works fine if the springs are assumed linear. The plots in Figure 5.6 were generated with this

approach and properly demonstrate zero interaction between the underlying modes of vibration.

The methodology does not work successfully once the bilinear nature of the springs is introduced. A perfectly symmetric support system with identical x and y initial conditions should display zero interaction regardless of the spring stiffness model. The slight discrepancy in initial conditions, once paired with the bilinear stiffness models, results in enough deviation to alter the correct response. Fortunately, the scope of this issue is limited to simulations requiring repeated simultaneous occurrence of events. In most cases this behavior is not required, but does limit the scope of studies possible in both free and forced vibrations. In the next section, free vibration results obtained from MATLAB are verified with ANSYS nonlinear transient simulation results, providing confidence in MATLAB simulations that avoid this issue.

5.3.2 Modeling MBS Support Systems with ANSYS

MBS support systems may also be simulated in the popular finite element software package ANSYS by defining physical systems with predefined elements. The principle of superposition is used to generate global mass, damping, and stiffness matrices which are then used to solve the requested analysis type, such as static, transient, or modal. Combin39, shown in Figure 5.9, is an ANSYS nonlinear spring element capable of representing general PWL springs [55].

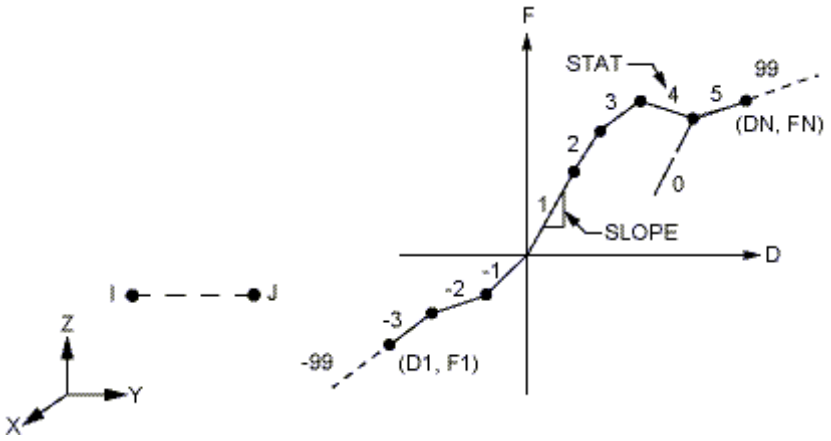

Figure 5.9: ANSYS Combin39 Nonlinear Spring Element [55]

The user defines the force versus displacement curve for the element by specifying up to 20 points on the curve. Compressive behavior can be explicitly defined, assumed to be a reflection of the tensile region, or set to 0 for all compressive loads.

Contrary to numerical integration of derived equations of motion in MATLAB, using ANSYS for simulation of the MBS support system does not require that the user hard code each of the piecewise differential equation sets ahead of time. The switching of equations of motion is handled automatically. During an ANSYS transient analysis, solutions are calculated via Newmark's Method at what are known as substeps. Substeps are usually chosen to satisfy a minimum time step increment for accurate time histories. When nonlinear analysis is conducted, additional equilibrium iterations are calculated at each substep to aid in convergence. The displacement results of the previous equilibrium iteration are used to determine what segment of the Combin39 force versus displacement curve should be active at each point of the transient simulation.

The Combin39 element does not have an explicit way to specify initial preload in the spring. This same difficulty was addressed in Chapter 4 in regards to AMS-02 strap team simulations in NASTRAN. It was shown that opting to shift the origin of the

stiffness curves and using a cut-to-length model, rather than modeling the preload, resulted in a slightly different problem. A simplistic solution to model preload when using the Combin39 element is to specify fixed displacements of the anchor nodes. These displacements are specified in addition to desired initial conditions of the mass. The initial displacement of the anchor nodes moves them to their desired location, preloads the system, and forces the mass to move to the proper equilibrium position. Once the springs are preloaded, ANSYS completes the nonlinear transient simulation. The ANSYS script capable of simulating the four-spring MBS support system is given in Appendix D. The simulation previously presented in Figure 5.7 was recreated in ANSYS and comparisons between the MATLAB and ANSYS results are presented in Figures 5.10 and 5.11.

Figure 5.10 presents the x and y dimensionless time histories at the beginning and end of the simulation. Initially, the two modeling approaches yield identical responses. The two results, which eventually deviate from each other as a result of numerical error that builds up as simulation time progresses, remain qualitatively similar throughout the simulation as seen in Figure 5.11. Similarity in trajectories exhibited in the phase plane portraits and two-dimensional plane of motion suggest that both modeling approaches are converged and yielding the correct solution. Presently, it is believed that MATLAB stays closer to the actual solution throughout the simulation. The period of motion in both the x and y time histories was estimated from data at the beginning of the simulation and projected through the rest of simulation time. It was found that MATLAB maintained the most consistent period (free response period should not change), and ANSYS deviated more through a gradual period elongation during the simulation.

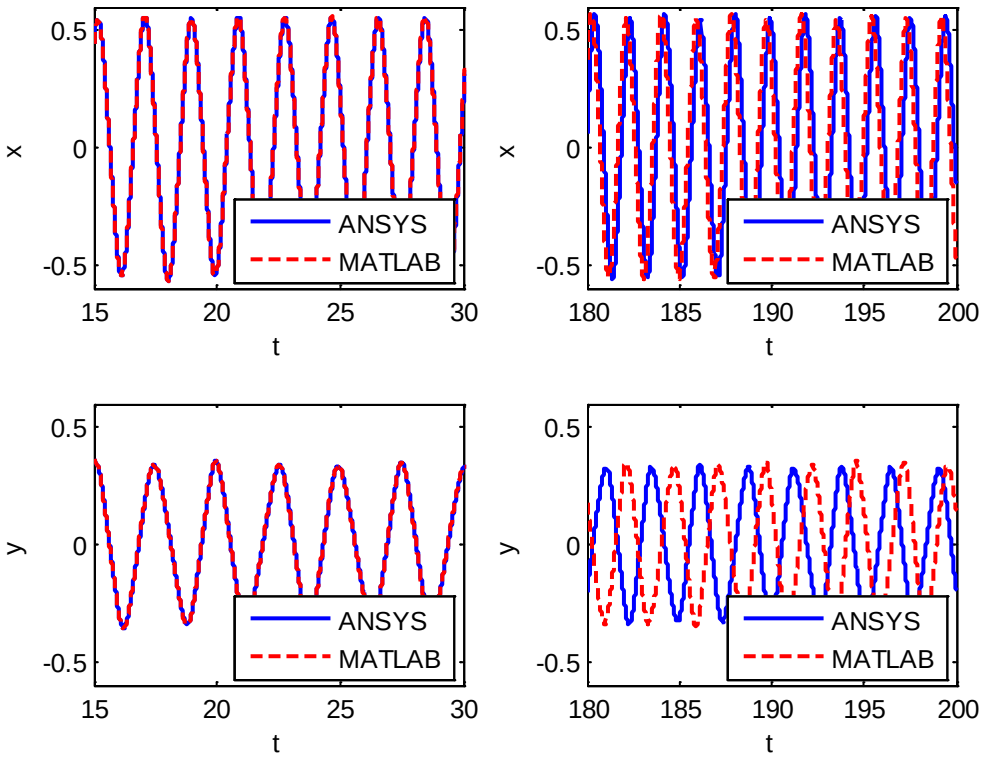

Figure 5.10: Time History Comparison between MATLAB and ANSYS Nonlinear Simulations

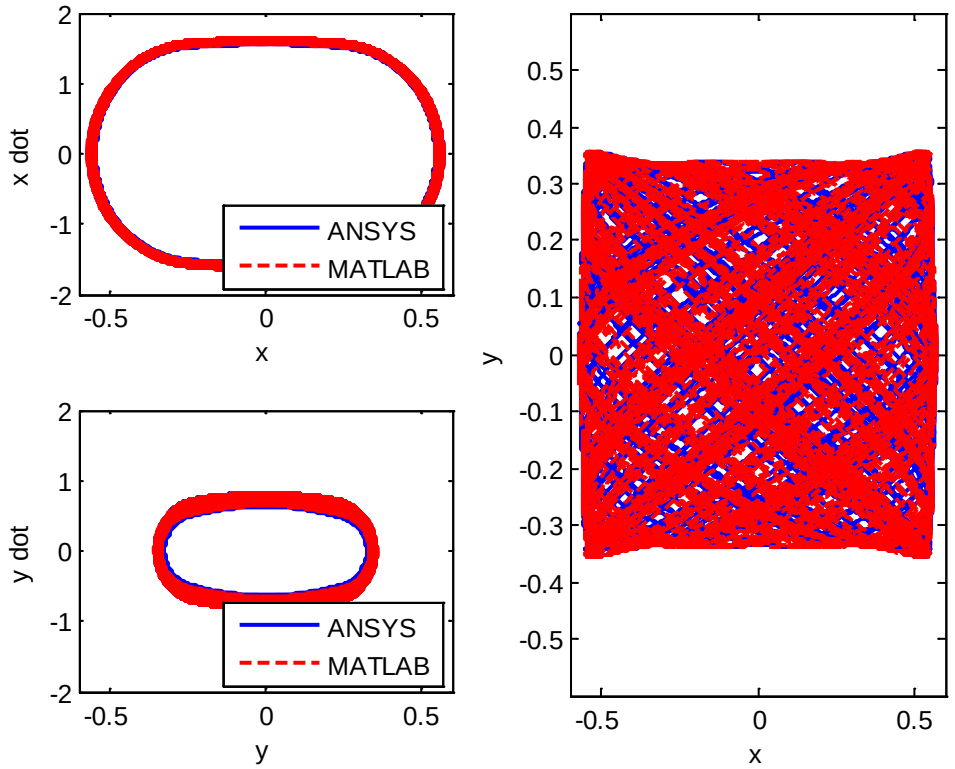

Figure 5.11: Phase Plane Portrait and Two-Dimensional Plane of Motion Comparison between MATLAB and ANSYS Nonlinear Simulations

The time step size is an important aspect of both simulation techniques. A practical rule of thumb states having at least ten time steps per natural period is required for converged results [39]. When numerically integrating in MATLAB, the user cannot directly specify the time step used to obtain the solution as can be done in ANSYS transient simulations. However, the time step was indirectly controlled through modifying the default absolute and relative error tolerances used by the ode45 command. With over one thousand time steps per natural period in ANSYS and MATLAB simulations, both approaches more than satisfied the minimum.

Another important aspect of the time step is how knee location and switching between equations of motion is handled. ANSYS checks at each iteration if a change is required, but maintains a set global time step. The MATLAB ode45 event detection algorithm attempts to intelligently locate the switching point. This detection, along with the starting and stopping of integration in MATLAB, implies that the time step gets smaller in the vicinity of a knee. This behavior is demonstrated in Figure 5.12. The regularly spaced blue dots represent time steps taken by ANSYS, and the red dots with variable spacing correspond to MATLAB time steps. If fixed time step data is desired from MATLAB, a cubic spline can be fit to the curves at desired nodes post simulation. This technique is used later when generating Poincaré maps and bifurcation diagrams, both of which require a consistent time step for sampling data.

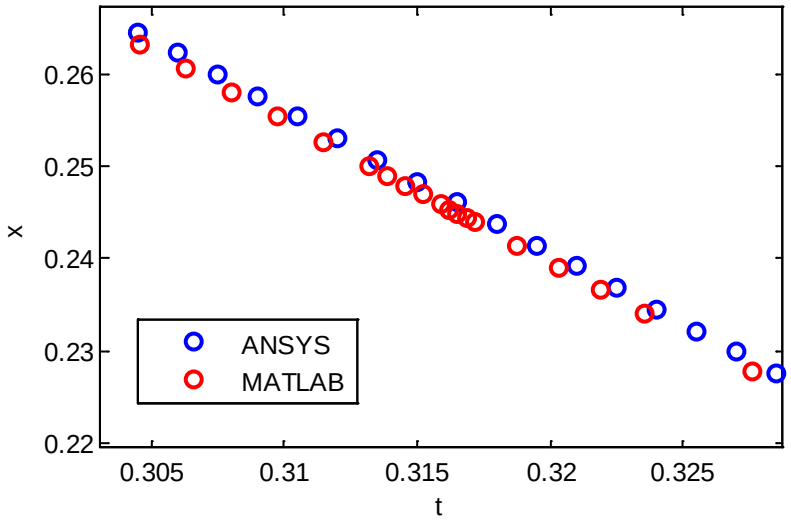

Figure 5.12: Comparing the Time Step Behavior near a Knee in MATLAB and ANSYS

The two methods differ in their required computational time. The runtime statistics for the two simulations are given in Table 5.2. ANSYS took approximately five hundred times longer than the corresponding MATLAB simulation, yet took less programming time beforehand. Generally speaking, runtimes on the order of seconds in MATLAB took on the order of hours in ANSYS.

Table 5.2: Comparing MATLAB and ANSYS MBS Free Vibration Runtime

	Time Step			Simulation Time	Runtime (s)
	Min	**Max**	**Mean**		
MATLAB	1.97E-06	0.004	0.002	200	16
ANSYS	0.0015	0.0015	0.0015	200	8100

This trade-off was the crucial factor when choosing which simulation approach to utilize. The four-spring system, which consists of 16 different differential equations sets, did not require an unreasonable amount of time to program into MATLAB. A much larger system, such as the 16 strap AMS-02 support system with over 65 thousand differential equation sets, could not practically be implemented into a MATLAB

simulation script with event detection, but could somewhat easily be programmed into ANSYS. In that case, opting to use a software package might be the only viable solution. However, for systems with less straps and thus less differential equation sets, or in work efforts where large quantities of simulations are desired, such as this thesis, the drastic reduction in simulation time was attractive and motivated the decision to use MATLAB for studying MBS support system dynamics.

5.3.3 Four-Spring MBS Forced Response

Applying a harmonic forcing function to the mass in the four-spring MBS system allows for further exploration of the nonlinear behavior possible in such a configuration. Nonlinear systems, as discussed in the literature review, are extremely sensitive to parameter values and initial conditions. An exhaustive parameter response plot, such as the example cited in the literature review created by Ueda [10], is not feasible for the four-spring MBS support system. The undeformed length and bilinear stiffness ratio for Springs 1-4, the primary stiffness ratio and knee ratio for Springs 2-4, the forcing amplitude and frequency, the initial position and velocity in the x and y directions, as well as the damping ratio, are all among the parameters whose effect on system response could be explored. Many papers discussed in the literature review examined the effect of a single parameter on the single bilinear spring oscillator. Here, rather than a thorough study of each parameters effect, select cases of interest with important engineering implications are presented for particular combinations of system parameters to demonstrate dynamic behavior possible with MBS support systems.

Simulations are addressed for the case of harmonic forcing applied along the global x-axis. When forcing is assumed along the x-axis, the y time history, the two-

dimensional plane of motion, and the y phase plane portrait are not shown due to their trivial nature. Similarly, forcing could be applied along the global y-axis and the corresponding x-axis plots be neglected.

5.3.3.1 Effect of α on Four-Spring MBS Forced Response

The effect of the bilinear stiffness ratio of the springs on the dynamic response is an important question associated with MBS support systems. The primary goal of the bilinear springs in an MBS support system is to restrict the motion of the mass to a region nearly within the knee-engagement curve. One may naïvely consider that increasing α will lead to less penetration outside of the knee-engagement curve without further thought of additional implications of the nonlinearities on the dynamic response.

In this section, bifurcation diagrams are generated for several values of α in the MBS support system using forcing frequency as the bifurcation parameter. The diagrams have been color coded so that response types, such as period-1 or period-3, have a unique color, as specified in the included legend. Three α values (used for all four springs) and two forcing amplitudes in the x-direction were considered. Figures 5.13 through 5.15 correspond to a forcing amplitude of Ax = 0.5 and all four α's = 5, 20, and 100, respectively. In Figures 5.16 through 5.18, the forcing amplitude is increased to Ax = 0.75 and the same three α values are considered. The remaining system parameter definitions are given in the figure captions.

It should be noted that a relatively coarse frequency step was used due to time limitations. Forced response studies require longer simulation times than free response studies because transient behavior must die out and steady state achieved before the

response type is classified. If in-depth analysis of a particular bifurcation is desired, a much smaller frequency interval in the region of interest would be required.

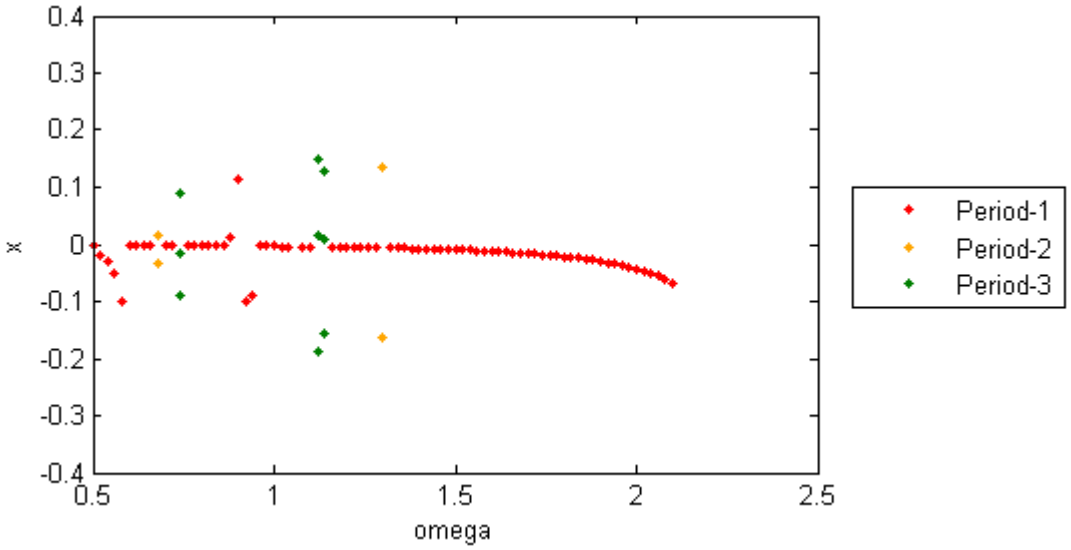

Figure 5.13: Four-Spring MBS Support System Bifurcation Diagram ($uL_1 = uL_2 = uL_3 = uL_4 = 4.25$, $\alpha_1 = \alpha_2 = \alpha_3 = \alpha_4 = 5$, $\beta_2 = \beta_3 = \beta_4 = 1$, $\sigma_2 = \sigma_3 = \sigma_4 = 1$, IC = (0, 0, 0, 0), Ax = 0.5, ζ =0.01, ω_x = 0.5 to 2.12)

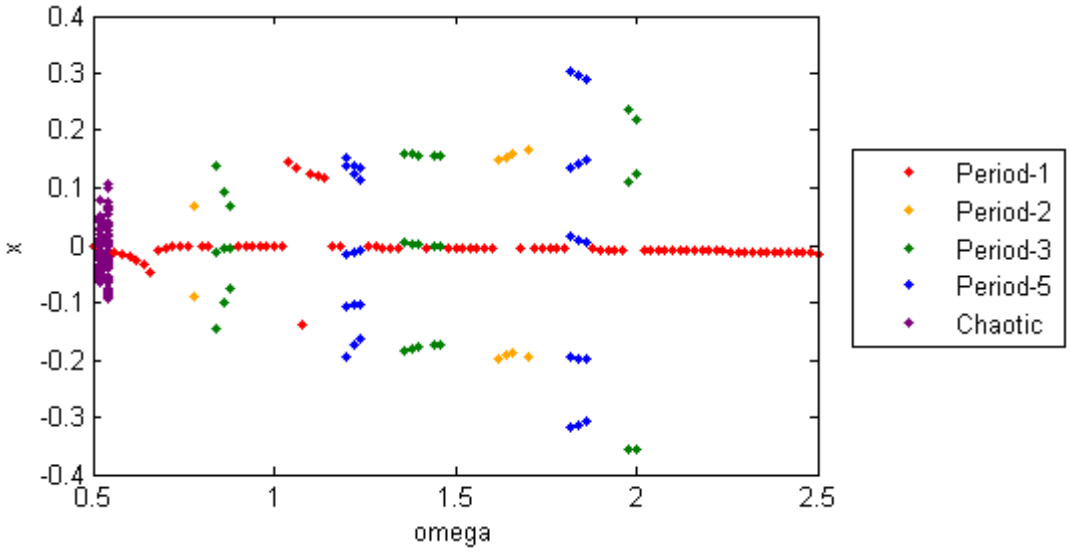

Figure 5.14: Four-Spring MBS Support System Bifurcation Diagram ($uL_1 = uL_2 = uL_3 = uL_4 = 4.25$, $\alpha_1 = \alpha_2 = \alpha_3 = \alpha_4 = 20$, $\beta_2 = \beta_3 = \beta_4 = 1$, $\sigma_2 = \sigma_3 = \sigma_4 = 1$, IC = (0, 0, 0, 0), Ax = 0.5, ζ =0.01, ω_x = 0.5 to 2.5)

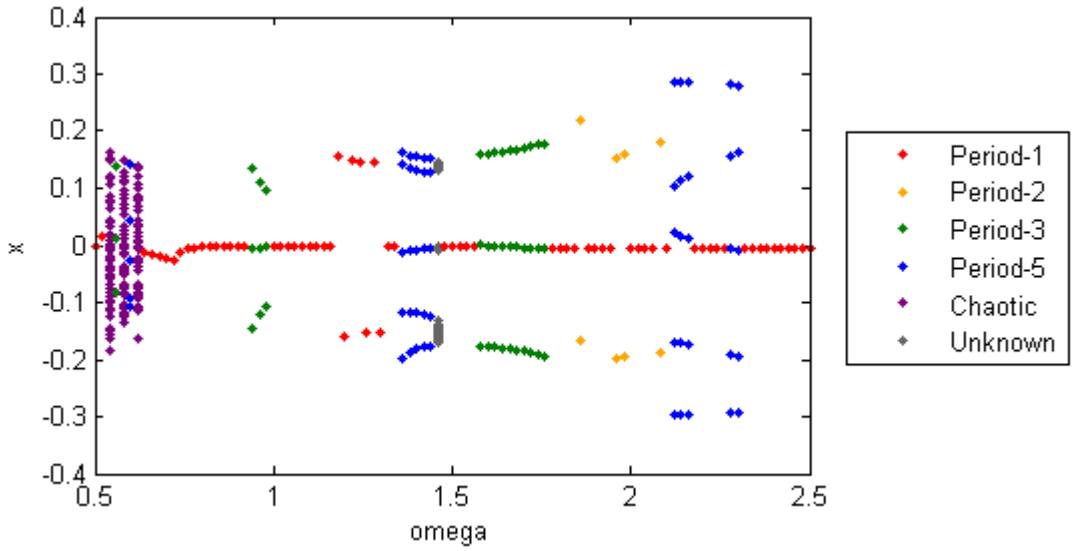

Figure 5.15: Four-Spring MBS Support System Bifurcation Diagram ($uL_1 = uL_2 = uL_3 = uL_4 = 4.25$, $\alpha_1 = \alpha_2 = \alpha_3 = \alpha_4 = 100$, $\beta_2 = \beta_3 = \beta_4 = 1$, $\sigma_2 = \sigma_3 = \sigma_4 = 1$, IC = (0, 0, 0, 0), Ax = 0.5, ζ =0.01, ω_x = 0.5 to 2.5)

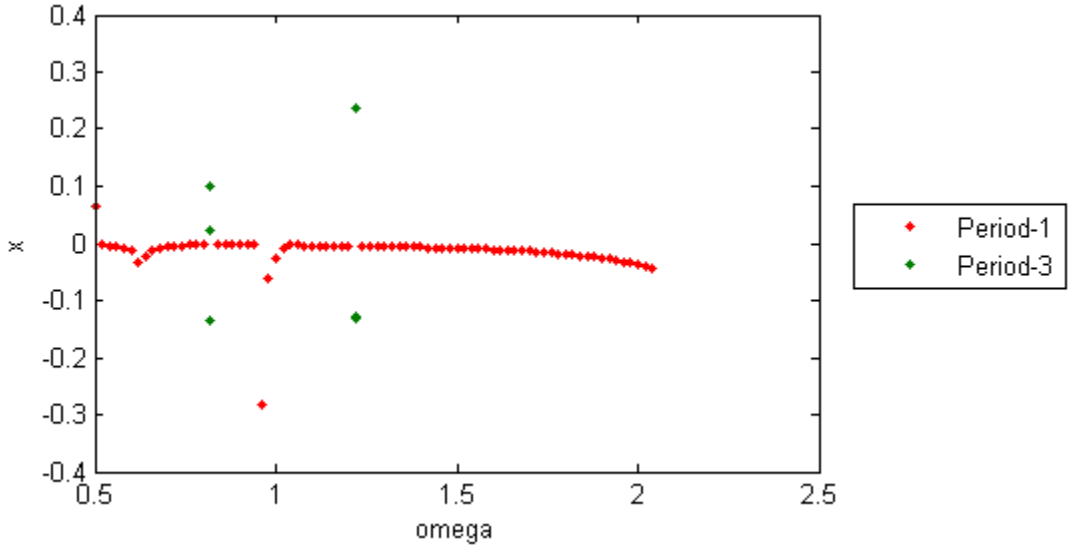

Figure 5.16: Four-Spring MBS Support System Bifurcation Diagram ($uL_1 = uL_2 = uL_3 = uL_4 = 4.25$, $\alpha_1 = \alpha_2 = \alpha_3 = \alpha_4 = 5$, $\beta_2 = \beta_3 = \beta_4 = 1$, $\sigma_2 = \sigma_3 = \sigma_4 = 1$, IC = (0, 0, 0, 0), Ax = 0.75, ζ =0.01, ω_x = 0.5 to 2.04)

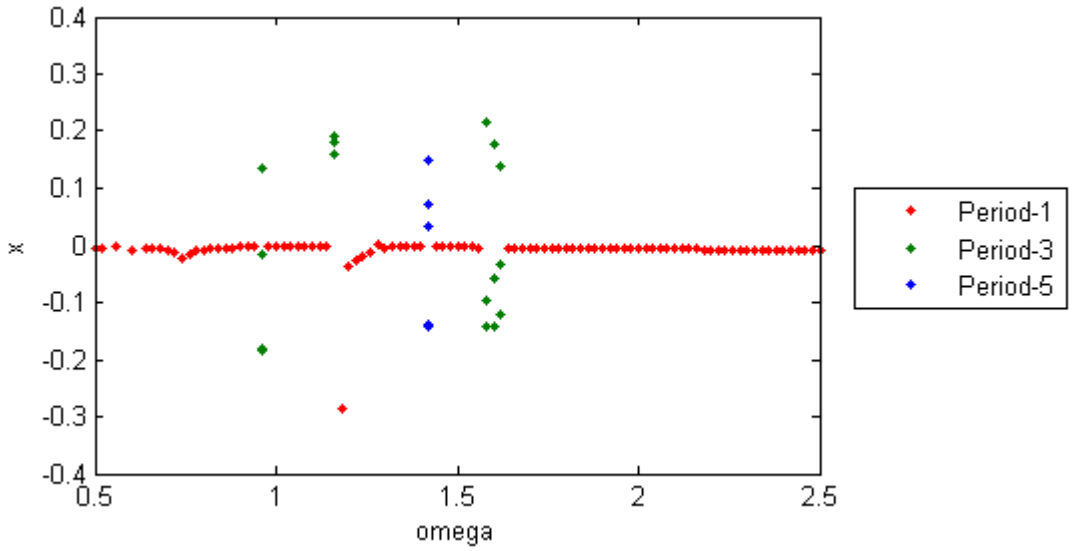

Figure 5.17: Four-Spring MBS Support System Bifurcation Diagram ($uL_1 = uL_2 = uL_3 = uL_4 = 4.25$, $\alpha_1 = \alpha_2 = \alpha_3 = \alpha_4 = 20$, $\beta_2 = \beta_3 = \beta_4 = 1$, $\sigma_2 = \sigma_3 = \sigma_4 = 1$, IC = (0, 0, 0, 0), Ax = 0.75, ζ =0.01, ω_x = 0.5 to 2.5)

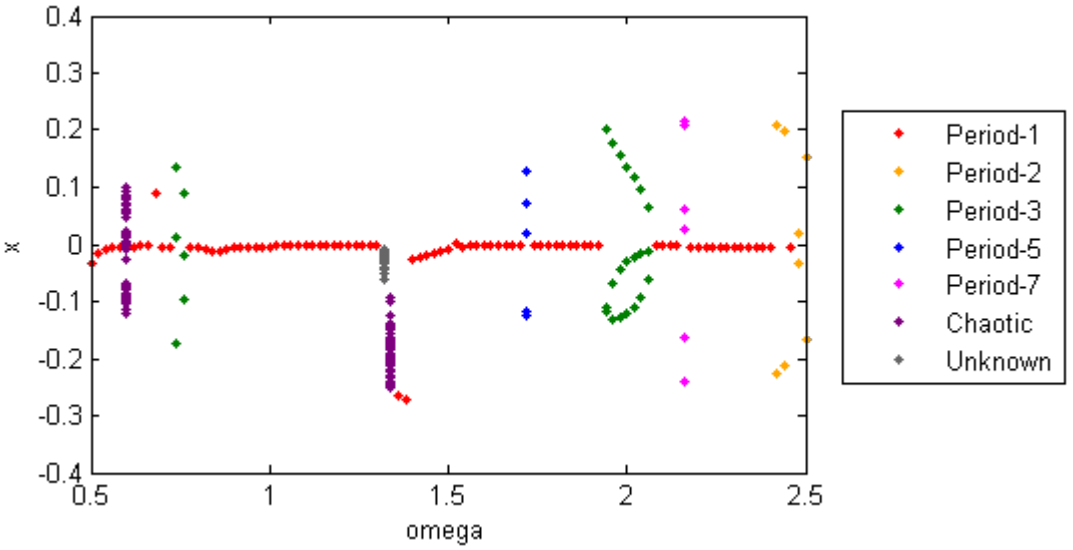

Figure 5.18: Four-Spring MBS Support System Bifurcation Diagram ($uL_1 = uL_2 = uL_3 = uL_4 = 4.25$, $\alpha_1 = \alpha_2 = \alpha_3 = \alpha_4 = 100$, $\beta_2 = \beta_3 = \beta_4 = 1$, $\sigma_2 = \sigma_3 = \sigma_4 = 1$, IC = (0, 0, 0, 0), Ax = 0.75, ζ =0.01, ω_x = 0.5 to 2.5)

The period-doubling bifurcations frequently noted in the single bilinear oscillator system are not readily seen in these studies. The subharmonic responses are predominately odd, such as period-3 or period-5, rather than even subharmonic responses that are typically discussed with period-doubling. The bifurcation diagrams also reveal

more subharmonic and chaotic responses as the value of α increases. This trend was apparent in the diagrams for both forcing function amplitude values. This behavior is consistent with Hossain et al, who noted that single bilinear oscillators with higher values of α exhibited more subharmonic and chaotic regions of motion than those with lower values of α [18]. The increase in α further restricts the motion of the mass, but the increase in subharmonic and chaotic response regions may be undesirable in practical applications.

Underlying the increase in nonlinear responses is sensitivity to small changes in forcing frequency. Slight changes in the forcing frequency value lead to very different response types. Consider the bifurcation diagram previously presented in Figure 5.14 with $A_x = 0.5$ and $\alpha = 20$. Period-1 and period-5 responses are found within a ω_x range of 1.18 to 1.20. The dimensionless time history and phase plane portraits for these responses are given in Figures 5.19 and 5.20. The plots suggest a bifurcation near ω_x = 1.19 leads to an abrupt change in behavior that may not be acceptable in physical uses.

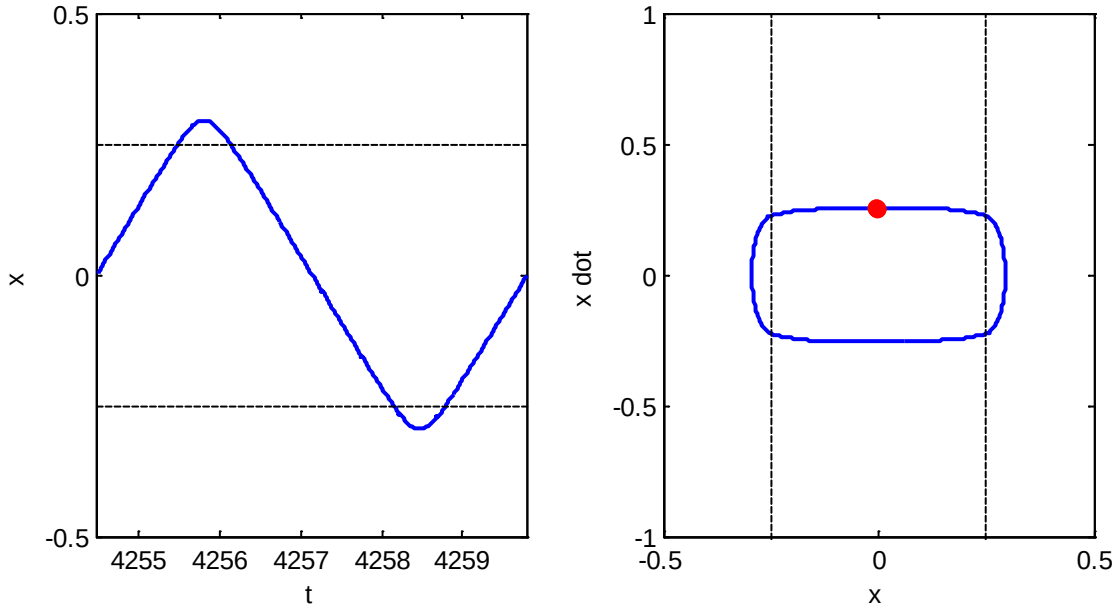

Figure 5.19: Period-1 Response, ($uL_1 = uL_2 = uL_3 = uL_4 = 4.25$, $\alpha_1 = \alpha_2 = \alpha_3 = \alpha_4 = 20$, $\beta_2 = \beta_3 = \beta_4 = 1$, $\sigma_2 = \sigma_3 = \sigma_4 = 1$, IC = (0, 0, 0, 0), Ax = 0. 5, ζ =0.01, $\omega_x = 1.18$)

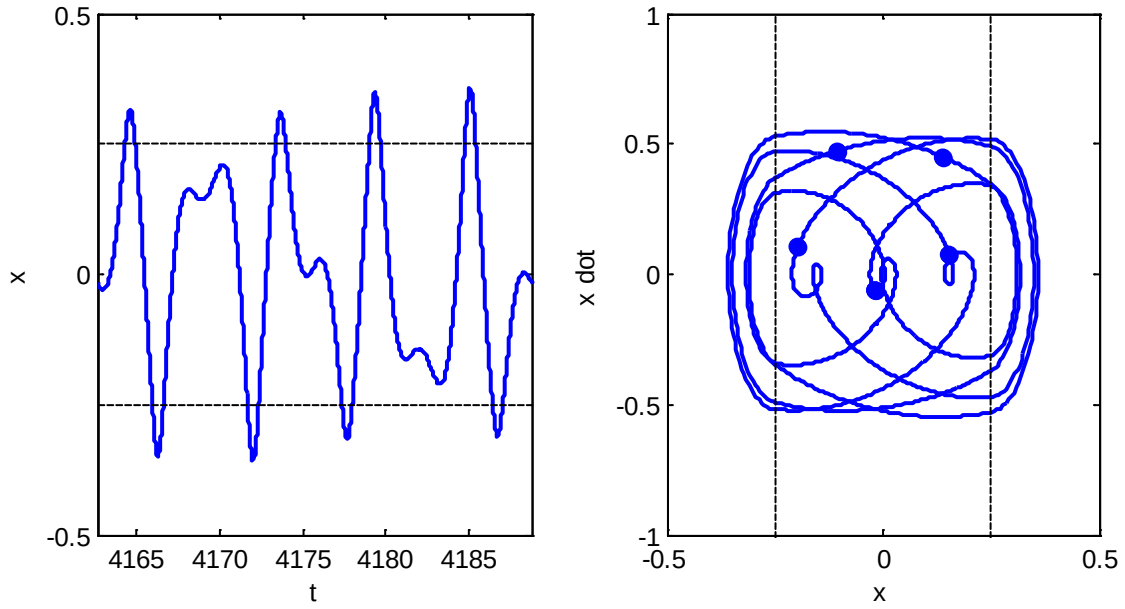

Figure 5.20: Period-5 Response, ($uL_1 = uL_2 = uL_3 = uL_4 = 4.25$, $\alpha_1 = \alpha_2 = \alpha_3 = \alpha_4 = 20$, $\beta_2 = \beta_3 = \beta_4 = 1$, $\sigma_2 = \sigma_3 = \sigma_4 = 1$, IC = (0, 0, 0, 0), Ax = 0. 5, ζ =0.01, $\omega_x = 1.2$)

5.3.3.2 Effect of Preload on Four-Spring MBS Forced Response

An important consideration associated with MBS support systems is how much initial preload to introduce into the system. This is accomplished by changing how close the bilinear springs are to the knee of their stiffness curves when in static equilibrium. The preloaded assumption, as opposed to the "cut-to-length" model discussed in Chapter 4, requires that the springs operate in tension, even at static equilibrium. However, the initial preload can be controlled by changing the undeformed length of each spring and/or the location of the fixed anchor points. In effect, changing the preload moves the knee-engagement curve and changes how close each spring is to its stiffness knee at equilibrium.

Hossain et al conducted a study on the equilibrium position relative to the knee location in the single bilinear oscillator [19]. In their study, it was found that moving the equilibrium position closer to the knee resulted in an increase in chaotic response

regimes. A similar study has been conducted here with the four-spring MBS support system. Previously, the bifurcation diagram in Figure 5.13 revealed period-1, period-2, and period-3 for the particular system parameters specified. A second bifurcation diagram was created with identical parameters, except the undeformed length, which was changed from 4.25 to 4.05, thus preloading all four-springs much closer to their knees. The anchor points, as previously stated, were kept at the positions specified in Table 5.1. The magnitude of this change is demonstrated in Figure 5.21, which compares the knee-engagement curves for the two different scenarios. When the undeformed length is shortened to 4.05 for each spring, the mass has a much smaller range of motion prior to knee engagement. Both scenarios are symmetric, implying all four bilinear springs are identical, and the equilibrium position lies at the origin of the two-dimensional plane. The new bifurcation diagram is given in Figure 5.22.

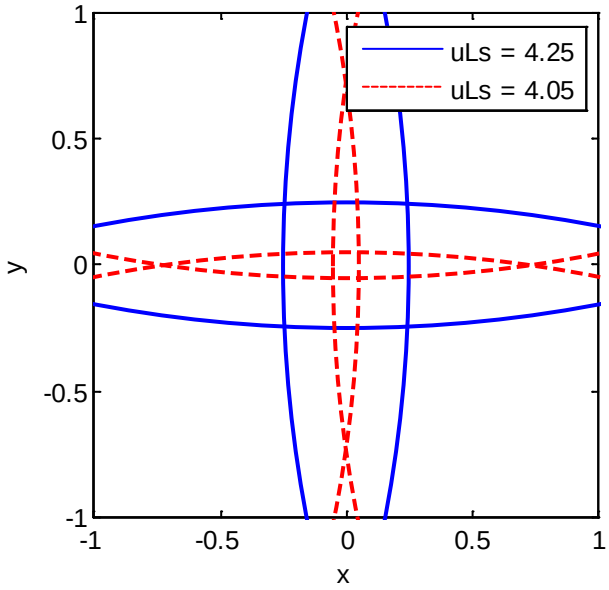

Figure 5.21: Comparing the knee-engagement curves for = uL_2 = uL_3 = uL_4 = 4.25 and 4.05. In both cases, σ_2 = σ_3 = σ_4 = 1

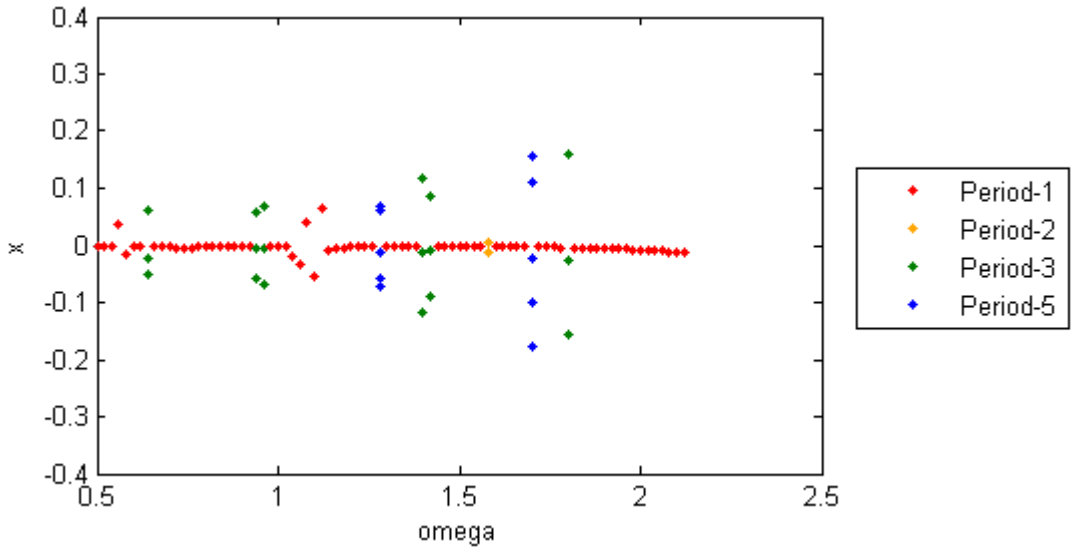

Figure 5.22: Four-Spring MBS Support System Bifurcation Diagram ($uL_1 = uL_2 = uL_3 = uL_4 = 4.05$, $\alpha_1 = \alpha_2 = \alpha_3 = \alpha_4 = 5$, $\beta_2 = \beta_3 = \beta_4 = 1$, $\sigma_2 = \sigma_3 = \sigma_4 = 1$, IC = (0, 0, 0, 0), Ax = 0.5, ζ =0.01, ω_x = 0.5 to 2.12)

The figure does not reveal any chaotic response regions, but does reveal an overall increase in the number of forcing frequencies at which subharmonic responses occur. Period-5 responses, which were not found when using an undeformed length of 4.25, have also been found with the new preload distance. This study, while not exhaustive, suggests that the preload in each spring, governed by the undeformed length and/or the fixed anchor point locations, does play a significant role in affecting the system response.

5.3.3.3 Asymmetric Four-Spring MBS Support Systems

The forced response studies up to this point have involved symmetric configurations, implying that the four bilinear springs have identical properties and that the equilibrium position of the mass corresponds to the origin of the two-dimensional plane of motion. The potential energy discussion in Chapter 4 addressed the fact that symmetric systems are unlikely to occur in real world applications and that variations about a nominal value are likely to be present. Asymmetry can be introduced into the

system in a variety of ways, such as discrepancies in undeformed lengths, bilinear stiffness ratios, primary stiffness ratios, and knee ratios of the bilinear springs.

Consider a period-1 response that occurs in a symmetric MBS support system configuration given in Figure 5.23. The system parameters are defined in the figure caption. The period-1 behavior can be converted to chaotic with one simple change that results in an asymmetric configuration. Consider Figure 5.24, which contains the response for a system with parameters identical to those used in Figure 5.23, except σ_3, which has been changed from 1 to 0.75. This places a knee at the origin of the two-dimensional plane of motion and leads to a chaotic response.

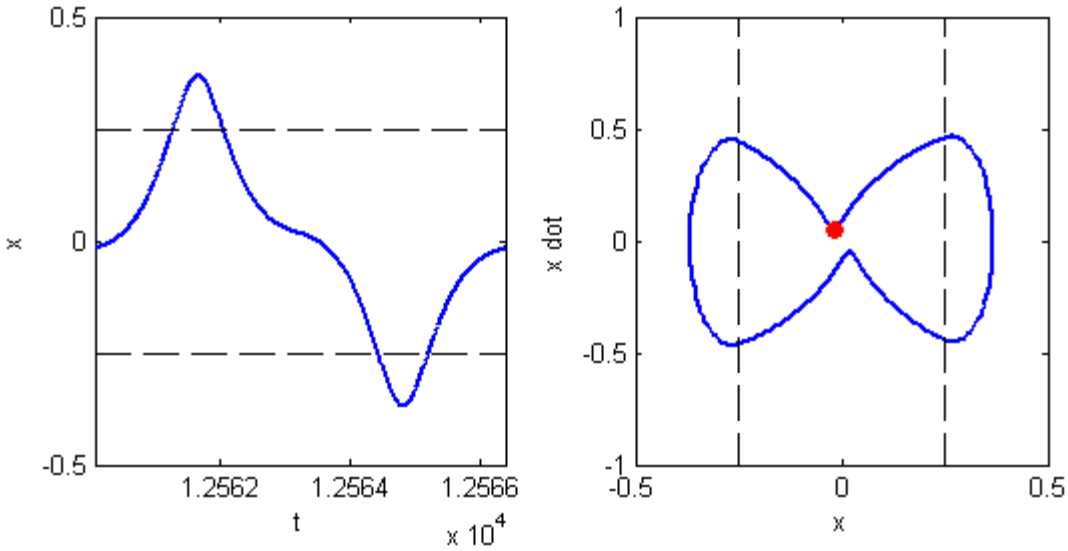

Figure 5.23: Period-1 Response, ($uL_1 = uL_2 = uL_3 = uL_4 = 4.25$, $\alpha_1 = \alpha_2 = \alpha_3 = \alpha_4 = 20$, $\beta_2 = \beta_3 = \beta_4 = 1$, $\sigma_2 = \sigma_3 = \sigma_4 = 1$, IC = (0, 0, 0, 0), Ax = 1, ζ =0.05, $\omega_x = 0.75$)

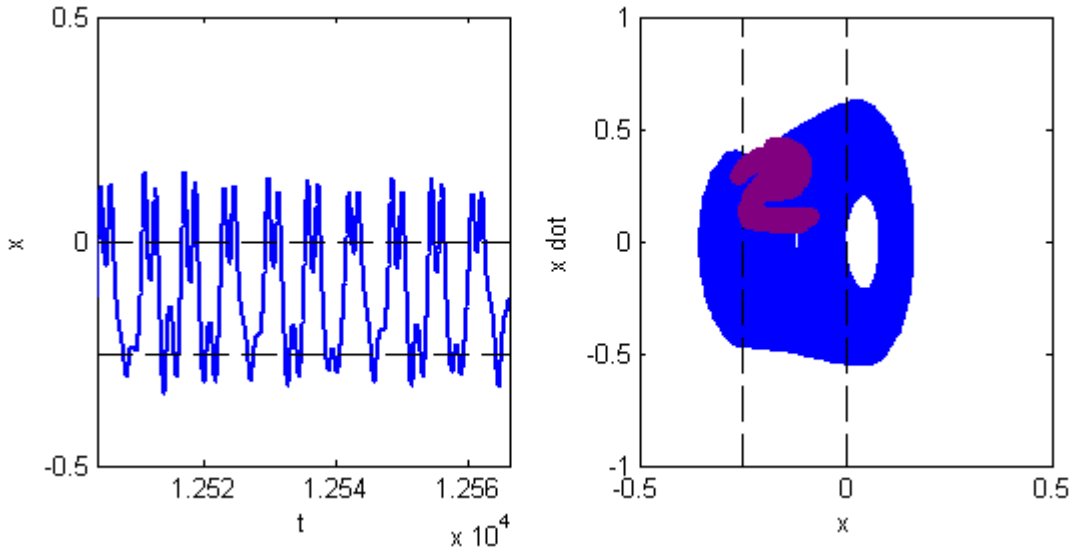

Figure 5.24: Chaotic Response, ($uL_1 = uL_2 = uL_3 = uL_4 = 4.25$, $\alpha_1 = \alpha_2 = \alpha_3 = \alpha_4 = 20$, $\beta_2 = \beta_3 = \beta_4 = 1$, $\sigma_2 = \sigma_4 = 1$, $\sigma_3 = 0.75$, IC = (0, 0, 0, 0), Ax = 1, ζ =0.05, $\omega_x = 0.75$)

The cluster of Poincaré points on the phase plane portrait in Figure 5.24 are part of a strange attractor. Strange attractors were discussed in the literature review section of Chapter 2. A closer view of the strange attractor is given in Figure 5.25. It is important to note that chaos is not completely random, thus the fractal, bounded shape of the attractor. Recall, this response was found by changing a single parameter which results in an asymmetric configuration, demonstrating the sensitive nature of MBS support systems. A more thorough investigation of asymmetric systems including cases where multiple parameters are changed would be a logical extension for future work.

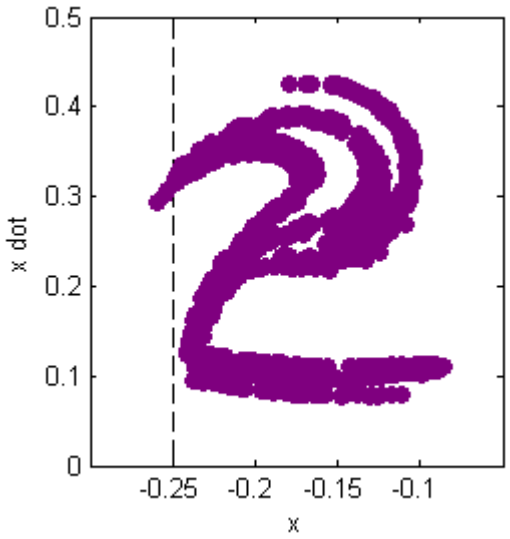

Figure 5.25: Close-up View of Strange Attractor in Figure 5.24

5.4 Utilizing Polynomial Approximations of Bilinear Stiffness Models

The objective of this section is to explore the feasability and effect of replacing bilinear springs with polynomial approximations in the MBS support system. Making use of polynomial approximations simplifies the analysis by eliminating the need to constantly switch among differential equation sets as individual springs move from their lower to upper stiffness regions, or vice versa. If successful, using polynomial approximations would simplify the piecewise equations of motion for the four-spring MBS support system into two expressions and expedite programming required prior to simulation.

Developing the equations of motion utilizing polynomial approximations requires that the bilinear stiffness models, now represented by dimensionless parameters, be fit with a polynomial of specified degree. In general, a polynomial approximation of degree n to a given set of data is given by

$$p_n = c_0 x^n + c_1 x^{n-1} + \ldots + c_n = \sum_{j=1}^{n+1} c_{j-1} x^{n+1-j} \qquad (5.1)$$

The coefficients of the best-fit polynomial can be determined via linear least-squares regression. The coefficients which define the polynomial approximation for each bilinear stiffness curve are unique, and will not be equal unless the bilinear springs are identical. During simulations, all four bilinear stiffness models are defined and used to calculate each polynomial approximation prior to integration of the equations of motion.

The user must specify the range of interest on each bilinear stiffness model to be used when determining the best-fit polynomial in addition to the degree of the approximation. Ideally, the range of interest used to solve for the coefficients will bracket the range of deformation the spring experiences during the desired simulation.

Lastly, the simplest form of linear regression will not ensure that the polynomial approximation pass through the origin of the stiffness curve as physically required. However, equality constraints can be applied that force the best-fit polynomial to pass through specified points, such as the origin. Throughout this section, a single constraint is assumed to be applied at the origin of all four bilinear stiffness curves.

Once the required coefficients have been determined, the governing differential equations of motion for the four-spring MBS support system, when using polynomial approximations of degree n, are given by

$$\begin{aligned}
&\sum_{j=1}^{n+1} c_{1,j-1}\left(\sqrt{(x_1-x)^2+y^2}-uL_1\right)^{n+1-j}\cos\left(a\tan\left(\frac{y}{(x_1-x)}\right)\right)\ldots \\
&-\sum_{j=1}^{n+1} c_{2,j-1}\left(\sqrt{x^2+(y_2-y)^2}-uL_2\right)^{n+1-j}\sin\left(a\tan\left(\frac{(y_2-y)}{x}\right)\right)\ldots \\
&-\sum_{j=1}^{n+1} c_{3,j-1}\left(\sqrt{(x-x_3)^2+y^2}-uL_3\right)^{n+1-j}\cos\left(a\tan\left(\frac{y}{(x-x_3)}\right)\right)\ldots \\
&-\sum_{j=1}^{n+1} c_{4,j-1}\left(\sqrt{x^2+(y-y_4)^2}-uL_4\right)^{n+1-j}\sin\left(a\tan\left(\frac{(y-y_4)}{x}\right)\right)-(2\zeta)\dot{x}+A_x\sin(\omega_x t)=\ddot{x}
\end{aligned} \tag{5.2}$$

and

$$
\begin{aligned}
&-\sum_{j=1}^{n+1} c_{1,j-1}\left(\sqrt{(x_1-x)^2+y^2}-uL_1\right)^{n+1-j}\sin\left(a\tan\left(\frac{y}{(x_1-x)}\right)\right)\ldots\\
&+\sum_{j=1}^{n+1} c_{2,j-1}\left(\sqrt{x^2+(y_2-y)^2}-uL_2\right)^{n+1-j}\cos\left(a\tan\left(\frac{(y_2-y)}{x}\right)\right)\ldots\\
&-\sum_{j=1}^{n+1} c_{3,j-1}\left(\sqrt{(x-x_3)^2+y^2}-uL_3\right)^{n+1-j}\sin\left(a\tan\left(\frac{y}{(x-x_3)}\right)\right)\ldots\\
&-\sum_{j=1}^{n+1} c_{4,j-1}\left(\sqrt{x^2+(y-y_4)^2}-uL_4\right)^{n+1-j}\cos\left(a\tan\left(\frac{(y-y_4)}{x}\right)\right)-(2\zeta)\dot{y}+A_y\sin(\omega_y t)=\ddot{y}
\end{aligned}
\tag{5.3}
$$

These equations are easily substituted into the existing MATLAB simulation script. The m-file which utilizes polynomial approximations is given in Appendix E.

The validity of this approximation was explored by comparing a bifurcation diagram produced with the bilinear assumption to bifurcation diagrams generated by using various order polynomial approximations. A known bifurcation in a symmetric configuration with all α's = 20 was studied using damping ratio as the bifurcation parameter. Some polynomial approximations utilized are presented in Figure 5.26.

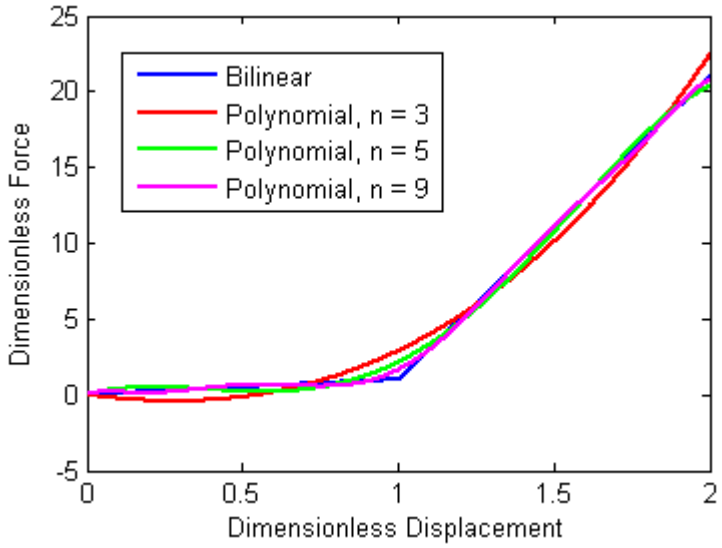

Figure 5.26: Various Order Polynomial Approximations of Bilinear Stiffness Model (α = 20, range of interest 0 to 2)

The bifurcation diagrams are presented in Figure 5.27. When using bilinear springs, three distinct bifurcations are seen. Period-3 bifurcates to period-1, period-1 bifurcates back to period-3, and period-3 bifurcates back to period-1.

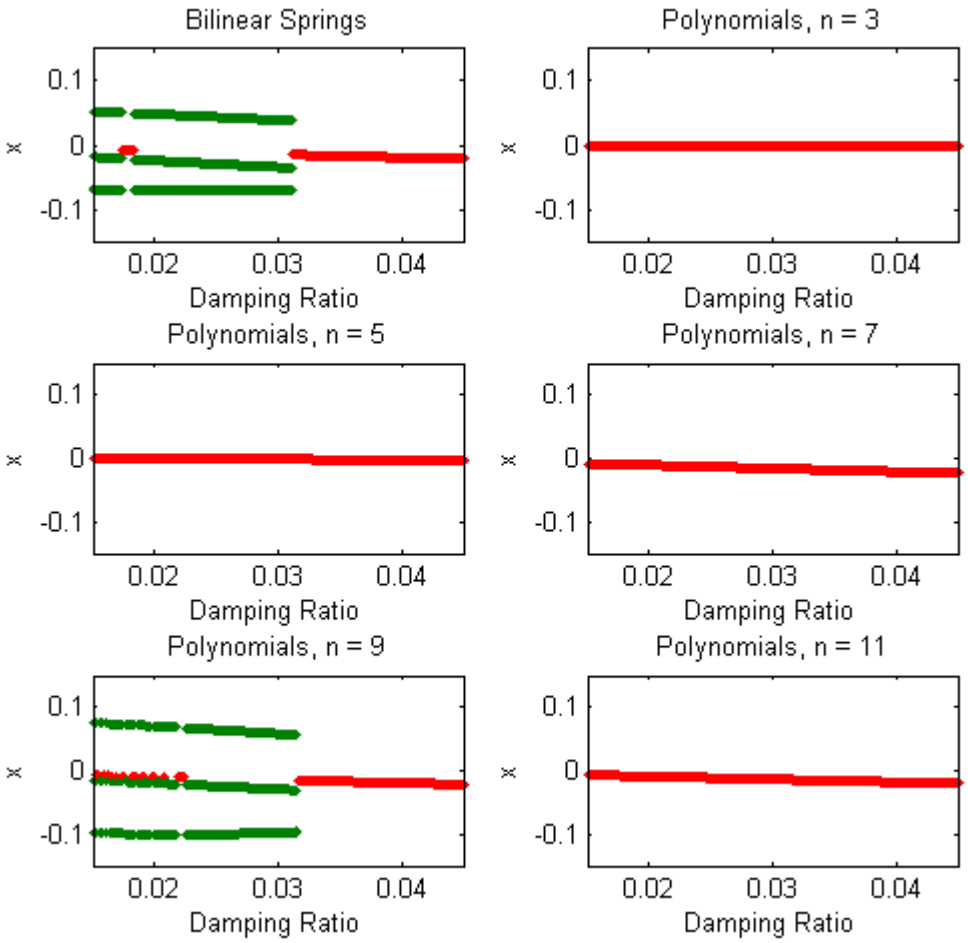

Figure 5.27: Bifurcation Diagrams for Four-Spring System ($uL_1 = uL_2 = uL_3 = uL_4 = 4.25$, $\alpha_1 = \alpha_2 = \alpha_3 = \alpha_4 = 20$, $\beta_2 = \beta_3 = \beta_4 = 1$, $\sigma_2 = \sigma_3 = \sigma_4 = 1$, IC = (0, 0, 0, 0), Ax = 0.75, $\omega_x = 0.75$, ζ =0.015 to 0.045) and Various Polynomial Approximations

The figure reveals that using polynomial approximations of degrees 3, 5, and 7 does not result in subharmonic motion or bifurcations, suggesting those order approximations are not adequate for capturing nonlinear behavior seen in the original system. The 9th order polynomial approximation does capture the nonlinear behavior, but has slight discrepancies such as the numerous regions of period-1 response found at low

damping ratios. The 11^{th} order polynomial approximation, however, does not capture any of the nonlinear behavior, yielding only period-1 response. The results suggest it is extremely difficult to predict which order approximation will be adequate for a given system. Simply increasing the polynomial degree does not guarantee a valid approximation, perhaps due to the increase in the number of concavity changes with higher order approximations.

Further investigation is required to conclusively state if polynomial approximations can accurately be used in place of bilinear stiffness models. In particular, the range of interest used to solve for coefficients and the placement of any additional linear constraint points to improve the polynomial approximation are two areas that may prove to greatly affect their validity. Another unanswered question is whether bilinear springs with lower α values are more accurately represented with polynomials. As α decreases, the harshness of the nonlinearity decreases, which may suggest that lower order polynomials would be sufficient approximations as opposed to the 9^{th} order polynomial when $\alpha = 20$.

5.5 Configurations for Future Study

For the range of parameters studied and forcing applied along the x-axis, the four-spring MBS system has essentially been a two knee system (Springs 1 and 3) with oblique springs (Springs 2 and 4). Encountering the knees associated with Springs 2 and 4 in the chosen geometric configurations was not possible unless extremely large forcing amplitude was applied. Realistically, it is feasible, and may be desired, for the knees of the oblique springs to be engaged when forced along a global axis. However, due to the previously discussed unresolved issue associated with repeated detection of simultaneous

events, the scope of symmetric forced four-spring MBS studies was limited. Once the issue has been resolved, studying the case of engaging oblique spring knees would serve as an interesting expansion upon the current work. The nonlinearities associated with additional knees will undoubtedly impact the system response.

Another interesting extension would involve applying the forcing function along an arbitrary axis at an angle with respect to the global coordinate system. Such a force would allow for all four knees to be more readily encountered during forced vibration simulations. Physically, this corresponds to discrepancies between the system orientation and the forcing function direction. A study of the effect of the arbitrary axis angle definition would be beneficial for real world systems where forcing and disturbances will not always be applied in the same foreknown direction.

Chapter 6: Conclusion

The main objective of this thesis was to develop numerical modeling techniques capable of simulating the dynamic response of a multi-bilinear-spring (MBS) support system motivated by a future International Space Station Experiment known as the Alpha Magnetic Spectrometer (AMS). One possible AMS design, denoted as AMS-02, features a cryogenic magnet supported in three-dimensional space by 16 straps with piecewise-linear (PWL) stiffness models. This highly nonlinear system has no previous flight heritage, and poses many questions in regards to possible dynamic responses. A two-dimensional, two DOF four-spring MBS support system was created by simplifying the AMS-02 geometry and feasible numerical modeling schemes were developed and used for analysis of the nonlinear system.

The following sections provide a summary of key material featured in the previous chapters of this thesis.

6.1 Literature Review

- A brief overview of terminology frequently used in the study of nonlinear dynamics was presented to aid the reader in understanding of material throughout this thesis.
- Literature concerning the one-dimensional, single DOF bilinear oscillator was reviewed. Classic nonlinear behavior, such as subharmonic motion, chaotic motion, and sensitivity to initial conditions was documented. Modeling approaches utilized in the various studies were also discussed.
- The AMS-02 support system consists of multiple PWL straps supporting a mass which moves in more than one dimension, contrary to the single DOF bilinear oscillator. The latter has been thoroughly documented in the literature, but the former

system type has not. Dynamic analysis of moored bodies was noted as the existing research most similar to analysis of MBS support systems.

- The concept of geometric nonlinearity, and its relevance to MBS support systems, was introduced.

6.2 Developing Numerical Models

- The piecewise differential equation of motion for the one-dimensional single DOF asymmetric bilinear oscillator was derived and nondimensionalized.
- A numerical integration scheme capable of switching which part of the piecewise-continuous equation is integrated based on spatial position of the mass was developed using MATLAB.
- Similar to the single bilinear oscillator, the piecewise-continuous differential equation of motion was derived for the two-dimensional, two DOF four-spring MBS support system.
- The MATLAB numerical integration script was adapted to handle the four-spring MBS support system piecewise equations of motion, which consist of 16 differential equation sets. The developed scheme switches which of the 16 sets are integrated as the mass moves in the two-dimensional plane.
- An effort to derive the equations of motion for the four-spring MBS support system via the Finite Element Method (FEM) formulation was documented. The approach derived in this work was proven to be inaccurate, but was included as reference for those who may consider a similar approach for future applications.

6.3 Potential Energy

- An expression for the PE in a single asymmetric bilinear spring was derived via integration of the restoring force equation. The scaled PE was defined as a scalar multiple of the non-scaled PE.
- The scaled PE equation for a single spring was used to create the scaled PE curves for the four-spring system. The scaled PE curves were used to quantify the difference between the preloaded model and the "cut-to-length" model assumptions, and revealed that accounting for the preload in the equations of motion for MBS support systems is required to perfectly capture the dynamic response.
- An exhaustive numerical search for multiple equilibrium positions, in the form of local potential energy minimums, was conducted. No such points were found, suggesting that MBS support systems are not capable of having multiple equilibrium positions, even with statistical variation in system parameters.

6.4 Dynamic Responses

- The distinct effects of the geometric and bilinear nonlinearities were demonstrated in the free response of the four-spring MBS system. The free response was also used to validate MATLAB numerical integration results with nonlinear transient analysis results from ANSYS. The MATLAB script proved to compute solutions quicker than ANSYS, but required more programming prior to simulation.
- Bifurcation diagrams were utilized to demonstrate the effect of increasing α for all springs in a harmonically forced four-spring MBS system. The diagrams revealed more regions of chaotic and subharmonic motion as the value of α increased.

- Changing the initial preload in each spring or introducing asymmetry into the support system by changing spring parameters both proved to alter the dynamic response, confirming that MBS support systems are extremely sensitive to slight changes in any defining parameters.
- The validity of approximating MBS support system bilinear stiffness models with polynomials was explored. Preliminary studies suggest that degree of the polynomial, the region of interest used to solve for coefficients, and the location of any linear constraint points all greatly influenced the obtained dynamic response. In most cases analyzed, the polynomial approximations were not sufficient to capture nonlinear behavior seen in the corresponding bilinear system.

6.5 Contribution

At the top level, this thesis has raised awareness of the AMS-02 and its unique support system that may be utilized on future space experiments. Although the analysis in this thesis was conducted on a simplified model of the physical experiment, it has answered many questions associated with MBS support systems in general. In this thesis, feasible numerical simulation techniques were developed using MATLAB that greatly reduce the computational time required as compared to more traditional finite element programs, such as ANSYS. The drastic reduction in run-time allowed for a broad range of simulations to be run. As a result, this thesis has demonstrated the extreme sensitivity of MBS support systems to variations in system parameters such as the initial preload and the bilinear stiffness ratio of the support springs. By revealing some of the nonlinear phenomena that can occur, this thesis will hopefully motivate any who may pursue a system similar to the AMS-02 design to conduct rigorous analysis of this highly

nonlinear system, thus insuring all possible behaviors are known. Lastly, the work contained herein has applied many of the analysis tools discovered in the literature on single bilinear oscillators to the more complicated and less frequently studied system of higher dimensions and multiple springs.

6.6 Future Work

There are many extensions of the work presented in this thesis that would be valuable. As stated in the Dynamic Responses chapter, a full examination of the effect of each system parameter was not possible due to the sheer number of variations. Studies could be conducted on parameters not emphasized in this thesis, such as the effect of changing the anchor points for each spring. Additional forcing functions, such as impulse and random, could be applied to the four-spring MBS model instead of the harmonic forcing used in this work. The model could also be used to further explore the interaction between the geometric and bilinear nonlinearities, which was briefly addressed via observations in the free response in Chapter 5.

In addition to the four-spring system, the work could be expanded by applying the methodology developed in this thesis to a three-dimensional system with additional support springs. This model would be closer to the physical AMS-02 configuration. An important question that could be addressed is what the minimum phenomenological representation is in three-dimensional space. Furthermore, the point mass assumption utilized in this thesis implied that rotational degrees-of-freedom were neglected. Including a rigid mass, such as the ring-like magnet shape seen in AMS-02, would further complicate the nonlinear system through coupling of the translational and rotational

degrees-of-freedom. This additional coupling may lead to nonlinear behavior not possible with the point mass assumption.

The topic of polynomial approximations could be further explored. Recall that the actual AMS-02 straps were PWL with three or more segments, depending on the temperature of operation. The straps were assumed bilinear due to the globally bilinear appearance of the stiffness curves. One question of interest is if polynomial approximations would yield more accurate results when compared to simulations using multi-PWL stiffness models as opposed to the bilinear models used in this thesis.

Last, two and three-dimensional support systems could be built and used for experimental validation of the numerical models developed in this work.

APPENDIX A

MATLAB script capable of simulating the response of the asymmetric bilinear oscillator

```
function [tout,qout,teout,qeout,ieout,tspan,qout_sp]= rk1bi_nd()
%********************DIMENSIONLESS*****************************
%clear all; close all; clc %Housekeeping

%% Dimensionless Parameters
alpha1 = 5;      %Bilinear Spring Stiffness Ratios (K12/K11)
Ax = 1;          %Forcing Amplitude
wx = 0.75;       %Forcing Frequency
dmprat = 0.01;  %Damping Ratio

%% State Space Function
qdots1 = @(t,q) [q(2); -q(1)-2*dmprat*q(2)+Ax*sin(wx*t)];
qdots2 = @(t,q) [q(2); -alpha1*q(1)-(1-alpha1)-
2*dmprat*q(2)+Ax*sin(wx*t)];

%% Time Information
T = 2*pi/wx;
Tmult = 100;
tspan = 0:T/100:T*Tmult;
tstart = tspan(1);
tend = tspan(end);

%Initial Conditions (position and velocity)
q0 = [0;0];

%% Determine which set of equations to start with
if (q0(1,1) > 1)
    flag1 = 1;
else
    flag1 = 0;
end

%Accumulators for ODE solve output
tout = tstart;   %global solution time
qout = q0.';          %global solution position
teout = [];         %time at which events occur
qeout = [];         %position at which events occur
ieout = [];         %flags which event triggered the switch

%Options for ODE solver
options = odeset('RelTol',1e-6,'AbsTol',1e-8,'Events',@events);

%% Main Loop
while (tout(end)<tend)
if flag1 == 1
[t,q,te,qe,ie] = ode45(qdots2,tspan,q0(:,1),options);
flag1 = 0;

else
[t,q,te,qe,ie] = ode45(qdots1,tspan,q0(:,1),options);
```

```
flag1 = 1;
end

%Accumulate output.
nt = length(t);
tout = [tout; t(2:nt)];
qout = [qout; q(2:nt,:)];
teout = [teout; te];    % Events at tstart are never reported.
qeout = [qeout; qe];
ieout = [ieout; ie];

tspan = [t(end), tend]; %reset time span,'where you just ended to tend'
q0 = [q(end,1);q(end,2)]; %reset IC as where you just ended
end %end while

%% ------------------------------------------------------------------------
function [value,isterminal,direction] = events(t,q)
value = [q(1)-1,q(1)-1];     % Detect zero of event functions
isterminal = [1,1];   % Stop the integration?
direction = [-1,1];   % Direction
%------------------------------------------------------------------------
end %end function events

%% Interpolate the data at desired time steps (via cubic spline)
tspan = 0:T/100:T*Tmult;
qout_sp(:,1) = spline(tout,qout(:,1),tspan);
qout_sp(:,2) = spline(tout,qout(:,2),tspan);

end %end function rk1bi_nd
```

APPENDIX B

MATLAB script capable of simulating the response of the four-spring MBS support system

```
function [tout,qout,teout,qeout,ieout,tspan,qout_sp] = rk4bi_nd_pre()
%********************DIMENSIONLESS*****************************
%clear all; close all; clc %Housekeeping

%% Dimensionless Parameters
alpha1 = 5;       %Bilinear Spring Stiffness Ratios (K_2/K_1)
alpha2 = 5;
alpha3 = 5;
alpha4 = 5;

beta2 = 1;       %Primary Stiffness Ratio (K_1/K11)
beta3 = 1;
beta4 = 1;

sigma2 = 1;     %Knee Ratio (s_/s1)
sigma3 = 1;
sigma4 = 1;

dmprat = 0.01;     %Damping Ratio

Amp = 1.0; Ang = 0;
Ax = Amp*cos(pi*Ang/180);         %x harmonic forcing amplitude
wx = 0.75;         %x " " frequency
Ay = Amp*sin(pi*Ang/180);         %y " "
wy = 0.75;         %y " "

x1 = 5; y1 = 0; %Anchor x & y coordinates
uL1 = 4.25; %Undeformed Length of Spring

x2 = 0; y2 = 5;
uL2 = 4.25;

x3 = -5; y3 = 0;
uL3 = 4.25;

x4 = 0; y4 = -5;
uL4 = 4.25;

%% Simulation Parameters
%Initial Conditions (Positions, Velocities)
IC = [0,0,0,0];  %(x y u v)

%Time Information
T = 2*pi/wx;
Tmult = 500;
tdiv = 400;
tspan = 0:T/tdiv:T*Tmult;  %Initial time span, changes as events occur
tstart = tspan(1);
```

```
tend = tspan(end);

%Determine Which Springs are Past the Knee Initially
fltrans = [1 1 %Translates the event number into proper flag setting
           2 2
           3 1
           4 2
           5 1
           6 2
           7 1
           8 2];

%% Calculate Stretches in Springs Initially
%Calculate stretch in each spring
d1 = sqrt((IC(1)-x1)^2+(IC(2)-y1)^2)-uL1;
d2 = sqrt((IC(1)-x2)^2+(IC(2)-y2)^2)-uL2;
d3 = sqrt((IC(1)-x3)^2+(IC(2)-y3)^2)-uL3;
d4 = sqrt((IC(1)-x4)^2+(IC(2)-y4)^2)-uL4;

%Check knee status of 1st spring
if (d1 < 1)
    fl(1) = 1;
else
    fl(1) = 2;
end

%Check knee status of 2nd spring
if (d2 < sigma2)
    fl(2) = 1;
else
    fl(2) = 2;
end

%Check knee status of 3rd spring
if (d3 < sigma3)
    fl(3) = 1;
else
    fl(3) = 2;
end

%Check knee status of 4th spring
if (d4 < sigma4)
    fl(4) = 1;
else
    fl(4) = 2;
end

%% Accumulators for ODE45 output (t,q start new after each ode45 call)
tout = tstart;      %global solution time
qout = IC;          %global solution position
teout = [];         %time at which events occur
qeout = [];         %position at which events occur
ieout = [];         %flags which event triggered the switch
```

```
%% ----------------------------------------------------------------------
%               RK Solver and Output Accumulators
%-----------------------------------------------------------------------
%Set options for the ODE solver
options = odeset('RelTol',1e-10,'AbsTol',1e-11,'Events',@events);

%Call the RK solver until tend reached (recall at each knee)
while (tout(end)<tend)
[t,q,te,qe,ie] = ode45(@qdots,tspan,IC,options);

%Determine how many events occured
ne = length(ie);

%Accumulate output.
nt = length(t);
tout = [tout; t(2:nt)]; %2:nt so ending and next IC are not reported 2x
qout = [qout; q(2:nt,:)];
teout = [teout; te];    % Events at tstart are never reported.
qeout = [qeout; qe];

tspan = [t(end), tend]; %reset time span,'where you just ended to tend'
IC = [q(end,1),q(end,2),q(end,3),q(end,4)]; %reset IC as
                                            %where you just ended
%Reset Proper Flags because of Event that triggered
for i = 1:ne
fl(ceil(ie(i)/2)) = fltrans(ie(i),2);
end %end flag setting
end %end while

%% ----------------------------------------------------------------------
%               State Space Function for Each Case (16 cases)
%-----------------------------------------------------------------------
function qdot = qdots(t,q)
%x and y components of deformed length for each spring
Lx1 = x1-q(1);    Ly1 = q(2);
Lx2 = q(1);        Ly2 = y2-q(2);
Lx3 = q(1)-x3;    Ly3 = q(2);
Lx4 = q(1);       Ly4 = q(2)-y4;

%Calculate Total Deformed Length @ each iteration (always (+))
L1 = sqrt((Lx1^2)+(Ly1^2));
L2 = sqrt((Lx2^2)+(Ly2^2));
L3 = sqrt((Lx3^2)+(Ly3^2));
L4 = sqrt((Lx4^2)+(Ly4^2));

%------------------------------1,2,3,4 Below--------------------------
if (fl(1) == 1 && fl(2) == 1 && fl(3) == 1 && fl(4) == 1)
    %Calculate Spring Force based on Stretch in Spring
    %(+) when any spring is in tension (+ direction depends on
orientation)
    fs1 = (L1-uL1);
    fs2 = beta2*(L2-uL2);
    fs3 = beta3*(L3-uL3);
    fs4 = beta4*(L4-uL4);
```

```
%------------------------------(1 Above) 2,3,4 Below-------------------
elseif (fl(1) == 2 && fl(2) == 1 && fl(3) == 1 && fl(4) == 1)
    fs1 = alpha1*(L1-uL1)+(1-alpha1);
    fs2 = beta2*(L2-uL2);
    fs3 = beta3*(L3-uL3);
    fs4 = beta4*(L4-uL4);

%------------------------------(2 Above) 1,3,4 Below-------------------
elseif (fl(2) == 2 && fl(1) == 1 && fl(3) == 1 && fl(4) == 1)
    fs1 = (L1-uL1);
    fs2 = alpha2*beta2*(L2-uL2)+(beta2-alpha2*beta2)*sigma2;
    fs3 = beta3*(L3-uL3);
    fs4 = beta4*(L4-uL4);

%------------------------------(3 Above) 1,2,4 Below-------------------
elseif (fl(3) == 2 && fl(1) == 1 && fl(2) == 1 && fl(4) == 1)
    fs1 = (L1-uL1);
    fs2 = beta2*(L2-uL2);
    fs3 = alpha3*beta3*(L3-uL3)+(beta3-alpha3*beta3)*sigma3;
    fs4 = beta4*(L4-uL4);

%------------------------------(4 Above) 1,2,3 Below-------------------
elseif (fl(4) == 2 && fl(1) == 1 && fl(2) == 1 && fl(3) == 1)
    fs1 = (L1-uL1);
    fs2 = beta2*(L2-uL2);
    fs3 = beta3*(L3-uL3);
    fs4 = alpha4*beta4*(L4-uL4)+(beta4-alpha4*beta4)*sigma4;

%------------------------------(1,2 Above) 3,4 Below-------------------
elseif (fl(1) == 2 && fl(2) == 2 && fl(3) == 1 && fl(4) == 1)
    fs1 = alpha1*(L1-uL1)+(1-alpha1);
    fs2 = alpha2*beta2*(L2-uL2)+(beta2-alpha2*beta2)*sigma2;
    fs3 = beta3*(L3-uL3);
    fs4 = beta4*(L4-uL4);

%------------------------------(1,3 Above) 2,4 Below-------------------
elseif (fl(1) == 2 && fl(3) == 2 && fl(2) == 1 && fl(4) == 1)
    fs1 = alpha1*(L1-uL1)+(1-alpha1);
    fs2 = beta2*(L2-uL2);
    fs3 = alpha3*beta3*(L3-uL3)+(beta3-alpha3*beta3)*sigma3;
    fs4 = beta4*(L4-uL4);

%------------------------------(1,4 Above) 2,3 Below-------------------
elseif (fl(1) == 2 && fl(4) == 2 && fl(2) == 1 && fl(3) == 1)
    fs1 = alpha1*(L1-uL1)+(1-alpha1);
    fs2 = beta2*(L2-uL2);
    fs3 = beta3*(L3-uL3);
    fs4 = alpha4*beta4*(L4-uL4)+(beta4-alpha4*beta4)*sigma4;

%------------------------------(1,2,3 Above) 4 Below-------------------
elseif (fl(1) == 2 && fl(2) == 2 && fl(3) == 2 && fl(4) == 1)
    fs1 = alpha1*(L1-uL1)+(1-alpha1);
    fs2 = alpha2*beta2*(L2-uL2)+(beta2-alpha2*beta2)*sigma2;
    fs3 = alpha3*beta3*(L3-uL3)+(beta3-alpha3*beta3)*sigma3;
    fs4 = beta4*(L4-uL4);
```

```
%------------------------------(1,2,4 Above) 3 Below-------------------
elseif (fl(1) == 2 && fl(2) == 2 && fl(4) == 2 && fl(3) == 1)
    fs1 = alpha1*(L1-uL1)+(1-alpha1);
    fs2 = alpha2*beta2*(L2-uL2)+(beta2-alpha2*beta2)*sigma2;
    fs3 = beta3*(L3-uL3);
    fs4 = alpha4*beta4*(L4-uL4)+(beta4-alpha4*beta4)*sigma4;

%------------------------------(1,3,4 Above) 2 Below-------------------
elseif (fl(1) == 2 && fl(3) == 2 && fl(4) == 2 && fl(2) == 1)
    fs1 = alpha1*(L1-uL1)+(1-alpha1);
    fs2 = beta2*(L2-uL2);
    fs3 = alpha3*beta3*(L3-uL3)+(beta3-alpha3*beta3)*sigma3;
    fs4 = alpha4*beta4*(L4-uL4)+(beta4-alpha4*beta4)*sigma4;

%------------------------------(2,3 Above) 1,4 Below-------------------
elseif (fl(2) == 2 && fl(3) == 2 && fl(1) == 1 && fl(4) == 1)
    fs1 = (L1-uL1);
    fs2 = alpha2*beta2*(L2-uL2)+(beta2-alpha2*beta2)*sigma2;
    fs3 = alpha3*beta3*(L3-uL3)+(beta3-alpha3*beta3)*sigma3;
    fs4 = beta4*(L4-uL4);

%------------------------------(2,4 Above) 1,3 Below-------------------
elseif (fl(2) == 2 && fl(4) == 2 && fl(1) == 1 && fl(3) == 1)
    fs1 = (L1-uL1);
    fs2 = alpha2*beta2*(L2-uL2)+(beta2-alpha2*beta2)*sigma2;
    fs3 = beta3*(L3-uL3);
    fs4 = alpha4*beta4*(L4-uL4)+(beta4-alpha4*beta4)*sigma4;

%------------------------------(2,3,4 Above) 1 Below-------------------
elseif (fl(2) == 2 && fl(3) == 2 && fl(4) == 2 && fl(1) == 1)
    fs1 = (L1-uL1);
    fs2 = alpha2*beta2*(L2-uL2)+(beta2-alpha2*beta2)*sigma2;
    fs3 = alpha3*beta3*(L3-uL3)+(beta3-alpha3*beta3)*sigma3;
    fs4 = alpha4*beta4*(L4-uL4)+(beta4-alpha4*beta4)*sigma4;

%------------------------------(3,4 Above) 1,2 Below-------------------
elseif (fl(3) == 2 && fl(4) == 2 && fl(1) == 1 && fl(2) == 1)
    fs1 = (L1-uL1);
    fs2 = beta2*(L2-uL2);
    fs3 = alpha3*beta3*(L3-uL3)+(beta3-alpha3*beta3)*sigma3;
    fs4 = alpha4*beta4*(L4-uL4)+(beta4-alpha4*beta4)*sigma4;

%------------------------------(1,2,3,4 Above)-------------------------
elseif (fl(1) == 2 && fl(2) == 2 && fl(3) == 2 && fl(4) == 2)
    fs1 = alpha1*(L1-uL1)+(1-alpha1);
    fs2 = alpha2*beta2*(L2-uL2)+(beta2-alpha2*beta2)*sigma2;
    fs3 = alpha3*beta3*(L3-uL3)+(beta3-alpha3*beta3)*sigma3;
    fs4 = alpha4*beta4*(L4-uL4)+(beta4-alpha4*beta4)*sigma4;
end
%-------------------------------------------------------------------------

%Calculate x and y components of spring forces
fx1 = fs1*cos(atan(Ly1/Lx1));     fy1 = -fs1*sin(atan(Ly1/Lx1));
fx2 = -fs2*sin(atan(Lx2/Ly2));    fy2 = fs2*cos(atan(Lx2/Ly2));
```

```
fx3 = -fs3*cos(atan(Ly3/Lx3));    fy3 = -fs3*sin(atan(Ly3/Lx3));
fx4 = -fs4*sin(atan(Lx4/Ly4));    fy4 = -fs4*cos(atan(Lx4/Ly4));

%Total Spring Forces in x and y direction on the mass (N2 Law)
fx = fx1+fx2+fx3+fx4+Ax*sin(wx*t);
fy = fy1+fy2+fy3+fy4+Ay*sin(wy*t);

%Calculate the qdot vector
qdot(1,1) = q(3);   %x velocity
qdot(2,1) = q(4);   %y velocity
qdot(3,1) = fx-2*dmprat*q(3);  %x accel = sum x forces
qdot(4,1) = fy-2*dmprat*q(4);  %y accel = sum y forces

end %function qdots

%% ---------------------------------------------------------------------
%               Events Function (Detects when knees are reached)
%----------------------------------------------------------------------
function [value,isterminal,direction] = events(t,q)
value = [(sqrt((q(1)-x1)^2+(q(2)-y1)^2)-uL1)-1,...
         (sqrt((q(1)-x1)^2+(q(2)-y1)^2)-uL1)-1,...
         (sqrt((q(1)-x2)^2+(q(2)-y2)^2)-uL2)-sigma2,...
         (sqrt((q(1)-x2)^2+(q(2)-y2)^2)-uL2)-sigma2,...
         (sqrt((q(1)-x3)^2+(q(2)-y3)^2)-uL3)-sigma3,...
         (sqrt((q(1)-x3)^2+(q(2)-y3)^2)-uL3)-sigma3,...
         (sqrt((q(1)-x4)^2+(q(2)-y4)^2)-uL4)-sigma4,...
         (sqrt((q(1)-x4)^2+(q(2)-y4)^2)-uL4)-sigma4]; %Detect 0s
isterminal = [1,1,1,1,1,1,1,1];   % Stop the integration for any event
direction = [-1,1,-1,1,-1,1,-1,1];   % Direction
end %function events

%% Interpoloate data at desired time steps (via cubic spline)
%Piecing together ode45 calls between knee engagements results in
%undesirable timestep.  This produces the desired global timestep.
tspan = 0:T/tdiv:T*Tmult;
qout_sp(:,1) = spline(tout,qout(:,1),tspan);
qout_sp(:,2) = spline(tout,qout(:,2),tspan);
qout_sp(:,3) = spline(tout,qout(:,3),tspan);
qout_sp(:,4) = spline(tout,qout(:,4),tspan);

end %function rk4bi_nd_pre
```

APPENDIX C

MATLAB script capable of calculating the scaled potential energy in the four-spring MBS support system

```
%clear all; close all; clc %Housekeeping

%Spring 1 Constants
k11 = 1;     %Lower stiffness
alpha1 = 20;       %Bilinear Spring Stiffness Ratios (K_2/K_1)
k12 = k11*alpha1;    %Upper stiffness
L1 = 4.25;
s1 = 1;         %Knee Location
x1 = 5;         %Anchor x coordinate
y1 = 0;         %Anchor y coordinate

%Spring 2 Constants
alpha2 = 20;
beta2 = 0;       %Primary Stiffness Ratio (K_1/K11)
sigma2 = 1;      %Knee Ratio (s_/s1)
L2 = 4.25;
x2 = 0;
y2 = 5;
k21 = beta2*k11;
k22 = alpha2*k21;
s2 = sigma2*s1;

%Spring 3 Constants
alpha3 = 20;
beta3 = 0;
sigma3 = 1;
L3 = 4.25;
x3 = -5;
y3 = 0;
k31 = beta3*k11;
k32 = alpha3*k31;
s3 =sigma3*s1;

%Spring 4 Constants
alpha4 = 20;
beta4 = 1;
sigma4 = 1;
L4 = 4.25;
x4 = 0;
y4 = -5;
k41 = beta4*k11;
k42 = alpha4*k41;
s4 = sigma4*s1;

%Vectors For Reasonable Box
x = -5:10/1200:5;
y = -5:10/1200:5;
```

```
%Initialize Scaled PE Matrix
U = zeros(numel(x),numel(y));

%Calculate the Potential Energy
for i = 1:numel(x)
    for j = 1:numel(y)

        %Calculate stretch in each spring
        d1 = (sqrt((x(i)-x1)^2+(y(j)-y1)^2)-L1);
        d2 = (sqrt((x(i)-x2)^2+(y(j)-y2)^2)-L2);
        d3 = (sqrt((x(i)-x3)^2+(y(j)-y3)^2)-L3);
        d4 = (sqrt((x(i)-x4)^2+(y(j)-y4)^2)-L4);

        %Check knee status of 1st spring
        if (d1 < s1)
            U(j,i) = U(j,i) + 0.5*k11*d1^2;
        else
            U(j,i) = U(j,i) + 0.5*k12*d1^2+0.5*(s1^2)*(k12-k11)+...
                (k11-k12)*s1*d1;
        end

        %Check knee status of 2nd spring
        if (d2 < s2)
            U(j,i) = U(j,i) + 0.5*k21*d2^2;
        else
            U(j,i) = U(j,i) + 0.5*k22*d2^2+0.5*(s2^2)*(k22-k21)+...
            (k21-k22)*s2*d2;
        end

        %Check knee status of 3rd spring
        if (d3 < s3)
            U(j,i) = U(j,i) + 0.5*k31*d3^2;
        else
            U(j,i) = U(j,i) + 0.5*k32*d3^2+0.5*(s3^2)*(k32-k31)+...
                (k31-k32)*s3*d3;
        end

        %Check knee status of 4th spring
        if (d4 < s4)
            U(j,i) = U(j,i) + 0.5*k41*d4^2;
        else
            U(j,i) = U(j,i) + 0.5*k42*d4^2+0.5*(s4^2)*(k42-k41)+...
                (k41-k42)*s4*d4;
        end
    end
end
```

APPENDIX D

ANSYS script capable of simulating the free response of the four-spring MBS support system

```
finish    !*******DIMENSIONLESS*********
/clear
/config,nres,250000  !The number of results able to store
/prep7
!------------Piecewise-Linear spring
et,1,combin39
keyopt,1,2,0  !Follow defined compression behavior (reflect if not given)
keyopt,1,4,3  !2d Longitudinal spring
keyopt,1,6,1  !Print Force Deflection table

!------------Lumped 2D Mass
et,2,mass21
keyopt,2,3,4   !2D w/out rotarty inertia

!Set the lumped mass value (always 1 for dimensionless simulation)
r,5,1

!------------Geometry Inputs
!Define coordinates for anchors and undeformed lengths(dimensionless)
x1 = 5
y1 = 0
uL1 = 4.25
move1 = x1-uL1

x2 = 0
y2 = 5
uL2 = 4.25
move2 = y2-uL2

x3 = -5
y3 = 0
uL3 = 4.25
move3 = x3+uL3

x4 = 0
y4 = -5
uL4 = 4.25
move4 = y4+uL4

!------------Define Dimensionless Parameters
alpha1 = 20
```

```
alpha2 = 20
alpha3 = 20
alpha4 = 20

beta2 = 1
beta3 = 1
beta4 = 1

sigma2 = 1
sigma3 = 1
sigma4 = 1

!------------the Bilinear Spring curve(s)
s1 = 1 !Knee Locations
s2 = sigma2*s1
s3 = sigma3*s1
s4 = sigma4*s1
k11 = 1 !Lower Stiffness Values
k21 = beta2*k11
k31 = beta3*k11
k41 = beta4*k11
xend1 = 10 !Just for reference(if exceeded slope is maintained)
xend2 = 10
xend3 = 10
xend4 = 10
compx1 = -10 !Used to define behavior under compression
compx2 = -10
compx3 = -10
compx4 = -10

!------------Autocalc
ys1 = s1*k11 !Force Value at Knee
ys2 = s2*k21
ys3 = s3*k31
ys4 = s4*k41
k12 = alpha1*k11 !Upper Stiffness Values
k22 = alpha2*k21
k32 = alpha3*k31
k42 = alpha4*k41
yend1 = ys1+k12*(xend1-s1)
yend2 = ys2+k22*(xend2-s2)
yend3 = ys3+k32*(xend3-s3)
yend4 = ys4+k42*(xend4-s4)
compy1 = compx1*k11
compy2 = compx2*k21
compy3 = compx3*k31
```

```
compy4 = compx4*k41

!Defining Bilinear Curves for each Spring
r,1,compx1,compy1,0,0,s1,ys1
rmore,xend1,yend1
r,2,compx2,compy2,0,0,s2,ys2
rmore,xend2,yend2
r,3,compx3,compy3,0,0,s3,ys3
rmore,xend3,yend3
r,4,compx4,compy4,0,0,s4,ys4
rmore,xend4,yend4

!Nodal Definitions
n,1,uL1,y1
n,2,x2,uL2
n,3,-uL3,y3
n,4,x4,-uL4
n,5,0,0

!Define Elements
type,1
real,1
e,1,5
real,2
e,2,5
real,3
e,3,5
real,4
e,4,5
type,2
real,5
e,5

!------------Turn the nonlinear behavior on
nlgeom,on

!------------Transient Analysis
/solu
sstif,on
antype,trans
solcontrol,on
ic,5,ux,0.55,0 !Initial Conditions
ic,5,uy,0.55,0
kbc,1
time,200
deltim,0.0015
```

```
!betad,0.9
outres,all,all

!Preload the springs initially by moving anchor points
d,1,ux,move1
d,1,uy,0
d,2,ux,0
d,2,uy,move2
d,3,ux,move3
d,3,uy,0
d,4,ux,0
d,4,uy,move4

solve

!Save the displacement and velocities of the mass
/post26
nsol,2,5,u,x,ux
nsol,4,5,vel,x,velx

nsol,3,5,u,y,uy
nsol,5,5,vel,y,vely

!Adjust number of lines before repeating header in any printouts
lines,200000
```

APPENDIX E

MATLAB script capable of simulating the response of the four-spring MBS support system using polynomial approximations for bilinear stiffness models

```
function [tout,qout] = rk4poly_nd_pre()
%********************DIMENSIONLESS*****************************
%clear all; close all; clc %Housekeeping

%% Dimensionless Parameters
alpha1 = 20;       %Bilinear Spring Stiffness Ratios (K_2/K_1)
alpha2 = 20;
alpha3 = 20;
alpha4 = 20;

beta2 = 1;       %Primary Stiffness Ratio (K_1/K11)
beta3 = 1;
beta4 = 1;

sigma2 = 1;     %Knee Ratio (s_/s1)
sigma3 = 1;
sigma4 = 1;

dmprat = 0.03;     %Damping Ratio

Ax = 1;         %x harmonic forcing amplitude
wx = 0.75;         %x " " frequency
Ay = 0;         %y " "
wy = 0;         %y " "

x1 = 5; y1 = 0; %Anchor x & y coordinates
uL1 = 4.25; %Undeformed Length of Spring

x2 = 0; y2 = 5;
uL2 = 4.25;

x3 = -5; y3 = 0;
uL3 = 4.25;

x4 = 0; y4 = -5;
uL4 = 4.25;

%% Generate Bilinear Stiffness Curves for Reference
xref = (0:0.001:2)'; %Try to bracket the range of spring deformation
fref1 = zeros(numel(xref),1);fref2=fref1; fref3 = fref1; fref4 = fref1;
for i = 1:numel(xref)
    if xref(i,1) <= 1
        fref1(i,1) = xref(i);
    else
        fref1(i,1) = alpha1*xref(i)+(1-alpha1);
    end
    if xref(i,1) <= sigma2
```

```
        fref2(i) = beta2*xref(i);
    else
        fref2(i,1) = alpha2*beta2*xref(i)+(beta2-alpha2*beta2)*sigma2;
    end
    if xref(i,1)<= sigma3
        fref3(i,1) = beta3*xref(i);
    else
        fref3(i,1) = alpha3*beta3*xref(i)+(beta3-alpha3*beta3)*sigma3;
    end
    if xref(i,1) <= sigma4
        fref4(i) = beta4*xref(i);
    else
        fref4(i,1) = alpha4*beta4*xref(i)+(beta4-alpha4*beta4)*sigma4;
    end
end

%% Specify polynomial degree and any linear constraints
polydeg = 5;
xpass = 0'; %input as row vector if multiple points
ypass = 0';

%% Generate Vandermonde Matrix for Reference Curve x values
V(:,polydeg+1) = ones(length(xref),1);
for j = polydeg:-1:1
V(:,j) = xref.*V(:,j+1);
end

%% Parameters for Linear Constraint
Aeq(:,polydeg+1)=ones(length(xpass),1); %Vandermonde matrix for xpass
for k = polydeg:-1:1
Aeq(:,k) = xpass.*Aeq(:,k+1);
end
beq = ypass; %desired value at xpass

%% Regression with Linear Constraints
options = optimset('LargeScale','off');
pc1 = lsqlin(V,fref1,[],[],Aeq,beq,[],[],[],options);
pc2 = lsqlin(V,fref2,[],[],Aeq,beq,[],[],[],options);
pc3 = lsqlin(V,fref3,[],[],Aeq,beq,[],[],[],options);
pc4 = lsqlin(V,fref4,[],[],Aeq,beq,[],[],[],options);

%% Simulation Parameters
%Initial Conditions (Positions, Velocities)
IC = [0,0,0,0];  %(x y u v)

%Time Information
T = 2*pi/wx;
Tmult = 100;
tdiv = 400;
tspan = 0:T/tdiv:T*Tmult;  %Initial time span, changes as events occur
```

```
%% ----------------------------------------------------------------------
%               RK Solver and Output Accumulators
%-----------------------------------------------------------------------
%Set options for the ODE solver
options = odeset('RelTol',1e-10,'AbsTol',1e-12);

%Call the RK solver
[tout,qout] = ode45(@qdots,tspan,IC,options);

%% ----------------------------------------------------------------------
%               State Space Function for Each Case (16 cases)
%-----------------------------------------------------------------------
function qdot = qdots(tout,qout)

%x and y components of deformed length for each spring
Lx1 = x1-qout(1);    Ly1 = qout(2);
Lx2 = qout(1);        Ly2 = y2-qout(2);
Lx3 = qout(1)-x3;    Ly3 = qout(2);
Lx4 = qout(1);       Ly4 = qout(2)-y4;

%Calculate Total Deformed Length @ each iteration (always (+))
L1 = sqrt((Lx1^2)+(Ly1^2));
L2 = sqrt((Lx2^2)+(Ly2^2));
L3 = sqrt((Lx3^2)+(Ly3^2));
L4 = sqrt((Lx4^2)+(Ly4^2));

fs1 = 0; fs2 = 0; fs3 = 0; fs4 = 0;
for m = 1:polydeg+1
     fs1 = fs1+(L1-uL1)^(polydeg-m+1)*pc1(m);
     fs2 = fs2+(L2-uL2)^(polydeg-m+1)*pc2(m);
     fs3 = fs3+(L3-uL3)^(polydeg-m+1)*pc3(m);
     fs4 = fs4+(L4-uL4)^(polydeg-m+1)*pc4(m);
end
%-----------------------------------------------------------------------
%Calculate x and y components of spring forces
fx1 = fs1*cos(atan(Ly1/Lx1));     fy1 = -fs1*sin(atan(Ly1/Lx1));
fx2 = -fs2*sin(atan(Lx2/Ly2));    fy2 = fs2*cos(atan(Lx2/Ly2));
fx3 = -fs3*cos(atan(Ly3/Lx3));    fy3 = -fs3*sin(atan(Ly3/Lx3));
fx4 = -fs4*sin(atan(Lx4/Ly4));    fy4 = -fs4*cos(atan(Lx4/Ly4));

%Total Spring Forces in x and y direction on the mass (N2 Law)
fx = fx1+fx2+fx3+fx4+Ax*sin(wx*tout);
fy = fy1+fy2+fy3+fy4+Ay*sin(wy*tout);

%Calculate the qdot vector
qdot(1,1) = qout(3);   %x velocity
qdot(2,1) = qout(4);   %y velocity
qdot(3,1) = fx-2*dmprat*qout(3);  %x accel = sum x forces
qdot(4,1) = fy-2*dmprat*qout(4);  %y accel = sum y forces

end %function qdots

end %function rk4poly_nd_pre
```

REFERENCES

[1] AMS-02 Project Page, <http://ams-02project.jsc.nasa.gov/html/Projectpage.htm>

[2] Lauritzen, C., "Pretest Analysis for the Alpha Magnet Spectrometer (AMS-02) Vacuum Case Sine Sweep Test," Jacobs Engineering, ESCG-4460-06-LODY-DOC-0216, 2006.

[3] Mott, P.B., "Alpha Magnetic Spectrometer 02 (AMS-02) Experiment/Vacuum Case (VC) Payload," NASA, JSC-29202, 2009.

Integration Hardware (PIH) Interfaces

[4] Klotz, I., "AMS to Get Longer Lease on Life," Aviation Week, 2010, <http://www.aviationweek.com/aw/generic/story_channel.jsp?channel=space&id=news/asd/2010/04/22/07.xml>

[5] Nayfeh, A.H, Balachandran, B., *Applied Nonlinear Dynamics: Analytical, Computational, and Experimental Methods*, John Wiley and Sons, 1995.

[6] Kelly, S. G., *Fundamentals of Mechanical Vibration*, McGraw-Hill, 1993, pp. 504-540.

[7] Den Hartog, J.P., *Mechanical Vibrations*, Third Edition, McGraw-Hill, 1947, pp 406-451.

[8] Minorsky, N., *Introduction to Non-Linear Mechanics: Topological Methods - Analytical Methods – Nonlinear Resonance – Relaxation Oscillations*, J.W Edwards, Ann Arbor, 1947.

[9] Thomson, W.T., Dahleh, M.D., *Theory of Vibration with Applications*, Fifth Edition, Prentice Hall, New Jersey, 1998, pp. 49-50.

[10] Ueda, Y, "Steady Motions Exhibited by Duffing's Equation: A Picture Book of Regular and Chaotic Motions," in New Approaches to Nonlinear Problems in Dynamics (ed. P.J. Holmes), *Society for Industrial and Applied Mathematics*, 1980.

[11] Thompson, J.M.T., Stewart, H.B., *Nonlinear Dynamics and Chaos*, John Wiley and Sons, 1986.

[12] Virgin, L.N., *Introduction to Experimental Nonlinear Dynamics*, Cambridge University Press, 2000.

[13] di Bernardo, M., Budd, C.J, Champneys, A.R, Kowalczyk, P., *Piecewise-Smooth Dynamical Systems: Theory and Applications*, in Applied Mathematical Sciences **163**, Springer, 2008.

[14] Plaut, R.H., Farmer, A.L., "Large Motions of a Moored Floating Breakwater Modeled as an Impact Oscillator," *Nonlinear Dynamics* **23**, 2000, pp. 319-334.

[15] Plaut, R.H., Archilla, J.C., Mays, T.W., "Snap Loads in Mooring Lines during Large Three-Dimensional Motions of a Cylinder," *Nonlinear Dynamics* **23**, 2000, pp. 271-284.

[16] Huang, S., Vassalos, D., "A Numerical Method for Predicting Snap Loading of Marine Cables," *Applied Ocean Research* **15**, 1993, pp. 235-242.

[17] Shaw, S.W., Holmes, P.J., "A Periodically Forced Piecewise Linear Oscillator," *Journal of Sound and Vibration* **90** (1), 1983, pp. 129-155.

[18] Hossain, M.Z, Mizutani, K., Sawai, H., "Chaos and Multiple Periods in an Unsymmetrical Spring and Damping System with Clearance," *Journal of Sound and Vibration* **250** (2), 2002, pp. 229-245.

[19] Hossain, M.Z, Mizutani, K., Sawai, H., Kato, M., "Preloading Effects on Clearance Problem in Rotor-coupling Vibration System: Experimentation and Simulation," *Chaos, Solitons, and Fractals* **14**, 2002, pp. 1371-1378.
[20] Kahraman, A., "On the Response of a Preloaded Mechanical Oscillator with a Clearance: Period-Doubling and Chaos," *Nonlinear Dynamics* **3**, 1992, pp. 183-198.

[21] Yoshitake, Y., Sueoka, A., Shoji, N., Hai, T., "Vibrations of Nonlinear Systems with Discontinuities (The Case of a Preloaded Compliance System)," Japan Society Mechanical Engineers International Journal **41** (4), 1998, pp. 710-717.
[22] Moon, F.C., Shaw, S.W., "Chaotic Vibrations of a Beam with Non-Linear Boundary Conditions," *International Journal of Non-Linear* Mechanics **18** (6), 1983, pp. 465-477.
[23] Pandey, U. K., Benipal, G.S., "Bilinear Dynamics of SDOF Concrete Structures under Sinusoidal Loading," *Advances in Structural Engineering* **9** (3), 2006, pp. 393-407.
[24] Den Hartog, J.P., Mikina, S.J., "Forced Vibrations with Non-Linear Spring Constants," Transactions of the American Society of Mechanical Engineers, APM-54-25, 1932, pp. 157-164.
[25] Den Hartog, J.P., Heiles, R.M., "Forced Vibrations in Nonlinear Systems with Various Combinations of Linear Springs," *Journal of Applied Mechanics*, 1936, pp. 127-130.
[26] Schulman, J.N., "Chaos in piecewise-linear systems," *Physical Review A* **28** (1), 1983, pp. 477-479.
[27] Luo, A.C.J, "The Mapping Dynamics of Periodic Motions for a Three-Piecewise Linear System under a Periodic Excitation," *Journal of Sound and Vibration* **283**, 2005, pp. 723-748.
[28] Hogan, S.J., Homer, M.E., "Graph Theory and Piecewise Smooth Dynamical Systems of Arbitrary Dimension," *Chaos, Solitons, and Fractals* **10** (11), 1999, pp. 1869-1880.
[29] Chicurel-Uziel, E., "Exact, Single Equation, Closed-Form Solution of Vibrating Systems with Piecewise Linear Springs," *Journal of Sound and Vibration* **245** (2), 2001, pp. 285-301.
[30] Vanden-Eijnden, E., "Introduction to Regular Perturbation Theory," Courant Institute, Lecture Notes, < http://www.cims.nyu.edu/~eve2/reg_pert.pdf>.
[31] Xu, L., Lu, M.W., Cao, Q., "Bifurcation and Chaos of a Harmonically Excited Oscillator with Both Stiffness and Viscous Damping Piecewise Linearities by Incremental Harmonic Balance Method," *Journal of Sound and Vibration* **264**, 2003, pp. 873-882.
[32] Narayanan, S., Sekar, P., "Periodic and Chaotic Responses of an SDF System with Piecewise Linear Stiffness Subjected to Combined Harmonic and Flow Induced Excitations," *Journal of Sound and Vibration* **184** (2), 1995, pp. 281-298.
[33] Lau, S.L., Cheung, Y.K., "Amplitude Incremental Variational Principle for Nonlinear Vibration of Elastic Systems," *Journal of Applied Mechanics* **48**, 1981, pp. 959-964.

[34] Lau, S.L., Zhang, W., "Nonlinear Vibrations of Piecewise-Linear Systems by Incremental Harmonic Balance Method," *Journal of Applied Mechanics* **59**, 1992, pp. 153-160.
[35] Li, T., Yorke, J.A., "Period Three Implies Chaos," *The American Mathematical Monthly* **82** (10), 1975, pp. 985-992.
[36] Ravindra, B., Mallik, A.K., "Chaotic Response of a Harmonically Excited Mass on an Isolator with Non-linear Stiffness and Damping Characteristics," *Journal of Sound and Vibration* **182** (3), 1995, pp. 345 – 353.
[37] Abou-Rayan, A.M., Nayfeh, A.H., Mook, D.T., "Nonlinear Response of a Parametrically Excited Buckled Beam," *Nonlinear Dynamics* **4**, 1993, pp. 499-525.
[38] Kincaid, D., Cheney, W., *Numerical Analysis: Mathematics of Scientific Computing*, Third Edition, Brooks/Cole, 2002.
[39] Koh, C.G., Liaw, C.Y., "Effects of Time Step Size on the Response of a Bilinear System, I: Numerical Study," *Journal of Sound and Vibration* **144** (1), 1991, pp. 17-29.
[40] Cao, Q., Xu, L., Djidjeli, K., Price, W.G., Twizell, E.H., "Analysis of Period-Doubling and Chaos of a Non-Symmetric Oscillator with Piecewise-Linearity," *Chaos, Solitons, and Fractals* **12**, 2001, pp. 1917-1927.
[41] Choi, S., Noah, S.T, "Response and Stability Analysis of Piecewise-Linear Oscillators under Multi-Forcing Frequencies," *Nonlinear Dynamics* **3**, 1992, pp. 105-121.
[42] Xueqi, C., Qiuhai, L., Zhichao, H., Tieneng, G., "A Two-Step Method to Identify Parameters of Piecewise Linear Systems," *Journal of Sound and Vibration* **320**, 2009, pp. 808-821.
[43] Wagg, D.J., Bishop, S.R., "A Note on Modelling Multi-Degree of Freedom Vibro-Impact Systems Using Coefficient of Restitution Models," *Journal of Sound and Vibration* **236** (1), 2000, pp. 176-184.
[44] Butcher, E.A., "Clearance Effects on Bilinear Normal Mode Frequencies," *Journal of Sound and Vibration* **224** (2), 1999, pp. 305-308.
[45] Butcher, E.A., "Order Reduction of Structural Dynamic Systems with Static Piecewise Linear Nonlinearities," *Nonlinear Dynamics* **49**, 2007, pp. 375-399.
[46] Luo, G.W., Lv, X.H., Zhu, X.F., "Dynamics of Vibro-Impact Mechanical Systems with Large Dissipation," *International Journal of Mechanical Sciences* **50**, 2008, pp. 214-232.
[47] Luo, G., Ma, L., Lv, X., "Dynamic Analysis and Suppressing Chaotic Impacts of a Two-Degree-of-Freedom Oscillator with a Clearance," *Nonlinear Analysis: Real World Applications* **10**, 2009, pp. 756-778.
[48] Ji, J.C., Hansen, C.H., "Approximate Solutions and Chaotic Motions of a Piecewise Nonlinear-Linear Oscillator," *Chaos, Solitons, and Fractals* **20**, 2004, pp. 1121-1133.
[49] Qinglong, M., "A Study of the Dynamic Behavior of Piecewise Nonlinear Oscillators with Time-Varying Stiffness," Dissertation, Ohio State University, 2005.

[50] Guest Editorial, “Special Issue on Geometrically Non-Linear Vibrations of Structures – Euromech 483,” *Journal of Sound and Vibration* **315**, 2008, pp. 371-374.
[51] Kovacic, I., Brennan, M.J., Waters, T.P., “A Study of a Nonlinear Vibration Isolator with a Quasi-Zero Stiffness Characteristic,” *Journal of Sound and Vibration* **315**, 2008, pp. 700-711.
[52] Gottlieb, O., Yim, S.C.S., “Nonlinear Oscillations, Bifurcations and Chaos in a Multi-Point Mooring System with a Geometric Nonlinearity,” *Applied Ocean Research* **14**, 1992, pp. 241-257.
[53] Umar, A., Ahmad, S., Datta, T.K., “Stability Analysis of a Moored Vessel,” *Journal of Offshore Mechanics and Artic Engineering* **126**, 2004, pp. 164-174.
[54] Aguilera, C.A.V, Extrema.m and Extrema2.m, MATLAB Central File Exchange, 2007, <http://www.mathworks.com/matlabcentral/fileexchange/12275>
[55] ANSYS Product Documentation, Release 12.0.1, SAS IP, Inc.
[56] MATLAB Product Documentation, Release 2009a, The Mathworks, Inc.

VITA

Trey Gilliam was born in Lexington, KY on December 22, 1985. He graduated from Paul Laurence Dunbar High School in 2004 and began undergraduate studies at the University of Kentucky in 2004 as well. Trey received his Bachelor of Science Degree in Mechanical Engineering from the University of Kentucky in 2008. In 2009, he began graduate studies in the Dynamic Structures and Controls Lab. During graduate studies, Trey was honored to receive funding from the University of Kentucky Center for Computational Sciences, as well as Otis A. Singletary and Kentucky Space Grant Consortium fellowships. His work was presented at the 13th Conference on Nonlinear Vibrations, Dynamics, and Multibody Systems at Virginia Tech as well as the 35th Dayton-Cincinnati Aerospace Sciences Symposium, where he was awarded Best Technical Presentation in the Space Applications category.